

UNCLASSIFIED

AD 295¹¹ 491

*Reproduced
by the*

**ARMED SERVICES TECHNICAL INFORMATION AGENCY
ARLINGTON HALL STATION
ARLINGTON 12, VIRGINIA**



UNCLASSIFIED

NOTICE: When government or other drawings, specifications or other data are used for any purpose other than in connection with a definitely related government procurement operation, the U. S. Government thereby incurs no responsibility, nor any obligation whatsoever; and the fact that the Government may have formulated, furnished, or in any way supplied the said drawings, specifications, or other data is not to be regarded by implication or otherwise as in any manner licensing the holder or any other person or corporation, or conveying any rights or permission to manufacture, use or sell any patented invention that may in any way be related thereto.

63-2-3

ASD-TDR-62-774

295 491

295491

ASTIA

AS AD 140.

DYNAMIC BUCKLING OF SHELL STRUCTURES SUBJECT TO LONGITUDINAL IMPACT

TECHNICAL DOCUMENTARY REPORT ASD-TDR-62-774

December 1962

Flight Dynamics Laboratory
Aeronautical Systems Division
Air Force Systems Command
Wright-Patterson Air Force Base, Ohio

Project No. 1467, Task No. 146703

ASTIA
FEB 19 1963

(Prepared under Contract No. AF 33(616)-8248
by General Electric Company
P.O. Box 8555, Philadelphia 1, Penna.
Authors: A. P. Coppa and W. A. Nash)

NOTICES

When Government drawings, specifications, or other data are used for any purpose other than in connection with a definitely related Government procurement operation, the United States Government thereby incurs no responsibility nor any obligation whatsoever; and the fact that the Government may have formulated, furnished, or in any way supplied the said drawings, specifications, or other data, is not to be regarded by implication or otherwise as in any manner licensing the holder or any other person or corporation, or conveying any rights or permission to manufacture, use, or sell any patented invention that may in any way be related thereto.

Qualified requesters may obtain copies of this report from the Armed Services Technical Information Agency, (ASTIA), Arlington Hall Station, Arlington 12, Virginia.

This report has been released to the Office of Technical Services, U. S. Department of Commerce, Washington 25, D. C. , in stock quantities for sale to the general public.

Copies of this report should not be returned to the Aeronautical Systems Division unless return is required by security considerations, contractual obligations, or notice on a specific document.

FOREWORD

This report was prepared by the General Electric Company, Missile and Space Division, King of Prussia, Pennsylvania. The work was sponsored by the Flight Dynamics Laboratory of the Aeronautical Systems Division, USAF, under Technical Area 750A "Mechanics of Flight". The work (administered under Contract AF 33(616)-8248) was accomplished in support of Project 1467 "Structural Analysis Methods" Task 146703 "Structural Plate and Shell Analysis". Mr. Adel Abdessalam served as project engineer for the laboratory.

The studies presented began on May, 1961, were concluded in June, 1962, and were performed by the Space Structures Operation, Space Sciences Laboratory, Missile and Space Division, General Electric Company. Mr. A. P. Coppa, Research Engineer, was responsible for the project at the General Electric Company.

The chief contributors to the project were: Mr. A. P. Coppa, theoretical and experimental activities, Professor W. A. Nash (University of Florida), theoretical analysis, Mr. S. A. Cimorelli (GE), experimentation, Mr. T. Coffin (GE), computations, Mr. F. L. Smith (GE), photography, and Mr. R. E. Herbert (University of Florida), computations.

This report is the final report and it concludes the work on Contract AF 33(616)-8248. The contractor's report number is TIS R62 SD77.

ASD-TR-62-774

ABSTRACT

Investigations dealing with the buckling of thin cylindrical and conical shells subject to axial impact are described. The studies consisted of experimental and theoretical efforts directed toward obtaining a qualitative and quantitative understanding of the dynamic buckling behavior of such shells under a variety of conditions. The conditions studied include different longitudinal conditions imposed on the impacted end of the shell and internal pressurization. In addition, methods of increasing the specific energy dissipation capacity of shells subject to axial impact were studied.

A number of interesting results were obtained. It was demonstrated experimentally that buckling of a cylindrical shell is initiated during the first passage of the axial compression stress wave due to the initial impact when the impact velocity is sufficiently high. Another significant experimental result obtained is that the asymmetrical (quasi-developable) form of shell buckling occurs as a result of a smooth transition from the symmetrical ("ring") form of buckling in some thin cylindrical shells subjected to an axially symmetric axial impact. Analytical results were obtained on the dynamical buckling behavior of cylindrical shells subject to a constant velocity end displacement. The method utilizes the finite deflection theory and is a refinement of the procedure due to A.S. Volmir. It shows that both the upper critical stress and the number of circumferential waves increase and the time to initiate buckling decreases with increasing velocity of impact. These trends are in agreement with the analytical results of Volmir and a phenomenological theory due to Coppa.

PUBLICATION REVIEW

This technical documentary report has been reviewed and is approved.


RICHARD F. HOENER
Chief, Structures Branch
Flight Dynamics Laboratory

TABLE OF CONTENTS

	Page
LIST OF SYMBOLS	vii
I. INTRODUCTION	1
II. SURVEY OF LITERATURE	3
III. EXPERIMENTAL INVESTIGATION	4
A. Apparatus	4
B. Specimens	5
C. Instrumentation	6
D. Results	7
1. Phase 1 — Effect of Longitudinal End Conditions	7
2. Phase 2 — Effect of Internal Pressure	11
3. Phase 3 — Optimization of Energy Absorption.	13
IV. ANALYTICAL INVESTIGATION	16
A. Introduction	16
B. Analysis	17
C. Conclusion	29
REFERENCES	31
FIGURES	34 thru 77

LIST OF FIGURES

Figure		Page
1.	Impact Test Apparatus for Impacting Unpressurized Shells . . .	34
2.	40 ft. Precision Impact Test Apparatus	35
3.	Apparatus for Impacting Pressurized Shells	36
4.	Test Set-Up for Impacting Cylindrical Shells with Initial Internal Pressure	37
5.	Internal Pressurization Scheme	38
6.	Apparatus for Impacting Shell Models into Non-Rigid Media . . .	39
7.	Test Set-Up for Hydrodynamic Impact	40
8.	Resultant Axial Strain in the Buckling Part	41
9.	Initial Strain Pulse After Impact ($V_0 = 46$ ft/sec)	42
10.	Initial Strain Pulse After Impact ($V_0 = 11.5$ ft/sec)	43
11.	Initial Strain Pulse After Impact ($V_0 = 25$ ft/sec)	44
12.	Strain Pulse After Impact ($V_0 = 11.5$ ft/sec)	45
13.	Axial Strain vs. Time ($V_0 = 11.5$ ft/sec)	46
14.	Buckling Process of a Cylindrical Shell Due to Axial Impact at 23 ft/sec (301 Stainless Steel, 5.700" Dia., 22.8" Lgth., .019 Thk.)	47
15.	Experimental Set-Up for Unpressurized Conical Shells	48
16.	Conical Shell Before and After Impact ($V_0 = 36$ ft/sec)	49
17.	Cylindrical Shells Before and After Hydrodynamic Impact	50
18.	Impact Penetration of a Cylindrical Shell Model into Water	51
19.	Axial Strain vs. Time at Two Circumferential Positions 120° Apart and 2 in. Behind Impacted End. Pressurized Cylindrical Shell ($V_0 = 11.5$ ft/sec, $p_0 = 8.5$ psig, $\bar{p} = .165$, $h = .008$ " , Aluminum)	52
20.	Axial Strain at 2 in. Behind Impact End vs. Time ($V_0 = 11.5$ ft/sec, $p_0 = 8.5$ psig, $\bar{p} = .165$, $h = .008$ " , Aluminum) Internally Pressurized Cylindrical Shell	53
21.	Axial Strain vs. Time for an Internally Pressurized Cylindrical Shell ($V_0 = 23$ ft/sec, $p_0 = 8.5$ psig, $\bar{p} = .165$, $h = .008$ in. Aluminum)	54
22.	Axial Strain at 2 in. Behind Impact End vs. Time ($V_0 = 11.5$ ft/sec, $p_0 = 17.0$ psig, $\bar{p} = .330$, $h = .008$ " , Aluminum) Internally Pressurized Cylindrical Shell	55
23.	Axial Strain vs. Time for an Internally Pressurized Cylindrical Shell ($V_0 = 23$ ft/sec, $p_0 = 17$ psig, $\bar{p} = .330$, $h = .008$ in. Aluminum)	56
24.	Axial Strain at 2 in. Behind Impact End vs. Time ($V_0 = 23$ ft/sec, $p_0 = 17$ psig, $\bar{p} = .330$, $h = .008$ " , Aluminum) Internally Pressurized Cylindrical Shell	57

LIST OF FIGURES (cont)

Figure		Page
25.	Cylindrical Shells After Impact ($V_0 = 23$ ft/sec, $p_0 = 17$ psig (Left) $p_0 = 8.5$ psig (Right), $h = .008$ " , Aluminum	58
26.	Partially Expanded Cylindrical Shell Showing Collapse Pattern	59
27.	Weight Ratio vs. Impact Velocity - Collapsible Shell (Vertical Cylinder) - Air Pressurized	60
28.	Weight Ratio vs. Impact Velocity - Collapsible Shell (Vertical Cylinder) - Helium Pressurized	61
29.	Deceleration of Collapsible Shell (Vertical Cylinder) with Constant Internal Pressure	62
30.	Arrays of Cylindrical Shells	63
31.	Collapsed Arrays of Cylindrical Shells.	64
32.	Shell Coordinates	65
33.	Shell Element Notations.	65
34.	Axial Stress vs. Time ($V_0 = 11.5$ ft/sec, $h = .004$ in., Aluminum)	66
35.	Lateral Deflection of Shell Wall vs. Time ($V_0 = 11.5$ ft/sec., $h = .004$ in. Aluminum)	67
36.	Axial Stress vs. Time ($V_0 = 23$ ft/sec, $h = .004$ in., Aluminum)	68
37.	Lateral Deflection of Shell Wall vs. Time ($V_0 = 23$ ft/sec. $h = .004$ in. Aluminum)	69
38.	Axial Stress vs. Time ($V_0 = 46$ ft/sec., $h = .004$ in., Aluminum)	70
39.	Lateral Deflection of the Shell Wall vs. Time ($V_0 = 46$ ft/sec, $h = .004$ in., Aluminum)	71
40.	Axial Stress vs. Time ($V_0 = 11.5$ ft/sec, $h = .008$ in., Aluminum)	72
41.	Lateral Deflection of the Shell Wall vs. Time ($V_0 = 11.5$ ft/sec, $h = .008$ in., Aluminum)	73
42.	Axial Stress vs. Time ($V_0 = 23$ ft/sec, $h = .008$ in., Aluminum)	74
43.	Lateral Deflection of the Shell Wall vs. Time ($V_0 = 23$ ft/sec, $h = .008$ in. Aluminum)	75
44.	Axial Stress vs. Time ($V_0 = 46$ ft/sec, $h = .008$ in., Aluminum)	76
45.	Lateral Deflection of the Shell Wall vs. Time ($V_0 = 46$ ft/sec, $h = .008$ in., Aluminum)	77

LIST OF SYMBOLS

- A_1, \dots, A_{10} , parameters defined by equation (19)
 c , speed of elastic compression waves = $\sqrt{\frac{E}{\rho}}$
 D , shell diameter or flexural rigidity = $\frac{Eh^3}{12(1-\nu^2)}$
 E , Young's Modulus
 e , end shortening
 f_0 , initial deflection parameter
 f_1 , time dependent deflection parameter
 G , shear modulus
 g , gravitational acceleration
 h , wall thickness
 K , aspect ratio of buckle = $\frac{l_y}{l_x}$
 K_1, \dots, K_{10} , parameters defined by equation (18)
 l_x, l_y , half wave length of buckle in x and y directions
 l_{cr} , critical length
 L , length of shell
 m , number of half waves of buckling in the axial direction
 M , bending moment
 n , number of circumferential buckles (In the analysis,
 n is taken as the number of circumferential half waves)
 P , total axial load
 p , mean axial stress
 Q , transverse shear force
 q , intensity of internal pressure
 R , radius of shell
 R_1, \dots, R_6 , parameters defined by equation (25)
 S_1, \dots, S_7 , parameters defined by equation (26)
 t , time
 t_{cr} , time at which buckling initiates
 u, v, w , components of displacement of the middle surface in the x, y, z
directions respectively.
 V, V_0 , speed of impact or end shortening
 V_0, \dots, V_6 , parameters defined by equation (33)
 W_0, \dots, W_7 , parameters defined by equation (34)
 w_0 , initial imperfection function

LIST OF SYMBOLS (cont)

w_1 , total lateral deflection

$w = w_1 - w_0$, net lateral deflection

x, y, z , orthogonal coordinates of shell

$$\alpha = \frac{m\pi}{L}$$

$$\beta = \frac{n}{R}$$

γ , weight density of shell material

ϵ , strain or unit end shortening

ϕ , Airy stress function

ν , Poisson's ratio

ψ_0 , initial deflection parameter of shell

ψ_1 , time dependent deflection parameter of deformed shell

ρ , mass density of shell material

σ_x, σ_y , components of stress in x, y direction

τ_{xy} , shear stress

ζ , dimensionless lateral deflection = $\frac{f_1 + \psi_1}{h}$

$\epsilon_x, \epsilon_y, \epsilon_{xy}$ normal and shearing membrane strains

I. INTRODUCTION

The advent of missile and space vehicles has created problem areas which require understanding and knowledge of heretofore neglected phenomena. Formerly, the initiation of any one of a number of possible failure mechanisms terminated the usefulness of a structure, but now the failure process itself may be assigned a useful function.

The structural behavior during impact is of governing importance, for example, to the success of the mission if it concerns the survivable landing of payloads on terrestrial, lunar and other planetary surfaces. An attractive system for accomplishing this utilizes a long cylindrical or conical shell mounted in front of the payload. As a result of fundamental investigations in dynamic buckling conducted at the Space Sciences Laboratory it is now known that, upon normal impact, a cylindrical shell will collapse in an orderly and progressive manner beginning at the impact end, with buckling remaining confined in the vicinity of the impacted end. During this process kinetic energy is absorbed from the payload and the deceleration pulses are maintainable within tolerable limits through-out the impact history. In this application not only must the time relationship between forces which produce structural failure and those which can damage the payload prior to their functioning be known, but also the amount of energy which can be absorbed and dissipated during structural collapse.

These studies were undertaken to extend previous investigations which were conducted at the Space Sciences Laboratory, General Electric Company, dealing with the behavior of shells subject to impact loading. One of the results of these previous investigations was a theory (Ref. 1) on the physical mechanism of buckling of a cylindrical shell subject to an axial impact. According to this theory, buckling of a cylindrical shell will be initiated on the first passage of the axial compression stress wave from the impacted end when the velocity is sufficiently high. In this event the peak value of the sustained stress is given by the relation,

$$\sigma_{cr} = \frac{V_0}{c} E \quad (1)$$

provided that σ is within the proportional limit of the shell material. If V_0 is not sufficiently high, then buckling will be initiated when the initial stress has been increased by reflections from the ends. Whether or not this can happen depends on the momentum of the impacting mass.

For buckling which occurs on the first passage of the stress wave, the time at which buckling initiates is, according to the theory, given by

$$t_{cr} = \frac{l_{cr}}{c} \quad (2)$$

The critical length, l_{cr} , is the greatest distance from the impacted end reached by the front of the stress wave prior to buckling. Since the critical length, on physical grounds, varies inversely with the axial stress, the critical time t_{cr} varies inversely with the impact velocity.

Manuscript released by the author September 1962 for publication as an
ASD Technical Documentary Report.

The form of buckling anticipated by the theory can be either of the two familiar types: (1) the symmetrical or ring form, or (2) the asymmetrical or triangular form. It appears that the flexural rigidity of the shell wall and the end constraint are dominant factors in determining which of the two types of buckling will occur initially.

It is shown that buckling in the asymmetrical form (equation 2) is an attempt on the part of the shell to shorten axially with a minimum amount of negative extensional strain resultant. The relation governing axial shortening with purely inextensional deformation (true only for $h \approx 0$) is given exactly by

$$\xi = 1 - \sqrt{1 - K^2 \tan^2 \frac{\pi}{2n}} \quad (3)$$

This relation states that for a given value of unit axial shortening ξ , there exists an infinite number of combinations of aspect ratio K and circumferential wave number. Equation (3) is valid for $0 \leq \xi \leq 1$ which covers the entire range of possible unit end shortenings. Thus for $\xi = 1$, which corresponds to total shortening, the aspect ratio K is given by

$$K = \frac{1}{\tan \frac{\pi}{2n}} \quad (4)$$

Comparison of the deformational patterns obtained experimentally from thin shells with patterns constructed according to equation (4) shows good agreement (see Fig. 18, Ref. 1).

The investigations conducted during the present program were undertaken to explore the predicted magnitudes and trends given by the theory and to extend the work accomplished up to the time of its initiation. The program consisted of three phases:

Phase 1 – The Effect of Longitudinal End Conditions – Under this phase, cylindrical and conical shells were impacted with rigid and non-rigid media. An example of a non-rigid medium employed is water.

Phase 2 – The Effect of Internal Pressure – The purpose of this part was to determine the effect of internal pressure on the dynamic buckling behavior of cylindrical and conical shells (comparing with the impact buckling of unpressurized shells) and conversely the effect of impact loading on internally pressurized shells (comparing with static buckling of pressurized shells).

Phase 3 – Optimization of the Energy Absorption Capacity – This phase covered studies of methods of increasing the specific energy absorption and dissipation capacity available in collapsing long thin walled cylindrical and conical shells.

The program was performed in the Space Sciences Laboratory of the General Electric Company by the Space Structures Operation, Dr. F.W. Wendt, Manager. Mr. A.P. Coppa, principal investigator, formulated the program and conducted the experimental research. Professor W.A. Nash, University of Florida, consultant, developed the mathematical analysis.

II. SURVEY OF LITERATURE

Papers dealing with the dynamic buckling of shells have appeared only in the past several years. The most notable of these are due to Russian investigators.

Schmitt (Ref. 2) presents results of an experimental program in which thin aluminum shells were impacted at velocities up to about 500 in./sec. Some useful data regarding the energy absorption during buckling are given and indicate an efficiency ranging from 1030 to 3160 lb ft/lb.

Bolotin (Ref. 3) gives an analysis of the dynamic stability of cylindrical and spherical shells without explaining the mechanism of instability. The problems of a cylindrical shell subject to axial compression and radial pressure are presented, as well as that of a spherical shell subject to uniform radial pressure. These analyses were made on the basis of infinitesimal deflection theory.

Agamirov and Volmir (Ref. 4) extend the analysis of Ref. 3 to include finite deflection effects. In this investigation it is assumed that impact velocities are small compared to the sonic velocity in the shell material. The analysis is reported to agree closely with experimental results.

Volmir (Ref. 5) has also analyzed the dynamic stability of a shallow cylindrical panel subject to axial compression on the basis of finite deflection theory.

Coppa (Ref. 1) presents a theory for the mechanism of buckling of a cylindrical shell under longitudinal impact. One dimensional wave propagation is used as a model for explaining the initiation of buckling both for low and high velocities of impact. According to this mechanism, buckling occurs at the impacted end if the impact velocity is sufficiently high but can occur at either end for sufficiently low velocities. Buckling progresses in a step-by-step manner with the cylinder adjacent to the buckling portion remaining essentially stable. An inverse relationship between the buckle size and the impact velocity is argued. It is also shown that the ratio of the circumferential to the axial wave length of diamond-shaped buckle wave-forms depends on the number of circumferential waves and the unit axial shortening.

Kadashevich and Pertsev (Ref. 6) analyze the stability of a cylindrical shell subject to a uniformly distributed dynamic radial pressure using finite deflection theory. The inertia corresponding to the axisymmetric circumferential displacements in addition to the lateral inertia is retained in the analysis. Because of this, the authors claim, the theory is valid for higher rates of loading than is Ref. 4 which retain's only the lateral inertia term.

Yao (Ref. 7) presents an analysis of a long cylindrical shell subject to an impulsive radial pressure. In this paper only the fundamental buckling mode ($n = 2$) is considered. Subject to this limitation, it is shown that if the magnitude of the pressure is greater than the static buckling pressure, the lateral displacement will increase monotonically as loading duration becomes long. The cylinder can withstand an impulsive loading greater than the static buckling pressure if the loading duration is very short compared with the free vibration period of the cylinder in the first mode.

III. EXPERIMENTAL INVESTIGATION

A. Apparatus

(1) Rigid Impact-Unpressurized

The experimental apparatus used on this phase was the Precision Drop Tester, located at the General Electric Company Space Sciences Laboratory (See Figures 1 and 2). This device consists of a hardened steel shaft 40 feet in length which is attached under tension between two vertically aligned points. A carriage situated concentrically with the shaft by means of two ball bushings rides along the shaft. The impact head, a hardened and ground steel disc, 10 inches in diameter is mounted to the carriage. The carriage assembly (drop head) is hoisted to the drop height by means of an electric winch which is attached to the carriage by an electro-magnet. The drop head is released merely by opening the circuit of the electro-magnet. A hardened and ground steel base, 8 inches thick and 20 inches in diameter is mounted at the bottom end of the shaft and situated concentrically with it. The base is mounted on three adjustable screws for the accurate positioning of the base in the horizontal plane. The carriage can also be adjusted with respect to the shaft so that the final alignment of the head with the impact end of the shell specimen can be accurately accomplished.

The drop head assembly contains ports for venting the air rapidly from the cylinder as it is collapsing. By means of this venting system, the buildup of internal pressure is prevented. The vent area can be decreased or completely closed according to specific requirements.

The specimen and its retainer are mounted on the base concentrically with the shaft. In order to do this the shaft must be raised clear of the base. This is accomplished by a manually operated winch.

(2) Rigid Impact-Pressurized

The apparatus on which experiments of pressurized shells under rigid impact are performed consists of a modification of the equipment described above (see Figures 3 and 4). A cross beam is mounted on the carriage in place of the vent chamber. The beam contains two mechanically actuated release mechanisms which are mounted on its extremities. The drop head is mounted to one of the mechanisms and a counterweight to the other. The shell specimen in its retainer can also be suspended from the beam for tests in which the specimen itself is dropped. In this apparatus, the base is moved so that it is centered vertically under the center of the drop head. The specimen in its retainer is secured to the base via the central hole of the base.

The cross beam assembly containing the drop head and counter weight is hoisted to the drop height and released. If so desired, the drop head can be released solely. When the cross beam assembly is dropped, it is decelerated by a shock absorber which is located at the lower end of the shaft. The initial deceleration force on the beam assembly is imposed via a foam pad so as to reduce the shock associated with the release of the drop head.

In order to preserve the unsupported edge condition of the impact end of the shell as used in the unpressurized tests, a special pressurization technique was devised for the experiments with pressurized cylinders. This was done to eliminate the different type of constraint which an end closure would impose on the edge of the shell. The pressurization rig, shown in Figure 5, utilizes a thin membrane of .0008 in. thick Mylar to form a pressure tight bag. The membrane is made by wrapping the Mylar film about a cylinder whose diameter equals that of the cylinder to be pressurized. The longitudinal joint is made simply by one strip of half inch width scotch tape. The ends are carefully folded so as to form under pressure a semi-toroidal configuration at both ends. At the impact end the membrane is supported by a plate which is attached to the cylinder mount via a transmission chain. This arrangement relieves the membrane from a large portion of the axial pressure loading and thereby greatly reduces the deflection of the membrane. Upon collapse of the cylinder the chain readily folds into the mount cavity shown at the bottom of the figure and thereby does not interfere with the axial shortening of the cylinder.

In Figure 5 the membrane is shown in its expanded position within a transparent plastic shell, this to check that the membrane is expanded against the entire surface of the shell.

The pressurization method produces an essentially radial pressure on the shell since the axial force is taken out by the tension in the chain and in the membrane. The only axial force which can be introduced into the metal shell is due to friction between the shell and the membrane.

(3) Non-Rigid Impact

The apparatus for conducting non-rigid impact experiments is essentially the same as that described above except that the cylindrical tank is put in place of the steel base (See Figures 6 and 7). The tank is 4 feet in diameter and 50 inches in depth and is equipped with a window for viewing purposes. The window is longer than the tank depth by an amount somewhat greater than the length of the specimen and hence provides an unobstructed view of the specimen before it strikes the surface of the impact medium and subsequently throughout the impact.

The apparatus allows the free dropping of the specimens into fluids and other deformable or penetrable media with a maximum amount of guidance prior to the impact.

B. Specimens

The specimens used in the experiments were cylindrical shells having the following dimensions: 5.70 in. inner diameter, 22.8 in. length and wall thicknesses of .004, .008, .016 and .019 inches. These correspond to a length to diameter ratio (L/D) of 4 and diameter to thickness ratios of 1425, 712, 356 and 300. The materials used were the aluminum alloys 2024 F, 2024 T3, and 5052 H-38 and 301 F.H. stainless steel.

In procuring specimens, efforts were made to obtain cylindrical shells having a deviation from a perfect cylindrical surface not exceeding one wall thickness. This limit was considered the maximum that could be allowed in order to limit sufficiently the scatter in the behavior of the shells near the critical point.

The specimens were fabricated from flat sheet by simply rolling the sheet into a cylinder and making a longitudinal joint. Both rubber base and epoxy adhesives were used as bonding agents for the joints and both lap and double butt strap configurations were employed.

The specimens were simply cylindrical, containing no stiffeners. In most cases, the shells were mounted on a rigid circular base. The impacted end was initially free of support and was unconstrained from radial displacement during the impact except by friction forces at the impact interface.

C. Instrumentation

(1) Strain Measurement

For the measurement of dynamic strains in the shell wall, metal foil strain gages (Tatnall Metalfilm, type C12-1X1-32A) were employed. For recording the strains, oscilloscopes (Tektronix Models 531 and 535) equipped with single sweeps were used together with Polaroid cameras.

(2) Acceleration Measurement

Cornell Models 200 and 504 high frequency accelerometers were employed to measure and oscilloscopes and cameras as described above to record the accelerations imparted to the drop head.

(3) Transient Pressure

Internal pressures during collapse of the shells were measured by means of a Kistler gage, model PZ 14 with a piezo calibrator, model 651-B. Recording was also accomplished by oscilloscopes and cameras.

(4) Photography

High speed photographs of the shell deformations following impact were made by a Fastax camera having a maximum filming rate of 16,000 frames per second. Various finishes were tried to improve the photographic clarity of the buckling patterns, and it was found that a photographic dulling spray is advantageous.

(5) Triggering

All recording components were initiated by a common trigger which consisted of a wire situated near the impact end of the shell. Later a system consisting of three pivoting rods was used. The trigger circuit was closed by

the contact of the drop head with the trigger. The position of the trigger end was such that the oscilloscopes were activated prior to the impact on the shell. A zero base line was thereby established on the record.

D. Results

(1) Phase 1 — Effect of Longitudinal End Conditions

a. Rigid Impact

As anticipated by the theory (Ref. 1), buckling should be initiated on the first passage of the stress wave if the velocity of impact is sufficiently high. Experiments were designed to test for this. Strain gages were mounted axially in back-to-back pairs on the cylinder wall near the impacted end. Other pairs of gages were mounted near the opposite end along the same generators as the forward gages. Oscilloscopes equipped with single sweep circuits and Polaroid cameras were used to record the strain-time variation. Using the value for the circumferential wave number, n , as determined from tests of similar specimens, the appropriate time scales for the oscilloscopes were chosen. Two times were determined for each measurement point, one short and the other long. The short time trace was based on the time required by the elastic strain wave to travel a length equal to one half the axial wave length of an inextensional buckle pattern having n circumferential buckles. This reference time, t_{cr} is given by the relation:

$$t_{cr} = \frac{1}{c} D \frac{\pi}{2n} \tan \frac{\pi}{2n} \frac{1}{\sqrt{2\left(\frac{V_0}{c}\right) - \left(\frac{V_0}{c}\right)^2}} \quad (5)$$

where D = diameter of the cylinder

n = number of circumferential waves

V_0 = impact velocity

c = speed of elastic waves in rods = $\sqrt{\frac{E}{\rho}}$

The long time trace was determined according to the time required to produce total collapse of the first row of inextensional axial half waves. This time is given by the relation:

$$t_f = \frac{1}{V_0} D \frac{\pi}{2n} \tan \frac{\pi}{2n} \quad (6)$$

As an example, if $V_0 = 23$ ft/sec, $c = 16,800$ ft/sec, $n = 6$, and $D = 5.70$ in.

$$t_{cr} = 38 \times 10^{-6} \text{ sec}$$

$$t_f = 1450 \times 10^{-6} \text{ sec}$$

The purpose of these experiments was to measure the time after impact at which instability initiates. According to the theory, the impact produces a compression stress wave whose magnitude is given to a first approximation by:

$$\sigma = \frac{V_0 E}{c} \quad (7)$$

Where E is the modulus of elasticity, provided that the impact strain, V_0/c is within the proportional limit of the material: Equation (7) is for the axial stress produced in an elastic rod when it is impacted by a perfectly rigid mass and therefore is an upper limit of the initial impact stress.

If σ is sufficiently high, buckling will initiate on the first passage of the stress wave through the cylinder. When this occurs, the axial compression stress decreases rapidly (Fig. 8) due to the lower axial rigidity of the buckling surface. The stress remains at a low level compared with the initial value until the surface that is buckling has been fully collapsed. When this has happened, an increase of axial stress is expected due to the increased axial rigidity of the region of the shell beyond the buckled part.

The experimental results were in general agreement with the anticipated behavior. The oscilloscope record shows a rapid rise in strain following impact to a value which is then sustained for a short interval of time. It then rapidly decreases to a low level and remains so for a relatively long time.

Typical strain records are reproduced in Figures 9, 10 and 11. These show the resultant compression strain near (one inch behind) the impacted end. The specimens were in each case 2024 H-19 aluminum cylinders of 5.700 in. dia., .008 in. wall thickness, and 22.8 in. length. The impact velocities are 46, 11.5, and 25 ft/sec. for Figures 9, 10, and 11 respectively. Figure 9, the short time record, has time and compression strain along the horizontal and positive vertical axes respectively. The time scale is 10 microseconds per unit grid spacing and the strain scale is .00196 in/in per unit spacing. A zero strain base is established (at the extreme left) by triggering the trace immediately prior to impact. It is seen that the strain rises within 10 microseconds to a peak strain of .00214 in/in and is sustained thereafter at an average level of .00194 in/in for 40 microseconds at which time it decreases substantially. At 80 microseconds after initiation of the pulse (+85 μ sec. after impact) the strain has decreased to zero. The time required for the initial elastic stress wave to return to the forward gage position is 216 μ sec. It is apparent from this that buckling has been initiated during the first passage of the stress wave.

Based on the theory, the axial compression strain pulse by an impact at a lower velocity was expected to have a lower strain sustained for a longer time than the higher velocity case. This is indeed evident in Figure 10 (also a short time trace) which corresponds to an impact velocity of 11.5 ft/sec. or one-fourth the velocity of the previously discussed test. The pertinent scales are 50 μ sec. per grid spacing (horizontal axis) and .000783 in/in strain per unit spacing (vertical axis). As before, the trace begins at the extreme left. The strain rises within 20 μ seconds to a value of .000802 in/in and after remaining at an average level of about .000622 in/in rises to a peak strain of approximately twice the initial peak. Thereafter, it decreases steadily and becomes equal to zero at 345 μ sec. after impact. It is interesting to note that the time at which the strain begins to rise to attain twice the initial value is slightly greater than 200 μ sec. after initiation of the signal. According to the

loading mechanism in the theory (Ref. 1) a rapid rise in strain to twice the initial value is expected at $216 \mu\text{sec.}$ when the compression wave reflected forward from the rear end arrives at the forward gage position. Another point of interest is that the time interval from the instant of impact to the occurrence of zero strain on this experiment (11.5 ft/sec impact velocity) is almost exactly four times as long as the previous experiment in which the impact velocity was four times as large (46 ft/sec.). These characteristics are being examined at the present time to determine their significance.

Results from an experiment conducted at an intermediate velocity of 25 ft/sec similarly appear to be in agreement with the theory. At this velocity, the theory predicts a critical strain of $\frac{25}{16800} = .00149$ in/in. The measured strain as shown in Figure 11 is initially .00146 in/in. or within 2% of the predicted value. Thereafter the strain fluctuates at a mean value similar to the above and drops off rapidly. Only the initial portion of the trace, however, is given as evidence since the measurement is due to a single axial gage. Bending strain components, therefore, are present in a substantial part of the later portion of the trace. Experience shows that the initial portion of the strain recorded from a single gage is valid as a measure of the axial strain.

The magnitudes of the initial strains corresponding to the three velocities under consideration agree reasonably closely with the values predicted from the theory. The experimental values are compared with the predicted values in Table 1.

Table 1

Impact Velocity ft/sec.	Measured Strain in/in	Predicted Strain in/in	Error %
46	.00214	.00274	-22%
25	.00146	.00149	-2%
11.5	.000802 .000622*	.000684	+17% -9%

*Average Strain during first passage of compression wave.

After buckling has been initiated, as indicated by the first reduction of axial strain, relatively small strains were measured during the entire long time trace. This was expected as previously discussed. In addition to the low total compression strain during this interval the measurements showed a considerable amount of bending of the shell wall. This is shown in Figures 12a and 12b which pertain to the test conducted at 11.5 ft/sec. These traces are from a pair of axial strain gages mounted back-to-back and wired to read separately. The time scale (horizontal axis) is $500 \mu\text{sec.}$ per grid spacing and the strain scales (vertical) are .000785 in/in (Fig. 12a) and .000783 in/in (Fig. 12b). After impact begins (at the extreme left) both traces show the compression strain pulse which is associated with the initiation of buckling. At about $400 \mu\text{sec.}$ the traces run

opposite each other, one reading tension and the other compression, thereby demonstrating axial bending of the wall. The bending strains run off the scale but the magnitude appears to be about .002 in/in or 2.5 times the maximum compression strain in the initial pulse. A composite plot of Figures 12a and 12b is shown in Figure 13, which reveals that the total compression strain present simultaneously with the bending strains is relatively low during the entire long time trace.

In conjunction with the measurement of strains in the shell during the impact, high speed photography was employed to record the deformational process during buckling. Using a Fastax camera, pictures were taken at a rate of 16,000 frames per second. Examples of these photographs are shown in Figure 14. The photographs show the behavior of a stainless steel cylinder (5.70 in. diameter, 22.8 in. length, and .019 in. thickness) impacted at 23 ft/sec. The pictures begin at impact and show buckling initiating in the form of an extensional type buckle (Fig. 14, plate 1). This buckle progresses through full collapse in one wave length. As full collapse of this buckle is almost complete, the circular cross section at the rear end of the buckle changes into the polygonal form (plate 2). In this region the diameter of the shell is less than the initial (unloaded) diameter and hence a state of compression stress exists. This stress apparently is the immediate cause of the inextensional type buckling. As the motion of the impact head proceeds, deformations of the inextensional type grow in a continuous fashion. The axial length of the buckles (plates 3-6) does not shorten as rapidly as has been observed for very thin shells ($D/h = 700-1400$), the shortening in the present case being due primarily to the motion of the impact head. This shows the presence of a relatively larger degree of extensional strain in the buckling surface since shortening due to the backward motion of the apex of the triangles is small, if any.

It is interesting to note how naturally and continuously the cylindrical surface changes from circular to polygonal cross-sections. It appears, from Figure 14, that the symmetrical buckle form serves as a transition from the circularly constrained form of the impacted end to a configuration which is rather independent of the edge constraint.

This transition is indicated even in very thin shells but in such cases, the symmetrical form of buckling only begins to develop and quickly degenerates into an inextensional type pattern which then serves as a transition to the buckling configuration more natural to the shell.

The experimentation on conical shells was chiefly exploratory in nature. A number of shells were subjected to impacts at velocities varying from 16 to 36 ft/sec. Several semi-vertex angles were tested ranging from 5° to 16° . The conical frusta buckled and collapsed in the orderly step-by-step fashion so typical of cylindrical shells in which some internal pressurization is present. The pressurization involved in these tests was that which occurred as a result of the reduction of the internal volume as collapse progressed. The experimental set-up for testing the conical shells is shown in Figure 15, which is essentially the same as used for the unpressurized, cylindrical shells. Shown in Figure 15 is the lighting array which was employed in the high speed photography of the buckling process.

The conical shell, before and after impact, is shown in Figure 16. The shell as fabricated has diameters of 6 and 3 in., length of 22.8 in., thickness of .008 in., and is of 5052 H-38 material. The shell is shown to have reduced to 42% of its initial length. The shell absorbed 740 lb. ft. through a distance of 1.1 ft.

A series of five conical shells as described above were instrumented for measurement of the initiation of buckling. The results of these tests are not available at this time.

(b) Non-Rigid Impact

Experiments were conducted in which thin aluminum shells were subjected to impacts with an undisturbed water surface. The experiments were conducted with the apparatus shown on Figures 6 and 7. The models used in these tests consisted of aluminum shells mounted in circular plates at both ends. The shells had the following dimensions: diameter = 5.700 in., length 12 and 22.8 in., thicknesses = .004 and .008 in. One of the models in its initial form is shown in Figure 17 at the left. The upper plate supported the model during the fall and served to impose inertia loading on the shell during impact. The lower plate was a circular plate of micarta plastic. This was designed to have a small inertia during water impact and a high penetration resistance.

The experiments consisted of the following: .004 thickness, 12 in. length shells impacted at initial velocities of 11.5 and 23 ft/sec. and a .008 thick, 22.8 in. length shell impacted at 32 ft/sec. In all cases Fastax motion pictures were taken and buckling was seen to initiate immediately after impact with the water surface. A photograph of one of the 12 in. length shell models is shown in Figure 18. The model is seen to have penetrated 60% of its length. A well defined cavitation envelope is seen extending from the flat disk to the water surface which except for the axially symmetrical splash is undisturbed. Some buckling deformation of the quasi-inextensional form is evident immediately behind the frontal plate. The high speed motion pictures show that the cavity is maintained until the velocity of the model is quite low, its shape, of course, varying from that of a slightly bulged conical frustum to a negatively bulged frustum. Finally the cavity collapses on the shell and causes buckling common to externally pressurized shells. This is evident in the shells shown in Figure 17. The buckling at the lower ends of the shells is due to the axial impact while the overall buckling is due to the subsequent collapse of the water cavity. It is clear that the deformation due to both causes is greater in the shell (extreme right of Fig. 17) which was subjected to the higher velocity impact (23 ft/sec compared with 11.5 ft/sec for the middle one).

(2) Phase 2 — The Effect of Internal Pressure

A series of experiments was conducted on cylindrical shells with initial internal pressure and subjected to axial impact. The impact velocities used were 11.5 and 23 ft/sec., a set of velocities common to the other portions of this program. The pressures used were 8.5 and 17 psig which were selected to correspond with those used by Thielemann (Ref. 8) in studies of internally pressurized shells under static axial compression.

Results of strain measurements are shown in Figures 19 to 24 inclusive. Strains were measured at three circumferential positions equally spaced at a station two inches beyond the impacted end. At each position, the gages were mounted directly opposite each other on the shell wall. Most gages were wired in series to cancel out the bending strain components. In some instances, however, they were wired separately in order to observe the bending strains.

Figure 19 shows the axial strains measured at two circumferential locations on a cylinder impacted at a velocity of 11.5 ft/sec. The initial internal pressure was 8.5 psig. At impact the strain proceeds into tension to a significant degree and after 120 to 200 μ seconds it rapidly goes into compression. The strains shown in Figures 19a and 19b peak at magnitudes of .000826 and .000750 in/in. By comparison the one dimensional elastic impact strain is .000685 in/in.

A composite of Figures 19a and 19b is shown in Figure 20. The strain rises to a peak of .000572 in/in at 410 μ seconds after impact and decreases to zero at 590 μ seconds. Thereafter several peaks of about .00040 in/in strain occur.

A trace of the strain measured in an experiment conducted at the same value of internal pressure but at twice the velocity as the previous test is shown in Figure 21a. The strain rises rapidly to a peak value of .00117 in/in and decreases to zero at 150 μ seconds, thereafter remaining at relatively low levels. The one dimensional elastic impact strain is by comparison .00149 in/in. The measured initial strain is, therefore within 21% of the predicted value.

The longer time trace of the above measurement is much more interesting and is shown in Fig. 21b. After the initial peak (which in this figure runs off the scale) occurs, other peaks are present having lower magnitudes than the initial peak. Considering these secondary peaks grossly, the first, which consists of many short duration pulses, has a strain level of .000545 in/in. and the next three have almost identical levels of .000828 in/in. These strain variations have durations of roughly one millisecond each, and probably correspond to the formation and collapse of buckles of the quasi-inextensional form. From motion pictures of the buckling of the cylinder with 8.5 psig pressure and a velocity of 11.5 ft/sec, it was observed that triangular buckles required times on the order of one millisecond to collapse fully.

Axial strain traces from three equally spaced circumferential positions were obtained from a test conducted at a velocity of 11.5 ft/sec and an internal pressure of 17 psig, twice that used in the previously described experiments. The initial strain peaks were as follows: .000827, .000666, and .00150 in/in. This latter value is greatly in excess of the value predicted by the one dimensional elastic impact theory of .000684 in/in. and its significance is being investigated. The three traces extended from the initiation of impact to 10 milliseconds thereafter. A composite of the three is shown in Figure 22. The strain rises to a peak value of .000580 in/in. at 300 μ second after impact and decreases to zero at 450 μ seconds. Thereafter many fluctuations occur whose mean magnitude rises to .0003 in/in compression and falls to about .00015 in/in. tension.

From this point the strain rises rapidly to a maximum compression strain of about .0011 in/in. at 9 milliseconds after impact. The strains on the individual traces at this time show .000790, .001090, and .001366 in/in.

The high speed motion pictures obtained from this test were studied to determine the reason for this unexpected behavior, especially the interval between 2.5 and 5.5 milliseconds in which the strain varied about zero and went into tension. Also the pictures were studied in order to understand the rapid rise at 6 milliseconds and the sustained high level of compression. No visual phenomena were observed in the brief study made up to this time, but a more extensive examination will be made.

In Figure 23 the initial strain from two locations are shown for an experiment run at a velocity of 23 ft/sec and a pressure of 17 psig. The initial strains were .00104 and .00158 in/in. compared with an expected value of .00149 in/in. A composite plot of three individual long strain traces, two of which include the short time traces of Figure 23, is shown in Figure 24. This shows what seems to be a more reasonable strain history than Figure 22. After the initial peak, the strain exhibits a number of peaks ranging in magnitude from .00064 to .00085 in/in. This behavior continues to 4 milliseconds after impact at which time the strain rises to a value of .0012 in/in at the end of the available trace.

Further experiments with initially pressurized shells subject to axial impact are being planned. Instrumentation will be designed to obtain an integrated average of the axial resistance of the shell during impact rather than a detailed measure of the strains at selected points. Definite and final conclusions regarding the behavior of shells under the loading conditions studied must await the completion of these further experiments. According to the pressurized experiments completed thus far, it can be stated that the initial peak value of the measured strain does in general agree well with the one dimensional elastic theory. The effect of the pressure on the overall deformations of the shell are decided, a higher energy mode corresponding to higher pressure.

The specimens tested at a velocity of 23 ft/sec are shown in Figure 25, the left and right cylinders corresponding to internal pressures of 17 and 8.5 psig respectively. The shells buckled in a very orderly manner but were damaged when the impact head struck them subsequent to rebound. The larger amount of axial shortening in the lower pressurized shell (right hand specimen) is evident.

(3) Phase 3 — Optimization of the Energy Absorption

a. Optimization by Internal Pressure

Experiments on cylindrical shells conducted during this program have shown that the presence of an internal radial pressure strongly influences the buckling behavior under impact loading. The effect of pressurization diminishes with decreasing diameter to thickness ratios. Tests on aluminum shells of D/h ratio ranging from 1425 to 712 showed orderly collapse in the asymmetric mode when internal pressure

was present. Figure 26 shows the collapse deformations in an aluminum shell of $D/h = 1425$.

In the absence of internal pressure the collapse was quite disorderly as should be expected for very thin shells. A full hard 301 stainless steel shell having a $D/h = 356$, which buckled in a disorderly manner without internal pressure was stabilized into collapsing in an orderly manner by a polystyrene core having a density of only 1.1 lb. per cu. ft. Hence, it is apparent that the proper stabilization of thin shells strongly increases the amount of energy that can be absorbed per unit combined weight of shell and pressurized agent.

Calculations were made of the energy absorption performance of cylindrical shells pressurized by air and helium. These are presented in Figures 27-29. Figures 27 and 28 show the ratio of the weight of the shell plus pressurizing agent to the weight of the payload whose velocity V_0 at impact is to be reduced to zero. Figure 29 compares the performance (including the deceleration imparted to the payload) of air and helium pressurized systems.

A constant internal pressure is assumed throughout the deceleration stroke. This implies the discharge of internal gas during the collapse of the volume.

b. Optimization by Constraint

Another approach taken toward increasing the energy absorption of collapsing shells was stiffening the shells by the mutual constraints imposed by attaching them together. The motivation for this approach was the reportedly large amounts of energy that can be absorbed by honeycomb structure without the effect of internal pressurization. This effect and its relationship with the collapse of thin cylindrical shells was discussed in Reference 9.

Arrays of cylindrical shells were designed to test for the effect of mutual constraints. The arrays consisted of aluminum sheet metal tubes having the following dimensions, diameter of 1 in. length of 8 in. Two wall thicknesses were employed, .002 and .004 inches. The arrays, shown in Figure 30, were made by joining the tubes tangent to each other, this resulting in a hexagonal periphery. The number of tubes per array increases in the following order: 7, 19, 37 and the hexagonal configurations corresponding to these have sides composed of two, three, and four tubes per side. The number of mutual constraints increases in the following sequence: 12, 42, and 89 for the three sizes and the numbers of constraints per tube are: 1.72, 2.21, and 2.40 for the three sizes in increasing order.

Since the number of constraints per tube increased with increasing size of the array it was expected that the energy absorbed per unit weight of material would increase. This however was not apparent from the experimental results. The specific energy turned out to vary between 4000 and 5000 lb. ft. per lb. with no apparent relationship between it and the size of the array.

The reason for this may have been the fact that the bond which joined the tubes together failed in a number of cases, thereby reducing the effect which was under study. Further work will be done in which adequately strong intertube bonds will be used.

The mutual constraints on the other hand did produce extremely well formed collapse patterns and in addition a moderately high value of specific energy. Pressure stabilization was present only in the tubes located on the periphery of the array whereas in all other tubes the pressure differential across the wall was negligible due to the pressure balance in adjacent tubes. Therefore the stabilization of the collapse of cylindrical shells by mutual constraints is evident.

Both for single tubes and the arrays, collapse would be readily accomplished over a very large percentage of the initial length. Single tubes having a length/diameter ratio of 8 were repeatedly crushed through 90% of their initial length, and arrays exhibited this behavior as well. Several arrays are shown after impact in Figure 31. The tubes in these arrays are of .002 in wall thickness. Failure of some of the intertubular bonds, apparent in the figure, is responsible for the imperfections in the collapse patterns. When the intertubular bonds are maintained, deformations are confined to the impacted end with essentially no deformation elsewhere.

IV. ANALYTICAL INVESTIGATION

A. Introduction

For the past several decades it has been well recognized that the problem of buckling of thin elastic shells must be attacked by nonlinear finite-deflection theory. This type of analysis thus stands in contrast to the problem of elastic buckling of bars, rings, and plates that may be successfully analyzed by classical infinitesimal deflection theory. For the case of these latter structures, the results of infinitesimal deflection theory are in satisfactory agreement with experimental evidence. For the case of buckling of a shell, however, this agreement no longer exists. For example, for the case of static axial compression of a circular cylindrical shell, experimental results range from twenty percent to sixty percent of the values predicted by linear small deflection theory.

In an effort to present a theory whose predictions are in more satisfactory agreement with experimental evidence, Donnell, in 1934, (Ref. 10) presented a theory based upon finite deformations together with a consideration of the initial imperfections present in the specimen. That theory was for statically applied axial compression of a circular cylindrical shell. Because of lack of suitable computers, certain drastic mathematical assumptions were introduced that rendered the final results somewhat less than satisfactory, but nevertheless, the beginnings had been made on a new type of analysis that showed promise of being in better agreement with experimental data. This work was continued by von Karman and Tsien (Ref. 11) in 1941 for the same case of axial compression of a cylindrical shell. These same authors in 1939 (Ref. 12) had studied the case of static buckling of a spherical shell by uniform external pressure. Perhaps the most satisfactory explanation of the static buckling of the axially compressed cylindrical shell has been offered by Kempner (Ref. 13). His analysis was on a sounder basis than any of its predecessors and presented an entirely realistic picture of the load-deflection characteristics of the shell. The analysis was based upon the principle of minimum potential energy of the system. More complete resumés of the finite-deflection buckling analyses of elastic shells are to be found in the survey papers by Fung and Sechler (Ref. 14) and the present author (Ref. 15). Another summary and critique, as well as an investigation of the effects of internal pressurization on buckling of an axially compressed cylinder, has been offered by Thielemann (Ref. 8).

The problem of dynamic buckling of thin elastic shells has only come into prominence in the past few years. One of the first treatments is due to Volmir (Ref. 5) who investigated the buckling of a shallow circular cylindrical panel subject to rapidly applied axial compression along its generators. The panel edges were taken to be simply supported. Finite deflection equations, incorporating a consideration of initial imperfections present in the specimen, were formulated and an approximate solution to these nonlinear equations was obtained by the Galerkin procedure. The final results were presented in the form of dimensionless axial load vs. time. It is interesting to observe that Volmir's solution indicates that the dynamically applied load increases to a value sixty-five percent greater than the upper critical load found from linear

theory for the case of static compression of such a panel. After this peak load is reached, there occurs an abrupt drop in axial load, and for a very short interval of time the load actually becomes negative, corresponding to an extension of the panel. As time increases still further the load fluctuates, indicating nonlinear oscillations of the panel.

Another study closely related to Reference 5 has been presented by Agamirov and Volmir (Ref. 4). Here, the authors apply finite deflection analysis, together with a consideration of initial imperfections, to the problem of dynamic buckling of a cylindrical shell subject to either hydrostatic pressure or axial compression. The analytic approach is identical to that employed by Volmir in Reference 5. However, the authors greatly simplified the mathematics by taking the values of certain parameters to be the same as formed for static analysis. This, of course, introduces an error of unknown magnitude. No numerical results were presented for the axial compression case. For the case of hydrostatic loading the authors found a critical pressure approximately twice the upper critical load formed from linear theory for the case of static compression.

An experimental investigation of buckling of cylindrical shells by dynamically applied hydrostatic pressure has been reported by Volmir and Mineev (Ref. 16). The shells were duraluminum, having a radius-thickness ratio of 112, and buckling loads up to four times the upper critical load formed from linear theory for static compression were measured. Further, it was found that with an increase in loading rate the number of waves around the circumference also increased.

B. Analysis

Let us consider the axially compressed cylindrical shell shown in Figure 32. The coordinate system consists of a coordinate x along a generator, y in the circumferential direction, and z in the inward radial direction. The components of displacement of a point in the middle surface of the shell in these directions are designated by u , v , and w respectively. Further, L denotes the length of the shell, R the radius to the middle surface, h the wall thickness, P the total axial compressive force, p the mean axial stress, and q the intensity of internal pressure.

We shall employ the following approximate nonlinear strain-displacement relations to describe the membrane strains:

$$\begin{aligned}\epsilon_x &= \frac{\partial u}{\partial x} + \frac{1}{2} \left(\frac{\partial w_1}{\partial x} \right)^2 - \frac{1}{2} \left(\frac{\partial w_0}{\partial x} \right)^2 \\ \epsilon_y &= \frac{\partial v}{\partial y} + \frac{1}{2} \left(\frac{\partial w_1}{\partial y} \right)^2 - \frac{1}{2} \left(\frac{\partial w_0}{\partial y} \right)^2 + \frac{w_1}{R} - \frac{w_0}{R} \\ \epsilon_{xy} &= \frac{\partial u}{\partial y} + \frac{\partial v}{\partial x} + \frac{\partial w_1}{\partial x} \cdot \frac{\partial w_1}{\partial y} - \frac{\partial w_0}{\partial x} \cdot \frac{\partial w_0}{\partial y}\end{aligned}\tag{8}$$

In these equations, ϵ_x and ϵ_y denote normal strains of the middle surface and ϵ_{xy} the shearing strain of that surface. The initial imperfections of the shell are represented by w_0 , the total deflection by w_1 , and consequently the net deflection by $w = w_1 - w_0$. By appropriate differentiations and linear combinations of equations (8) we obtain

$$\frac{\partial^2 \epsilon_x}{\partial y^2} + \frac{\partial^2 \epsilon_y}{\partial x^2} - \frac{\partial^2 \epsilon_{xy}}{\partial x \partial y} = \left[\left(\frac{\partial^2 w_1}{\partial x \partial y} \right)^2 - \frac{\partial^2 w_1}{\partial x^2} \cdot \frac{\partial^2 w_1}{\partial y^2} \right] \quad (9)$$

$$- \left[\left(\frac{\partial^2 w_0}{\partial x \partial y} \right)^2 - \frac{\partial^2 w_0}{\partial x^2} \cdot \frac{\partial^2 w_0}{\partial y^2} \right] - \frac{1}{R} \left[\frac{\partial^2 w_1}{\partial x^2} - \frac{\partial^2 w_0}{\partial x^2} \right]$$

Let us now introduce the Airy function $\phi(x, y)$ of the membrane stresses. This function is defined by the relations

$$\begin{aligned} \sigma_x &= \frac{\partial^2 \phi}{\partial y^2} \\ \sigma_y &= \frac{\partial^2 \phi}{\partial x^2} \\ \tau_{xy} &= - \frac{\partial^2 \phi}{\partial x \partial y} \end{aligned} \quad (10)$$

where σ_x and σ_y denote normal stresses of the middle surface and τ_{xy} represents the shearing stress of that surface. If the relations (10) together with the biaxial stress-strain relations are introduced into equation (9), one obtains the compatibility equation

$$\frac{1}{E} \nabla^4 \phi = \left[\left(\frac{\partial^2 w_1}{\partial x \partial y} \right)^2 - \frac{\partial^2 w_1}{\partial x^2} \cdot \frac{\partial^2 w_1}{\partial y^2} \right] \quad (11)$$

$$- \left[\left(\frac{\partial^2 w_0}{\partial x \partial y} \right)^2 - \frac{\partial^2 w_0}{\partial x^2} \cdot \frac{\partial^2 w_0}{\partial y^2} \right] - \frac{1}{R} \left[\frac{\partial^2 w_1}{\partial x^2} - \frac{\partial^2 w_0}{\partial x^2} \right]$$

where

$$\nabla^4 = \frac{\partial^4}{\partial x^4} + 2\frac{\partial^4}{\partial x^2 \partial y^2} + \frac{\partial^4}{\partial y^4}$$

and E represents Young's modulus.

We shall now consider the equilibrium of an element of the shell. A free-body diagram is shown in Figure 33. There, double-headed vector representations are employed for the bending moments M_x and M_y and the twisting moment M_{xy} . Further, Q_x and Q_y denote the resultant transverse shearing forces. It is to be observed that M_x , M_y , M_{xy} , Q_x , and Q_y are all resultants per unit length of the middle surface of the shell.

Summing moments about the x and y axes and neglecting higher order terms, we obtain

$$\frac{\partial M_x}{\partial x} + \frac{\partial M_{xy}}{\partial y} - Q_x = 0 \quad (12)$$

$$\frac{\partial M_y}{\partial y} + \frac{\partial M_{xy}}{\partial x} - Q_y = 0$$

Summing forces in the radial direction we obtain

$$\frac{\partial Q_x}{\partial x} + \frac{\partial Q_y}{\partial y} + \sigma_x h \frac{\partial^2 w_l}{\partial x^2} + \sigma_y h \left(\frac{1}{R} + \frac{\partial^2 w_l}{\partial y^2} \right) \quad (13)$$

$$+ 2\tau_{xy} h \frac{\partial^2 w_l}{\partial x \partial y} - \frac{\gamma}{g} h \frac{\partial^2 w}{\partial t^2} - q = 0$$

Here γ denotes the weight density of the shell material and g represents the gravitational acceleration.

We shall employ the usual moment-curvature relations of shell theory:

$$M_x = -D \left(\frac{\partial^2 w}{\partial x^2} + \nu \frac{\partial^2 w}{\partial y^2} \right)$$

$$M_y = -D \left(\frac{\partial^2 w}{\partial y^2} + \nu \frac{\partial^2 w}{\partial x^2} \right) \quad (14)$$

$$M_{xy} = -\frac{Gh^3}{6} \cdot \frac{\partial^2 w}{\partial x \partial y}$$

where G represents the shear modulus of the material, ν is Poisson's ratio, and D is the flexural rigidity defined by

$$D = \frac{E h^3}{12 (1 - \nu^2)}$$

Here w , rather than w_1 , appears in (14) because the moments depend only upon changes of curvature. If the relations (14) are now substituted in (12), we find Q_x and Q_y as functions of w . These results, together with the relations (10) may now be substituted in (13) to yield the equilibrium equation

$$\begin{aligned} \nabla^4 (w_1 - w_0) = \frac{h}{D} \left[\frac{\partial^2 \phi}{\partial x^2} \cdot \frac{\partial^2 w_1}{\partial y^2} + \frac{\partial^2 \phi}{\partial y^2} \cdot \frac{\partial^2 w_1}{\partial x^2} + 2 \frac{\partial^2 \phi}{\partial x \partial y} \cdot \frac{\partial^2 w_1}{\partial x \partial y} \right. \\ \left. + \frac{1}{R} \cdot \frac{\partial^2 w_1}{\partial x^2} - \frac{\gamma}{g} \frac{\partial^2 w}{\partial t} \right] - \frac{q}{D} \end{aligned} \quad (15)$$

We now select for w_0 and w_1 the functions

$$w_0 = f_0 \sin \alpha x \sin \beta y + \psi_0 \sin^2 \alpha x \sin^2 \beta y \quad (16)$$

$$w_1 = f_1 \sin \alpha x \sin \beta y + \psi_1 \sin^2 \alpha x \sin^2 \beta y$$

where $\alpha = \frac{m \pi}{L}$ and $\beta = \frac{n}{R}$. Here m is the number of half waves in the axial direction of the shell and n the number of half waves in the circumferential direction. In equations (16) f_0 and ψ_0 are initial deflection parameters of the shell, which will either be known or will be assumed. Further, f_1 , and ψ_1 are time-dependent deflection parameters of the deformed shell. The configuration (16) implies diamond-shaped buckles. The relations (16) correspond to an elastically supported shell, one whose ends are neither damped nor simply supported. However, as in the case of static buckling of shells, it is unlikely that boundary conditions are of extreme significance provided the length of the shell is greater than approximately 1.5 diameters.

If the relations (16) are substituted in the compatibility equation (11), we obtain the following solution of (11) for the Airy stress function

$$\begin{aligned} \phi = & \kappa_1 \sin \alpha x \sin \beta y + \kappa_2 \sin 3 \alpha x \sin \beta y \\ & + \kappa_3 \sin \alpha x \sin 3 \beta y + \kappa_4 \cos 2 \alpha x + \kappa_5 \cos 2 \beta y \\ & + \kappa_6 \cos 2 \alpha x \cos 2 \beta y + \kappa_7 \cos 4 \alpha x + \kappa_8 \cos 4 \beta y \end{aligned}$$

$$+ K_9 \cos 4\alpha \times \cos 2\beta y + K_{10} \cos 2\alpha \times \cos 4\beta y - \frac{py^2}{2} + \frac{qR}{2h} x^2 \quad (17)$$

where

$$K_1 = \frac{(f_1 - f_0) \left(\frac{a^2}{R}\right) - (f_1 \psi_1 - f_0 \psi_0) a^2 \beta^2}{A_1}$$

$$K_2 = \frac{3(f_1 \psi_1 - f_0 \psi_0) a^2 \beta^2}{2A_2}$$

$$K_3 = \frac{3(f_1 \psi_1 - f_0 \psi_0) a^2 \beta^2}{2A_3}$$

$$K_4 = \frac{(f_1^2 - f_0^2 + \psi_1^2 - \psi_0^2) \left(\frac{a^2 \beta^2}{2}\right) - (\psi_1 - \psi_0) \left(\frac{a^2}{R}\right)}{A_4}$$

$$K_5 = \frac{(f_1^2 - f_0^2 + \psi_1^2 - \psi_0^2) a^2 \beta^2}{2A_5} \quad (18)$$

$$K_6 = \frac{(\psi_1 - \psi_0) \left(\frac{a^2}{R}\right) - (\psi_1^2 - \psi_0^2) a^2 \beta^2}{A_6}$$

$$K_7 = - \frac{(\psi_1^2 - \psi_0^2) a^2 \beta^2}{2A_7}$$

$$K_8 = - \frac{(\psi_1^2 - \psi_0^2) a^2 \beta^2}{2A_8}$$

$$K_9 = \frac{(\psi_1^2 - \psi_0^2) a^2 \beta^2}{2A_9}$$

$$K_{10} = \frac{(\psi_1^2 - \psi_0^2) a^2 \beta^2}{2A_{10}}$$

and

$$A_1 = \frac{(a^2 + \beta^2)^2}{E}$$

$$A_2 = \frac{(9a^2 + \beta^2)^2}{E}$$

$$A_3 = \frac{(a^2 + 9\beta^2)^2}{E}$$

$$A_4 = \frac{16a^4}{E}$$

$$A_5 = \frac{16\beta^4}{E}$$

$$A_6 = \frac{16(a^2 + \beta^2)^2}{E}$$

$$A_7 = \frac{256a^4}{E}$$

$$A_8 = \frac{256\beta^4}{E}$$

$$A_9 = \frac{16(4a^2 + \beta^2)^2}{E}$$

$$A_{10} = \frac{16(a^2 + 4\beta^2)^2}{E}$$

(19)

We have now found a stress function satisfying compatibility. Equilibrium must now be satisfied. If we substitute the above values of w_1 , w_0 , and ϕ in the equilibrium equation, it will not in general be satisfied. However, we may satisfy it approximately by the Galerkin technique. For this purpose, let

$$H = D \nabla^4 (w_1 - w_0) - h \left[\frac{\partial^2 \phi}{\partial x^2} \cdot \frac{\partial^2 w_1}{\partial y^2} + \frac{\partial^2 \phi}{\partial y^2} \cdot \frac{\partial^2 w_1}{\partial x^2} - 2 \frac{\partial^2 \phi}{\partial x \partial y} \cdot \frac{\partial^2 w_1}{\partial x \partial y} + \frac{1}{R} \cdot \frac{\partial^2 \phi}{\partial x^2} - \frac{\gamma}{g} \cdot \frac{\partial^2 w}{\partial t^2} \right] + q \quad (20)$$

That is, H is the residual of the equilibrium equation after approximate values of w_1 , w_0 , and ϕ have been substituted. To minimize H we employ the Galerkin method, viz.

$$\int_0^{2\pi R} \int_0^L H \frac{\partial w}{\partial f_1} dx dy = 0 \quad (21)$$

$$\int_0^{2\pi R} \int_0^L H \frac{\partial w}{\partial \psi_1} dx dy = 0$$

These equations become

$$\int_0^{2\pi R} \int_0^L H \sin \alpha x \sin \beta y dx dy = 0 \quad (22)$$

$$\int_0^{2\pi R} \int_0^L H \sin^2 \alpha x \sin^2 \beta y dx dy = 0$$

For the above values of w_1 , w_0 , and ϕ , H may now be determined from equation (20). This value of H, together with the above Galerkin equations, yields the coupled nonlinear differential equations in f_1 and ψ_1 :

$$\frac{\gamma}{g} \frac{d^2 f_1}{dt^2} = R_1 f_1 + R_2 f_1^3 + R_3 \psi_1 + R_4 f_1 \psi_1 + R_5 f_1 \psi_1^2 + R_6 \quad (23)$$

$$\frac{9\gamma}{4g} \frac{d^2 \psi_1}{dt^2} = S_1 \psi_1 + S_2 \psi_1^2 + S_3 \psi_1^3 + S_4 f_1 + S_5 f_1^2 + S_6 f_1^2 \psi_1 + S_7 \quad (24)$$

where the coefficients are defined as follows:

$$R_1 = - \frac{D(a^4 + 2a^2\beta^2 + \beta^4)}{h} + a^4\beta^4(f_0^2 + \psi_0^2) \left(\frac{1}{A_4} + \frac{1}{A_5} \right) \\ - \frac{2a^4\beta^2\psi_0}{RA_4} - \frac{a^4}{R^2A_1} + pa^2 + \frac{qR\beta^2}{h}$$

$$R_2 = -a^4\beta^4 \left(\frac{1}{A_4} + \frac{1}{A_5} \right) \quad (25)$$

$$R_3 = f_0 a^4 \beta^2 \left[\frac{R\psi_0\beta^2}{RA_1} + \frac{9\psi_0\beta^2}{4} \left(\frac{1}{A_2} + \frac{1}{A_3} \right) \right]$$

$$R_4 = \frac{2a^4\beta^2}{R} \left(\frac{1}{A_1} + \frac{1}{A_4} \right)$$

$$R_5 = -a^4\beta^4 \left(\frac{1}{A_1} + \frac{9}{4A_2} + \frac{9}{4A_3} + \frac{1}{A_4} + \frac{1}{A_5} \right)$$

$$\begin{aligned}
R_6 &= \frac{f_0 D}{h} (a^4 + 2a^2 \beta^2 + \beta^4) - \frac{f_0 a^4}{R^2 A_1} (R \psi_0 \beta^2 - 1) \\
S_1 &= -\frac{D (12a^4 + 8a^2 \beta^2 + 12\beta^4)}{h} + 4a^4 \beta^4 \left[f_0^2 \left(\frac{1}{A_4} + \frac{1}{A_5} \right) \right. \\
&\quad \left. + \psi_0^2 \left(\frac{1}{A_4} + \frac{1}{A_5} + \frac{2}{A_6} + \frac{1}{A_7} + \frac{1}{A_8} + \frac{1}{2A_9} + \frac{1}{2A_{10}} \right) \right] \\
&\quad - \frac{8a^4 \beta^2 \psi_0}{R} \left(\frac{1}{A_4} + \frac{1}{A_6} \right) - \frac{4a^4}{R^2} \left(\frac{2}{A_4} + \frac{1}{A_6} \right) + 3a^2 p - \frac{3qR\beta^2}{h} \\
S_2 &= \frac{2a^4 \beta^2}{R} \left(\frac{6}{A_4} + \frac{6}{A_6} \right) \\
S_3 &= -2a^4 \beta^4 \left(\frac{2}{A_4} + \frac{2}{A_5} + \frac{4}{A_6} + \frac{2}{A_7} + \frac{2}{A_8} + \frac{1}{A_9} + \frac{1}{A_{10}} \right) \\
S_4 &= f_0 a^4 \beta^2 \left[\frac{4}{A_1} (\psi_0 \beta^2 - \frac{1}{R}) + 9\beta^2 \psi_0 \left(\frac{1}{A_2} + \frac{1}{A_3} \right) \right] \\
S_5 &= \frac{4a^4 \beta^2}{R} \left(\frac{1}{A_1} + \frac{1}{A_4} \right) \tag{26} \\
S_6 &= -a^4 \beta^4 \left(\frac{4}{A_1} + \frac{9}{A_2} + \frac{9}{A_3} + \frac{4}{A_4} + \frac{4}{A_5} \right) \\
S_7 &= \frac{4\psi_0 D}{h} (3a^4 + 2a^2 \beta^2 + 3\beta^4) + \frac{a^4 \psi_0}{R^2} \left(\frac{8}{A_4} + \frac{4}{A_6} \right) \\
&\quad - \frac{2a^4 \beta^2}{R} \left[\frac{2(f_0^2 + \psi_0^2)}{A_4} + \frac{2\psi_0^2}{A_6} \right] - \frac{16q}{9h} + \frac{4q}{h}
\end{aligned}$$

It is to be observed that R_1 and S_1 each contain p , the mean axial stress, which is defined by the relation

$$p = \frac{P}{2 \pi R h} \quad (27)$$

where P is the applied axial load. Let us consider the relation between end shortening e and axial displacement which is given by

$$e = \int_0^L \frac{\partial u}{\partial x} dx \quad (28)$$

If now the first of equations (8) is solved for $\partial u / \partial x$ and this value, together with the value of ϵ_x found from Hooke's law, substituted in (28), we obtain

$$e = \frac{PL}{E} + \frac{\alpha^2 L}{8} (f_1^2 + \frac{3}{4} \psi_1^2) + \frac{\nu q RL}{Eh} \quad (29)$$

If V denotes the constant rate of end shortening, from which $e = Vt$ where t denotes time, we have from (29)

$$p = \frac{EVt}{L} - \frac{E\alpha^2}{8} (f_1^2 + \frac{3}{4} \psi_1^2) - \frac{\nu q R}{h} \quad (30)$$

This result may now be substituted in equations (23) and (24) to obtain the governing equations for constant rate of end shortening, viz:

$$\frac{\gamma}{g} \frac{d^2 f_1}{dt^2} = v_0 f_1 t + v_1 f_1 + v_2 f_1^3 + v_3 \psi_1 + v_4 f_1 \psi_1 + v_5 f_1 \psi_1^2 + v_6 \quad (31)$$

$$\begin{aligned} \frac{9\gamma}{4g} \frac{d^2 \psi_1}{dt^2} = & w_0 \psi_1 t + w_1 \psi_1 + w_2 \psi_1^2 + w_3 \psi_1^3 + w_4 f_1 \\ & + w_5 f_1^2 + w_6 f_1^2 \psi_1 + w_7 \end{aligned} \quad (32)$$

where

$$V_0 = \frac{E a^2 v}{L}$$

$$V_1 = \frac{D(a^2 + \beta^2)^2}{h} + a^4 \beta^4 (f_0^2 + \psi_0^2) \left(\frac{1}{A_4} + \frac{1}{A_5} \right) \\ - \frac{2 a^4 \beta^2 \psi_0}{R A_4} - \frac{a^4}{R^2 A_1} - \frac{\nu q R a^2}{h} + \frac{q R \beta^2}{h}$$

$$V_2 = R_2 - \frac{E a^4}{8}$$

$$V_3 = R_3$$

$$V_4 = R_4$$

$$V_5 = R_5 - \frac{3 E a^4}{32}$$

(33)

$$V_6 = R_6$$

$$W_0 = \frac{3 E a^2 v}{L}$$

$$W_1 = - \frac{D (12 a^4 + 8 a^2 \beta^2 + 12 \beta^4)}{h} + 4 a^4 \beta^4 \left[f_0^2 \left(\frac{1}{A_4} + \frac{1}{A_5} \right) \right. \\ \left. + \psi_0^2 \left(\frac{1}{A_4} + \frac{1}{A_5} + \frac{2}{A_6} + \frac{1}{A_7} + \frac{1}{A_8} + \frac{1}{2A_9} + \frac{1}{2A_{10}} \right) \right] \\ - \frac{8 a^4 \beta^2 \psi_0}{R} \left(\frac{1}{A_4} + \frac{1}{A_6} \right) - \frac{4 a^4}{R^2} \left(\frac{2}{A_4} + \frac{1}{A_6} \right) \\ - \frac{3 \nu q R a^2}{h} - \frac{3 q R \beta^2}{h}$$

$$\begin{aligned}
W_2 &= S_2 \\
W_3 &= S_3 - \frac{9E a^2}{32} \\
W_4 &= S_4 \\
W_5 &= S_5 \\
W_6 &= S_6 - \frac{3E a^2}{8} \\
W_7 &= S_7
\end{aligned}
\tag{34}$$

Because of the complexity of the quantities involved in equations (33) and (34), it is desirable to proceed from this stage onward only by numerical techniques. Since the equations (31) and (32) are coupled nonlinear equations, no closed-form solution is known to exist. However, with given initial conditions, these two equations may be readily integrated numerically by the Runge-Kutte method. We shall investigate the initial conditions

$$\begin{aligned}
f_1 &= f_0 \\
\psi_1 &= \psi_0 \\
\frac{df_1}{dt} &= 0 \\
\frac{d\psi_1}{dt} &= 0
\end{aligned}
\tag{35}$$

The numerical solutions of equations (31) and (32) have been carried out on an IBM 1620 for shells having the following constants

$$\begin{aligned}
E &= 10.6 \times 10^6 \text{ #/IN}^2 \\
\nu &= 0.33
\end{aligned}$$

$L = 22.8 \text{ IN}$
 $R = 2.85 \text{ IN}$
 $h = 0.004 \text{ IN AND } 0.008 \text{ IN}$
 $V = 11.5, 23, \text{ AND } 46 \text{ ft/sec}$

$$f_0 = \psi_0 = h/2$$

Further, α was taken to be equal to β , which implies a wave aspect ratio of unity. Figures 34-45 on the following pages illustrate the results of these computations. For each set of parameters, both a dimensionless axial stress

$$\sigma = pR/Eh$$

and a dimensionless lateral deflection

$$\zeta = \frac{f_1 + \psi_1}{h}$$

were plotted as functions of time.

Since the rate of end shortening has been taken to be constant, this implies that these same two quantities are just as readily presented as functions of unit end shortening. It is to be observed from these figures that it is necessary to make a selection of which curve is the appropriate one to consider, i. e. for a given rate of end shortening and a given thickness shell, there is plotted a family of curves for various values of n , the number of half waves in the circumferential direction. The question arises as to which curve is the one that realistically describes the load-time relation of the shell. The criteria was adopted that the ζ - t curve that is first to deviate from the abscissa axis and is also first to reach its peak value is the one that should be considered.

C. Conclusion

On the basis of this criteria, inspection of the curves reveals certain extremely interesting results:

- a) With increasing rates of end shortening, the first maximum load, termed the buckling load, corresponding to the first maximum dimensionless axial stress, is attained sooner.
- b) With increasing rates of end shortening, the buckling load as defined in (a) is increased.
- c) With increasing rates of end shortening, the number of half waves that form around the circumference increases.

It is interesting to observe that these results are in qualitative agreement with those found by Agamirov and Volmir (Ref. 4) for the case of a cylindrical shell loaded by hydrostatic pressure. Further, for the parameters investigated here, the maximum load was always greater than would be anticipated for static buckling. A reliable estimate of the static buckling load may be found from

Kempner's theory (Ref. 13). Obviously it is desirable to obtain more information concerning behavior of these same geometries, particularly when different initial imperfections and still greater rates of end shortening are considered.

REFERENCES

1. Coppa, A.P., "On the Mechanism of Buckling of a Circular Cylindrical Shell under Longitudinal Impact", General Electric Co. TIS Rep. R60SP 494, Tenth International Congress of Applied Mechanics, Sept., 1960.
2. Schmitt, A.F., "Dynamic Buckling Tests of Aluminum Shells", Aeronautical Engineering Review, 15, 9, 54-58, 1956.
3. Bolotin, V.V., "Dynamic Stability of Elastic Systems", Gos. Isdat. Tekh-Teor. Lit. Moscow, 1956.
4. Agamirov, V.L. And Volmir, A.S., "Behavior of Cylindrical Shells under Dynamic Loading by Hydrostatic Pressure or by Axial Compression", Bulletin of the Academy of Sciences, USSR, Division Technical Sciences, Mechanics and Machine Construction, No. 3, 1959, pp. 78-83. Translated in Journal of the American Rocket Society, Vol. 31, No. 1, pp. 98-101, 1961.
5. Volmir, A.S., "On the Stability of Dynamically Loaded Cylindrical Shells", Proceedings of the Academy of Sciences, USSR, Vol. 123, pp. 806-808, 1958.
6. Kadashevich, Yu, I., and Pertsev, A.K., "Loss of Stability of a Cylindrical Shell under Dynamic Loads", Bulletin of the Academy of Sciences USSR, Div. Tech. Sci., Mechanics and Machine Construction, No. 3, pp. 30-33, 1960. Translation in ARS Journal, Jan. 1962.
7. Yao, V.C., "Stability of a Cylinder under Dynamic Radial Pressure", ARS Journal, Dec. 1961.
8. Thielemann, W.F., "New Developments in the Nonlinear Theories of the Buckling of Thin Cylindrical Shells", Aeronautics and Astronautics, Proceedings of the Durand Centennial Conference, Pergammon Press, New York, 1961.
9. Coppa, A.P., Collapsible Shell Structures for Lunar Landings, General Electric Co. TIS Rep. R62SD9, Feb. 1962 (Presented at the A.R.S. Space Flight Report to the Nation, Oct., 1961).
10. Donnell, L.H., "A New Theory for the Buckling of Thin Cylinders under Axial Compression and Bending", ASME Transactions, Vol. 56, No. 11, pp. 795-806, 1934.
11. von Karman, T. and Tsien, H.S., "The Buckling of Thin Cylindrical Shells under Axial Compression", Journal of the Aeronautical Sciences, Vol. 8, No. 8, pp. 303-312, 1941.
12. von Karman, T. and Tsien, H.S., "The Buckling of Spherical Shells by External Pressure", Journal of the Aeronautical Sciences, Vol. 7, No. 2, pp. 43-50, 1939.

13. Kempner, J., "Postbuckling Behavior of Axially Compressed Circular Cylindrical Shells", *Journal of the Aeronautical Sciences*, Vol. 21, No. 5, pp. 329-335, 342, 1954.
14. Fung, Y.C. and Sechler, E.E., "Instability of Thin Elastic Shells", *Structural Mechanics*, Pergammon Press, London, 1960.
15. Nash, W.A., "Recent Advances in the Buckling of Thin Shells", *Applied Mechanics Reviews*, April 1960.
16. Volmir, A. S. and Mineev, V. E., "An Experimental Investigation of the Buckling of a Shell under Dynamic Load", *Proceedings of the Academy of Sciences, USSR*, (incomplete).

Figures

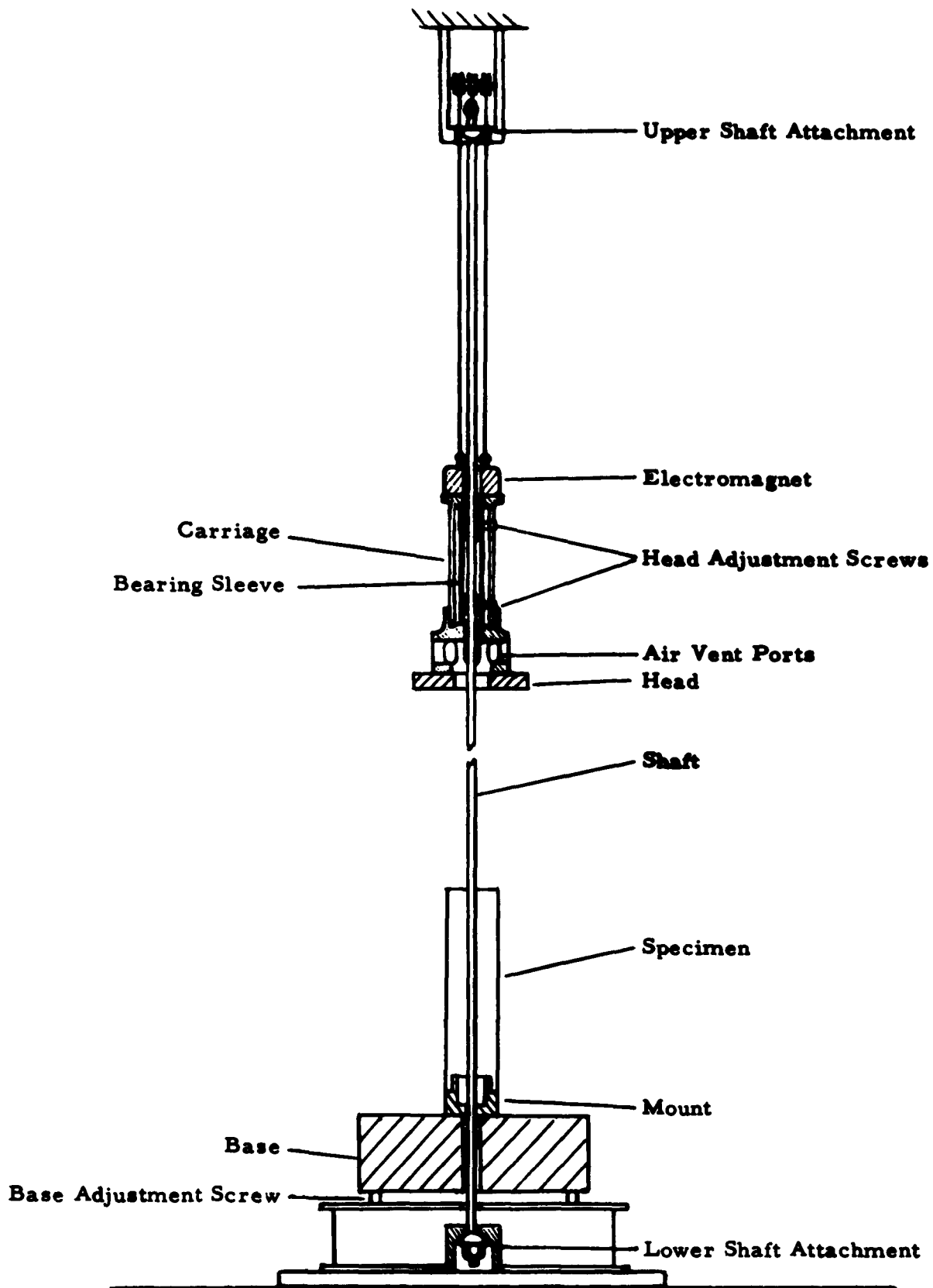


Figure 1. Impact Test Apparatus for Impacting Unpressurized Shells

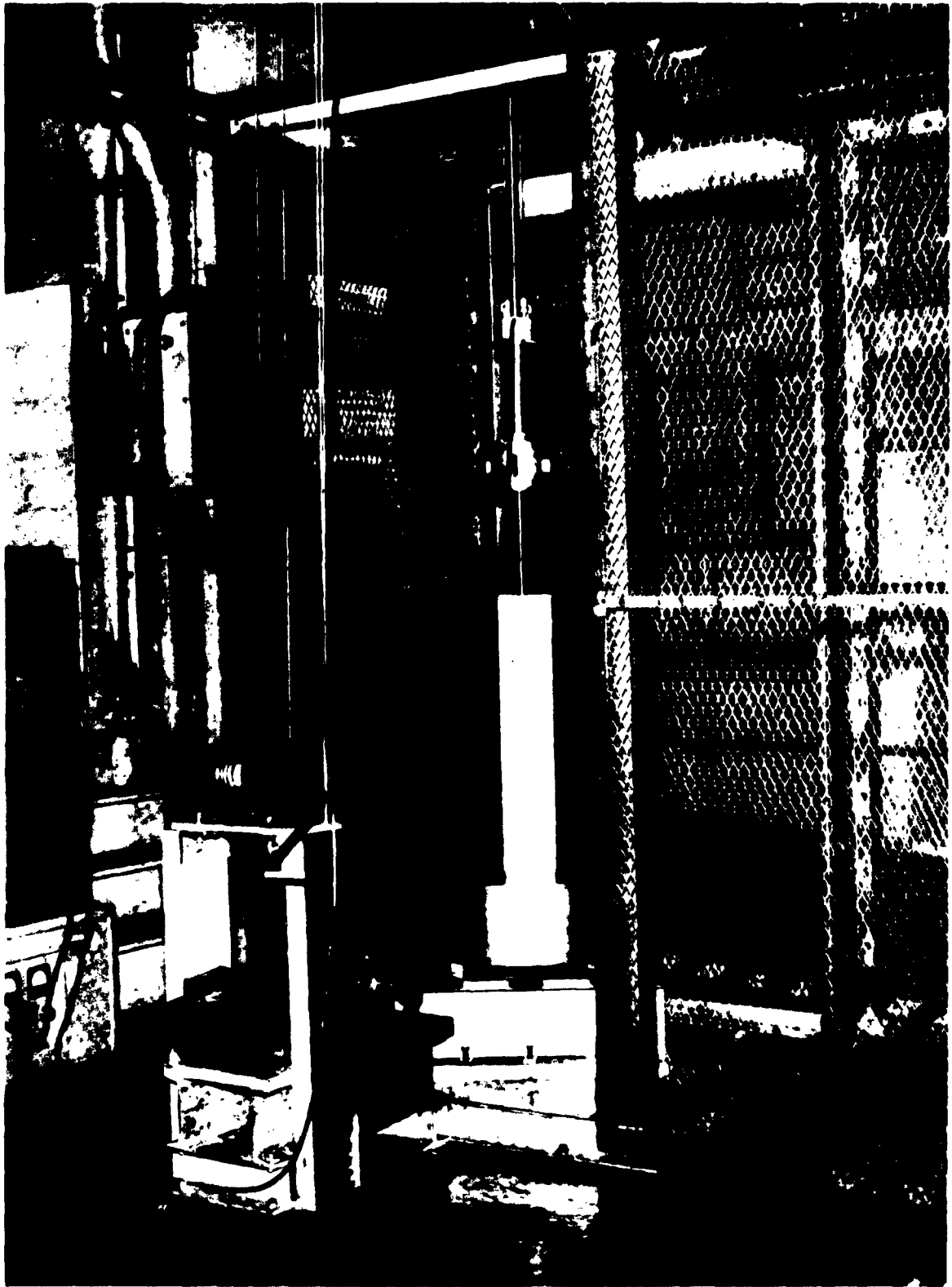


Figure 2. 40 ft. Precision Impact Test Apparatus

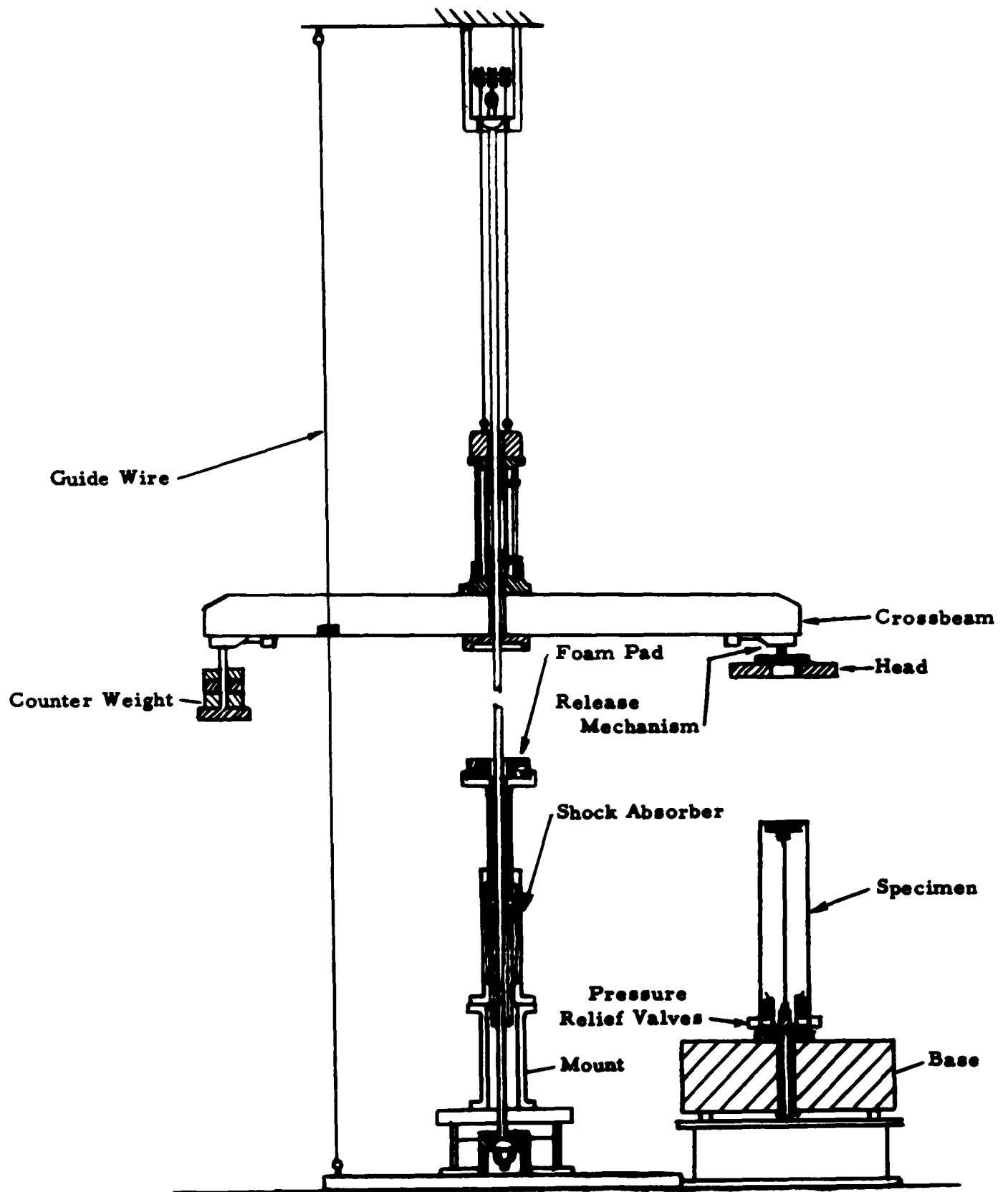


Figure 3. Apparatus for Impacting Pressurized Shells

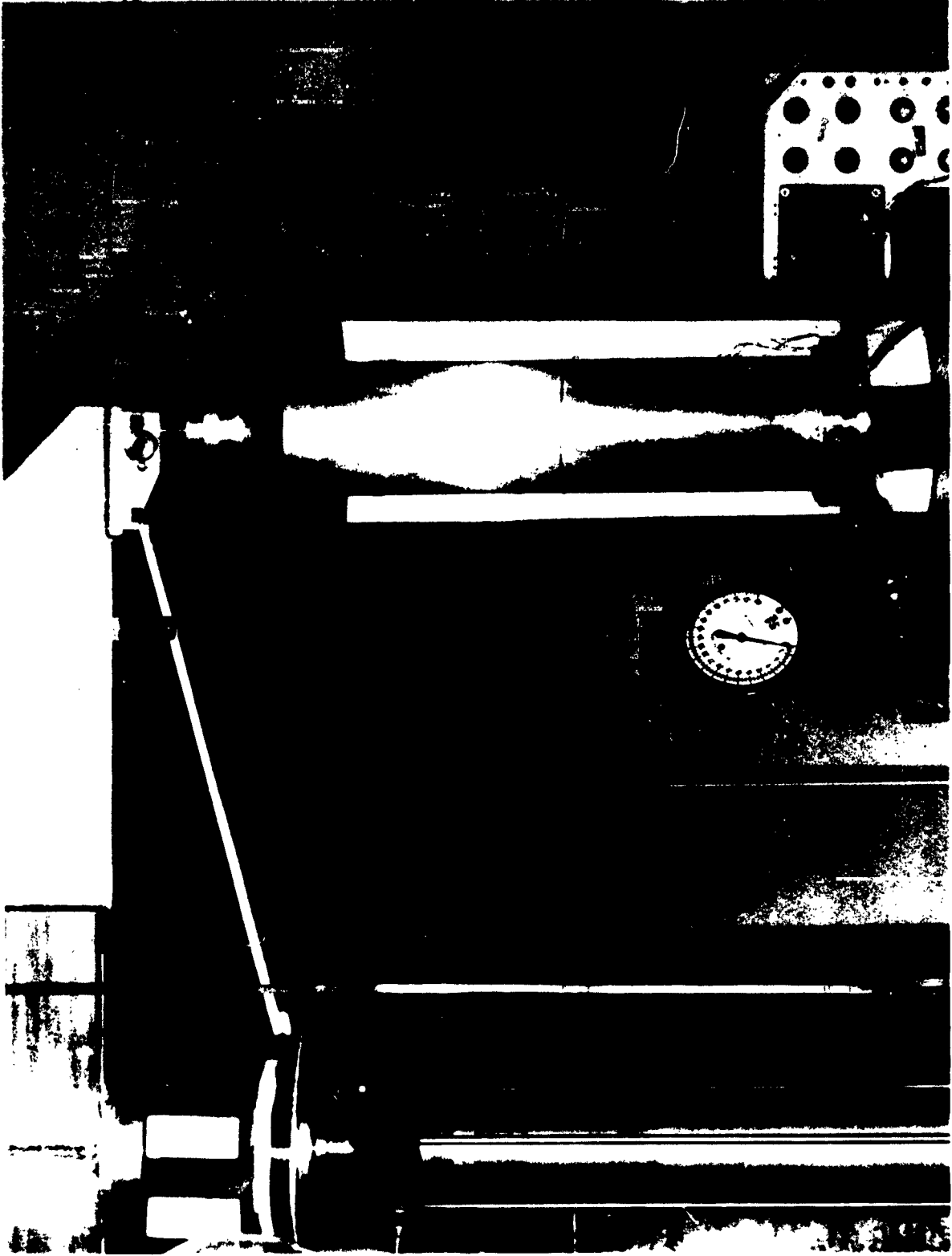


Figure 4. Test Set-Up for Impacting Cylindrical Shells with Initial Internal Pressure

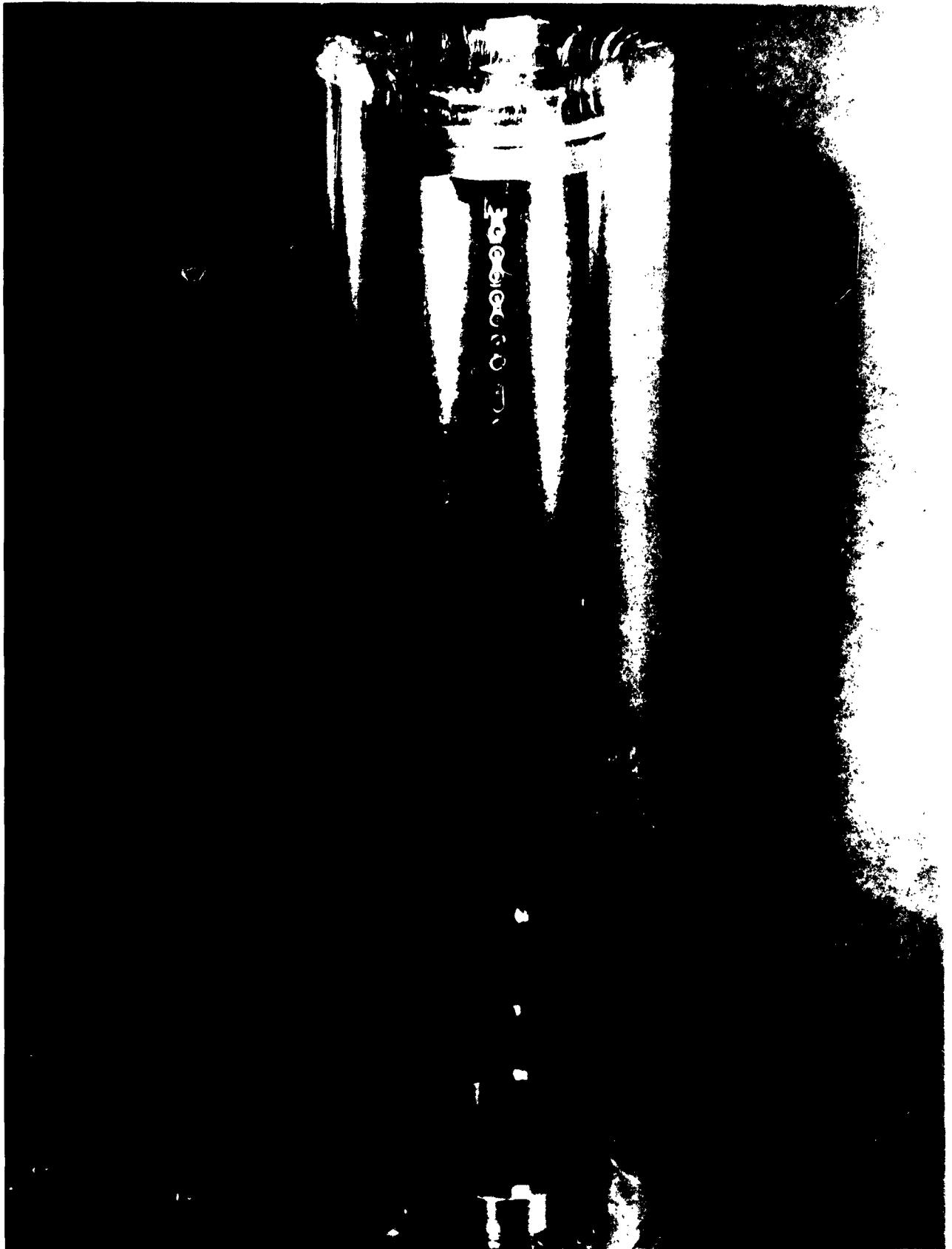


Figure 5. Internal Pressurization Scheme

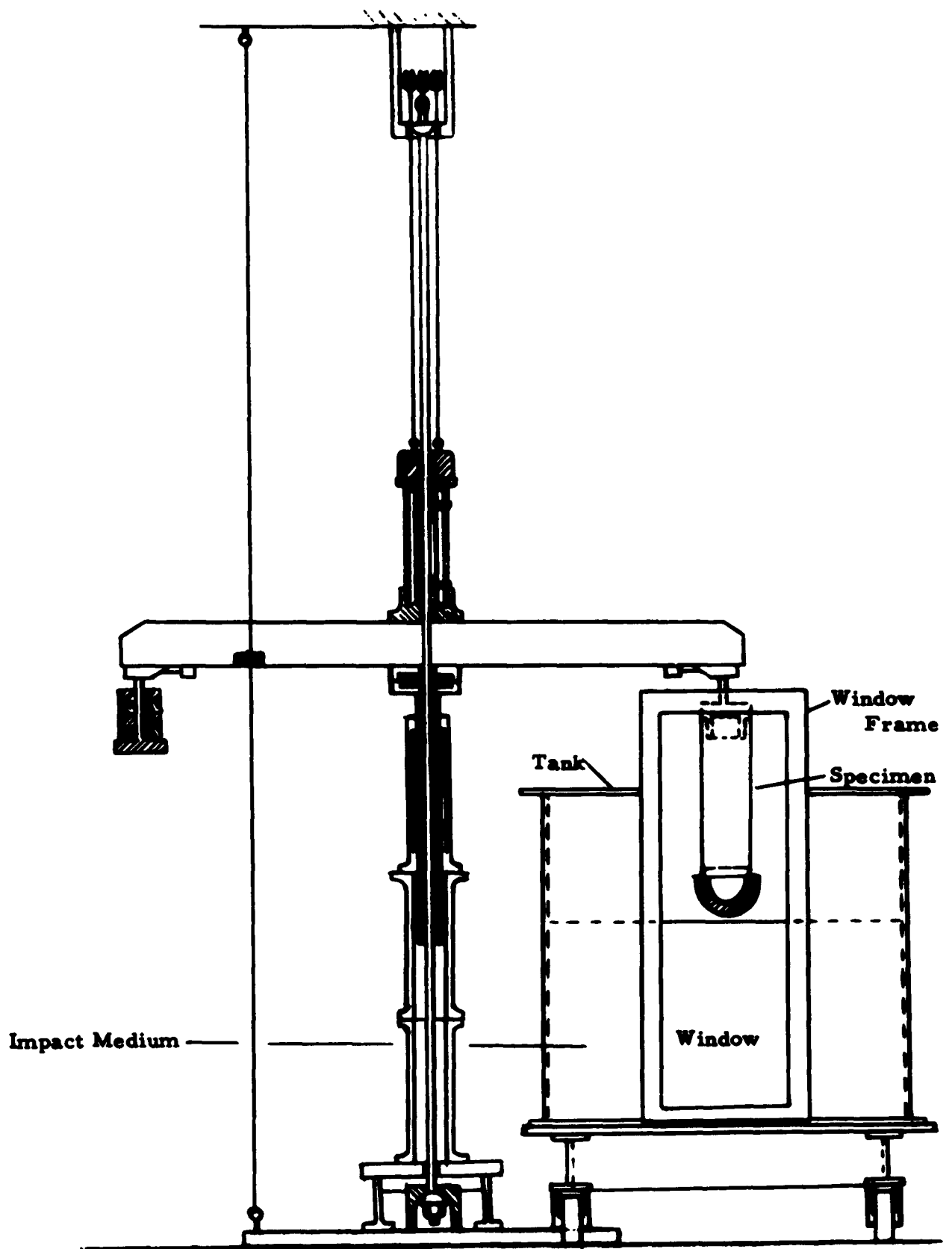


Figure 6. Apparatus for Impacting Shell Models into Non-Rigid Media

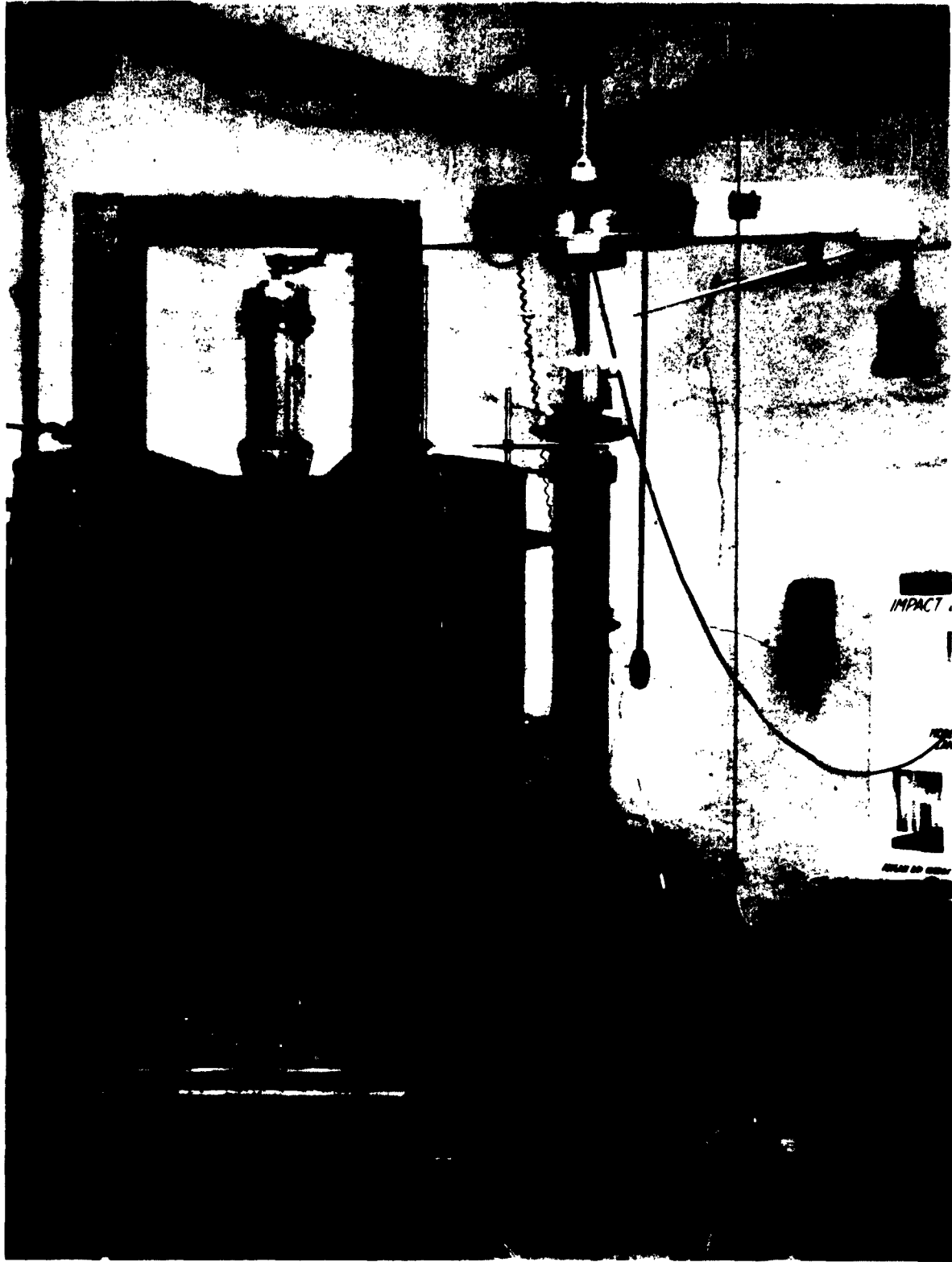


Figure 7. Test Set-Up for Hydrodynamic Impact

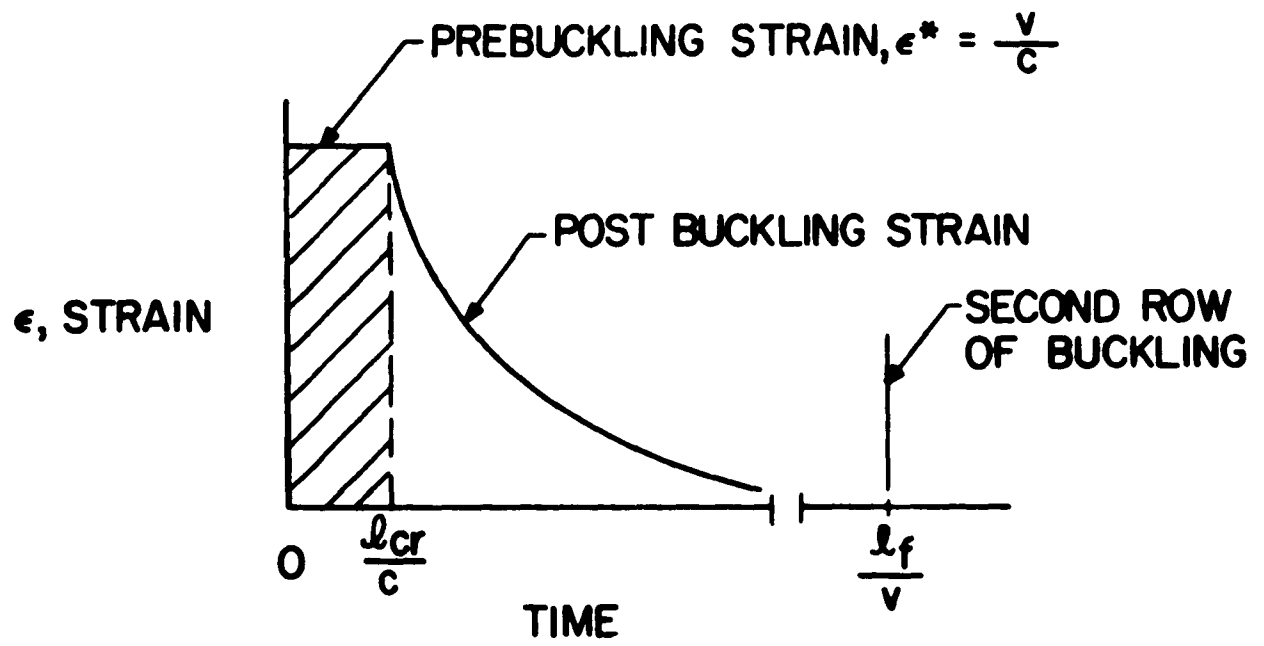
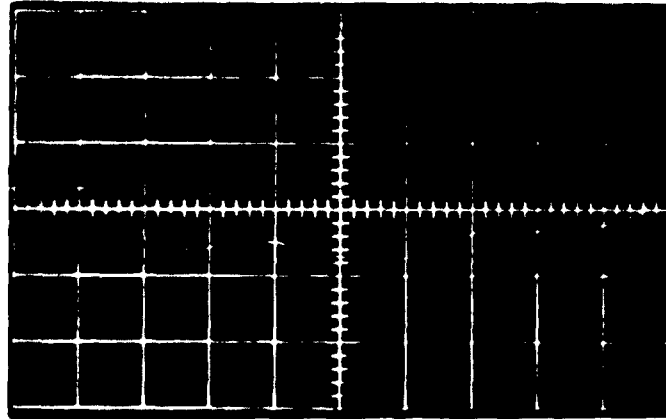


Figure 8. Resultant Axial Strain in the Buckling Part

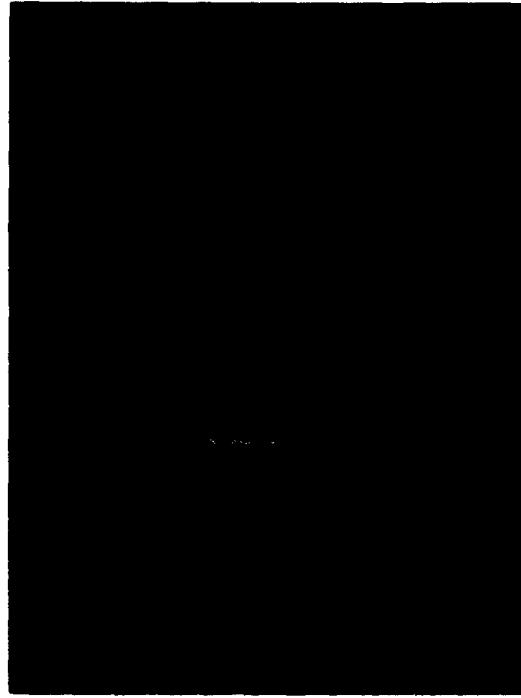
Axial Strain (.00196 in/in/grid spacing)
← Compression



Time (10 μ sec/grid spacing)

Figure 9. Initial Strain Pulse After Impact
(2024 H-19 Al Cylindrical Shell,
5.700" Dia., 22.8" Lgth, .008"
Thk. Impact Velocity = 46 ft/sec)

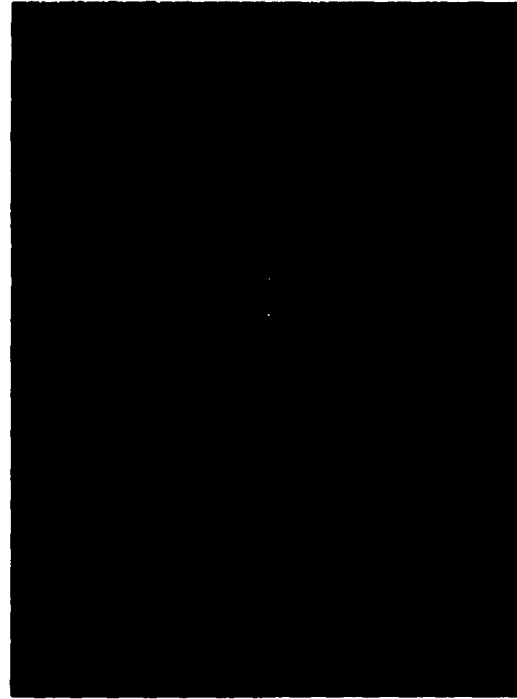
Axial Strain (.000783 in/in per grid spacing)
Compression →



Time After Impact (50 μ sec/grid spacing)

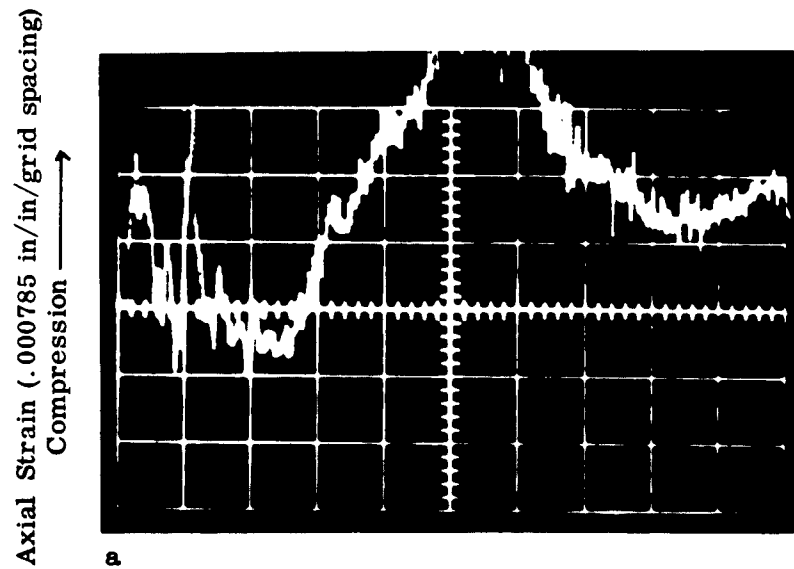
Figure 10. Initial Strain Pulse After Impact
(2024 H-19 Al Cylindrical Shell,
5.700" Dia., 22.8" Lgth, .008"
Thk. Impact Velocity = 11.5 ft/sec)

Axial Strain (.00196 in./in./grid spacing)
Compression →



Time (10 μ sec/grid spacing)

Figure 11. Initial Strain Pulse After Impact
(2024 H-19 Al Cylindrical Shell,
5.700" Dia., 22.8" Lgth, .008"
Thk. Impact Velocity = 25 ft/sec)



Time After Impact (500 μ sec/grid spacing)



Time After Impact (500 μ sec/grid spacing)

Figure 12. Strain Pulse After Impact (2024 H-19 Al Cylindrical Shell, 5.700" Dia., 22.8" Lgth, .008" Thk. Impact Velocity = 11.5 ft/sec)

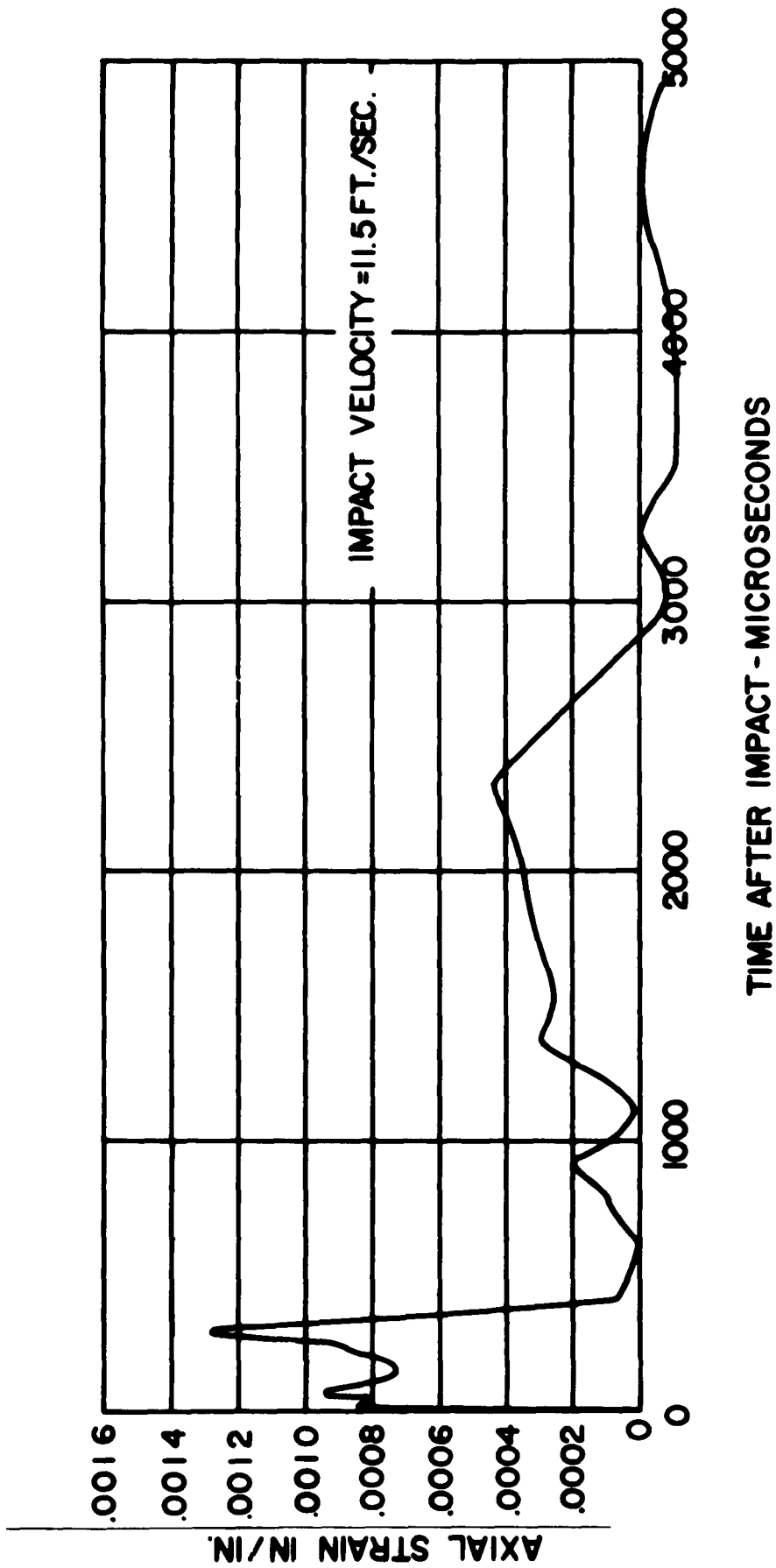


Figure 13. Axial Strain vs. Time (2024 H-19 Al Cylindrical Shell, 5.700" Dia., 22.8" Lgth, .008" Thk.
Impact Velocity = 11.5 ft/sec)

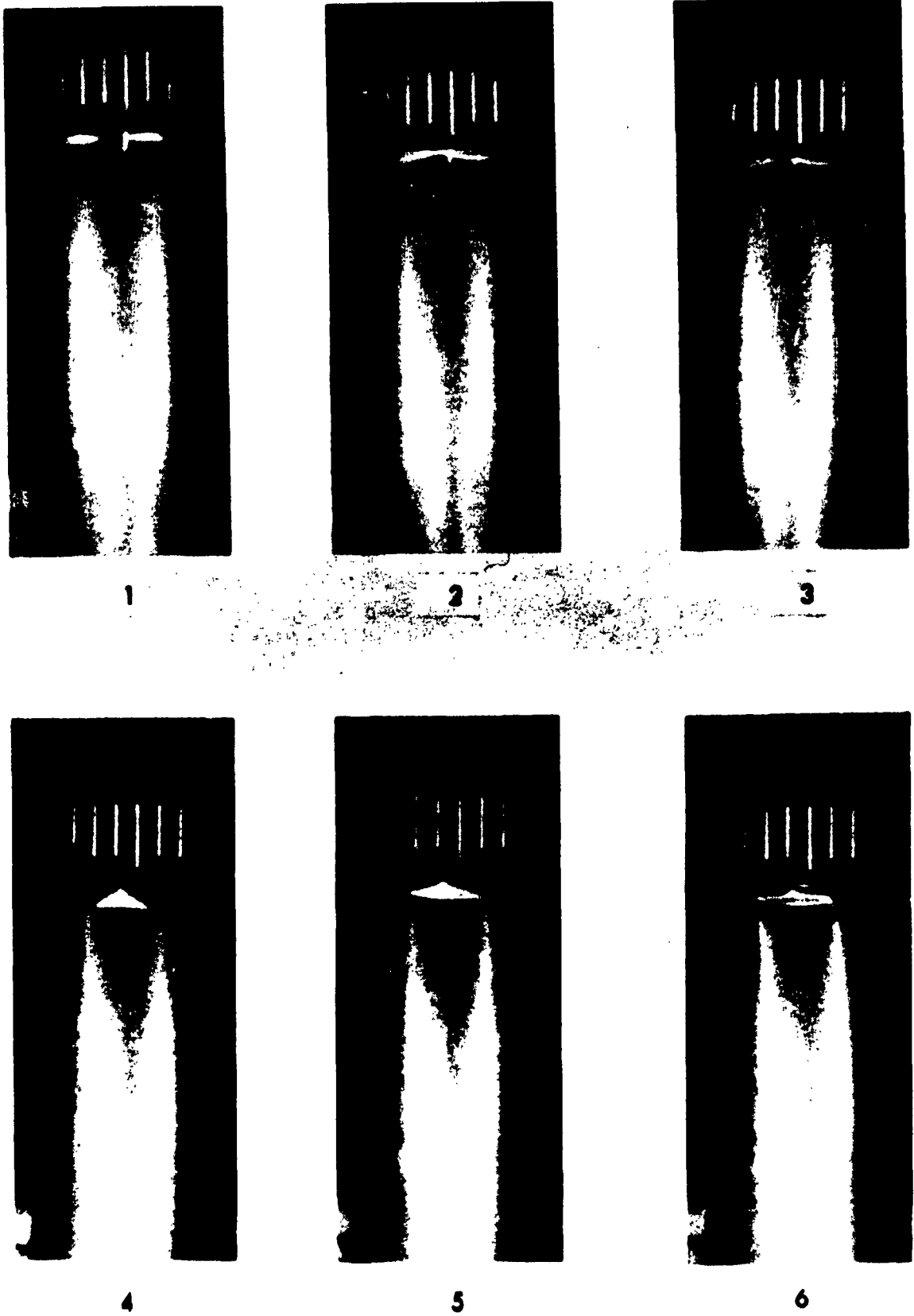


Figure 14. Buckling Process of a Cylindrical Shell Due to Axial Impact at 23 ft/sec (301 Stainless Steel, 5.700" Dia., 22.8" Lgth., .019" Thk.)

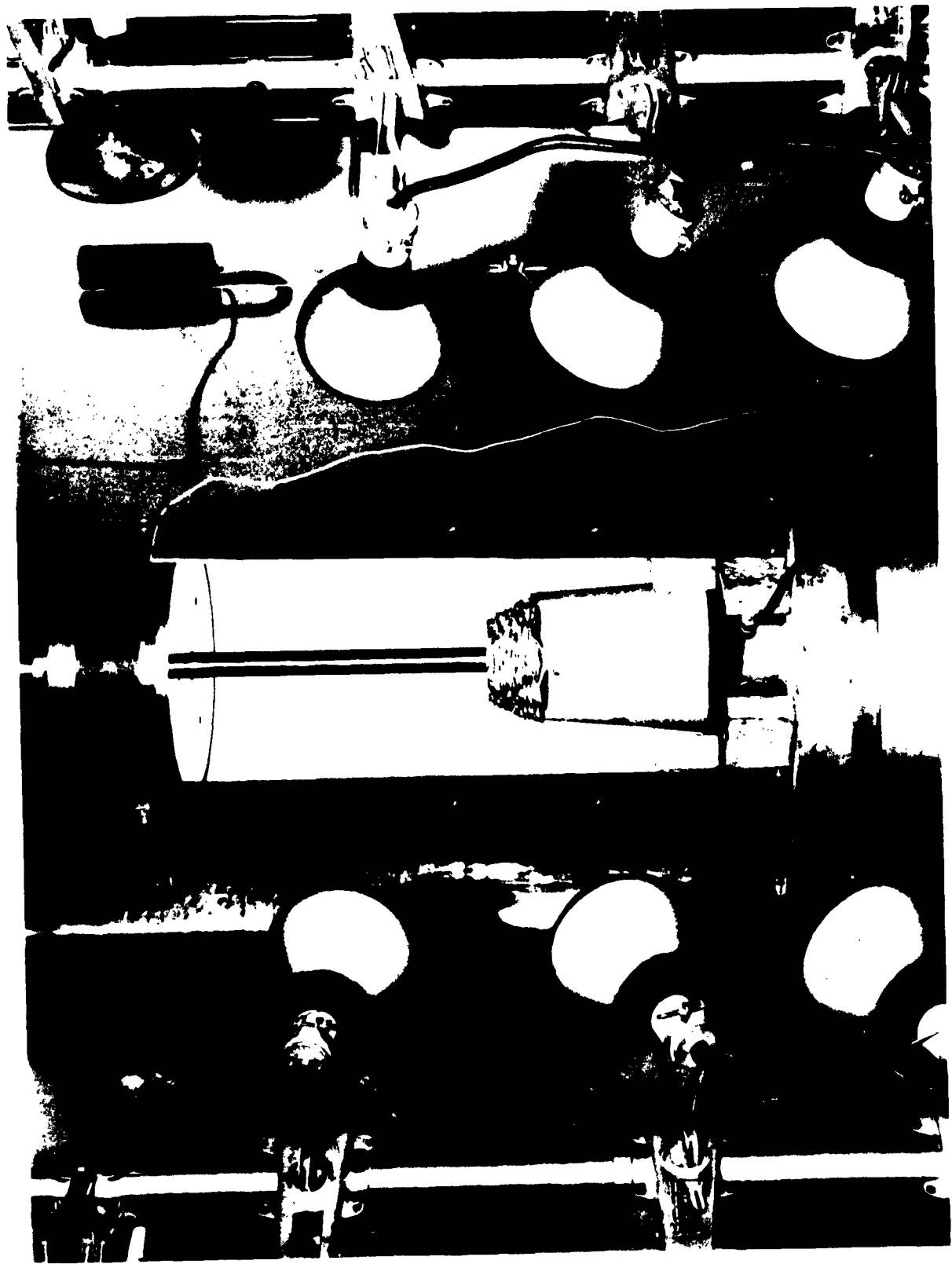


Figure 15. Experimental Set-Up for Unpressurized Conical Shells



Figure 16. Conical Shell Before and After Impact (5052 H-38 Aluminum,
3" and 6" Dia. at ends, 22.8" Lgth, .008" Thk.
Impact Velocity 36 ft/sec)

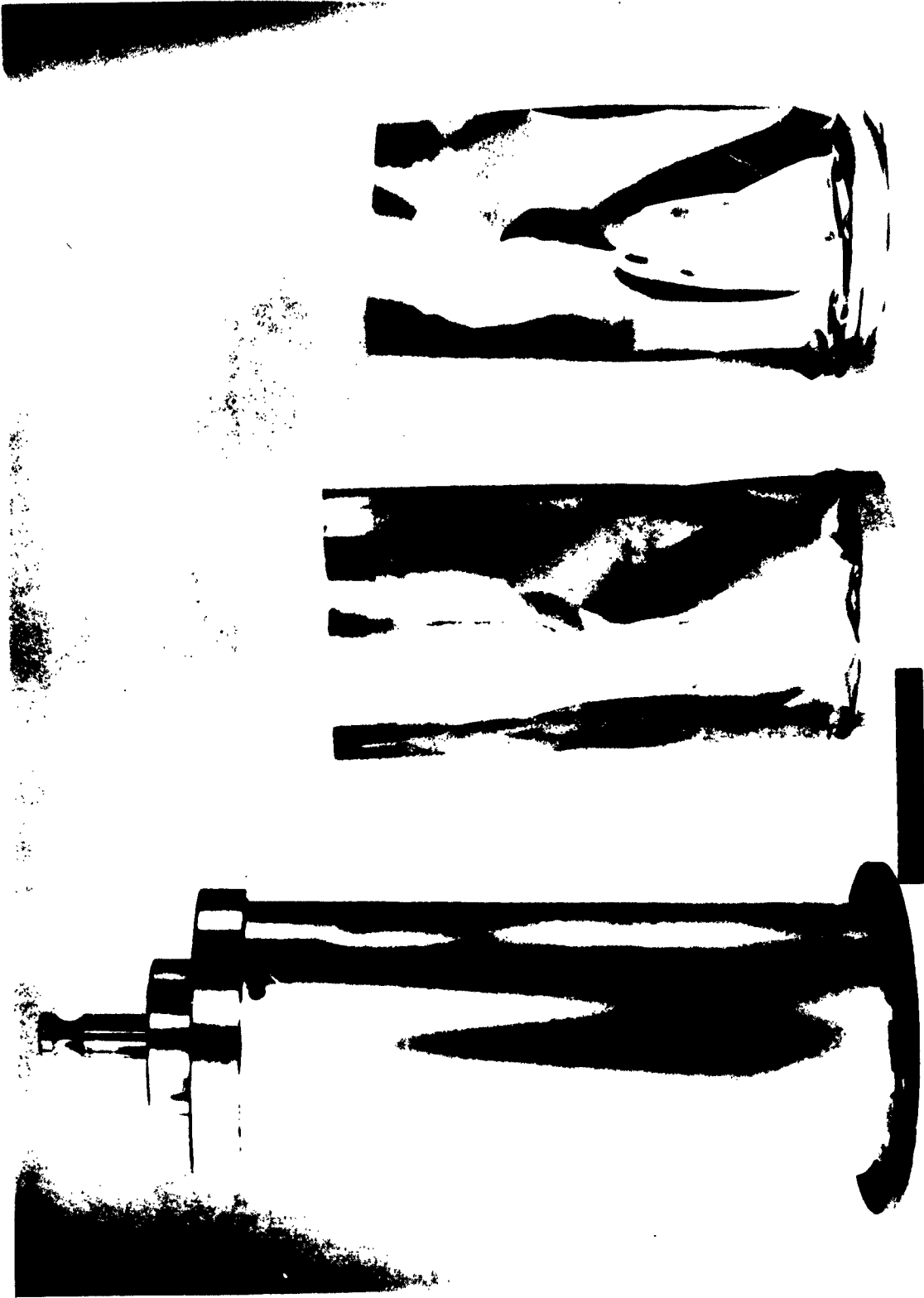


Figure 17. Cylindrical Shells Before and After Hydrodynamic Impact

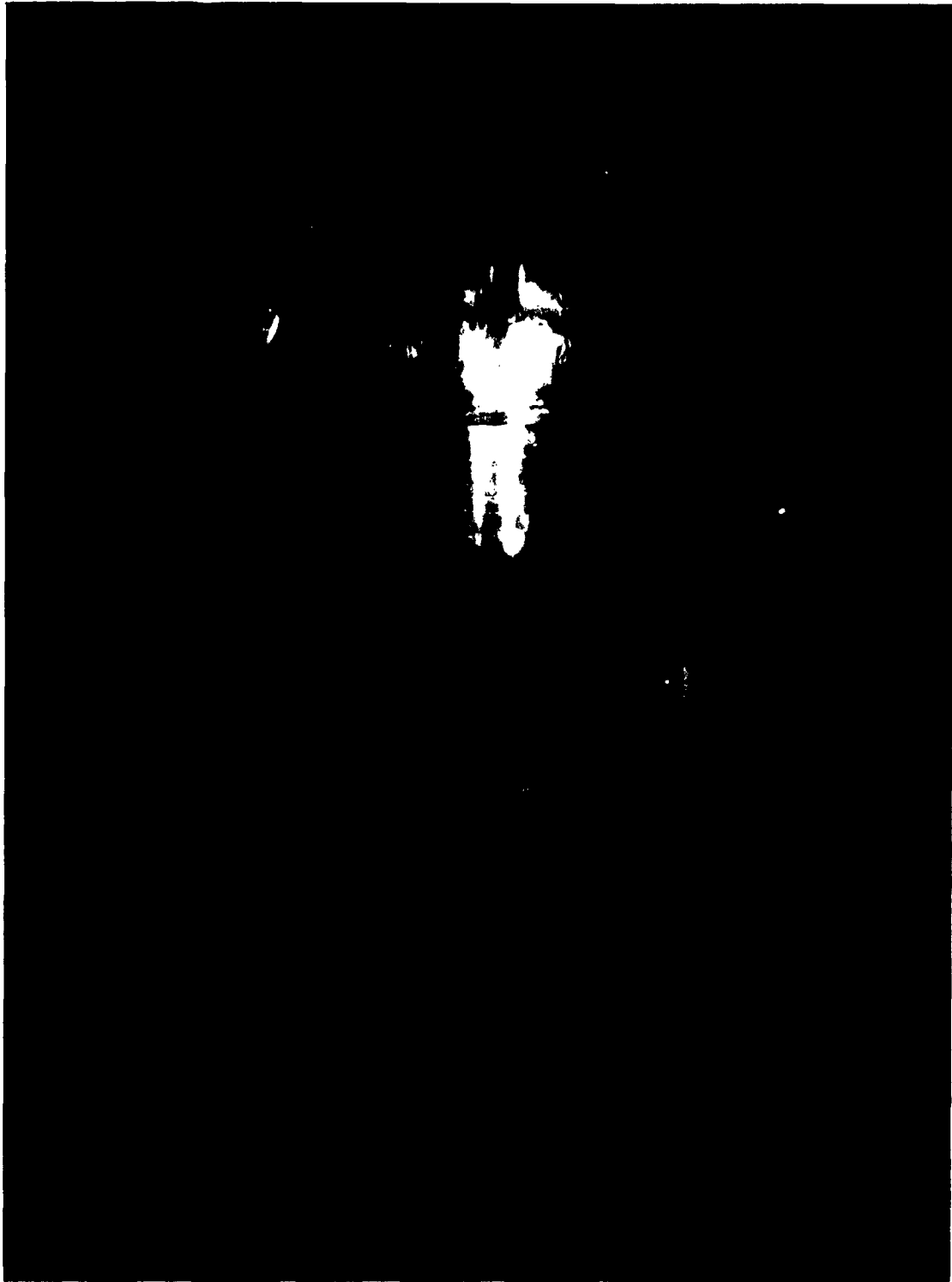
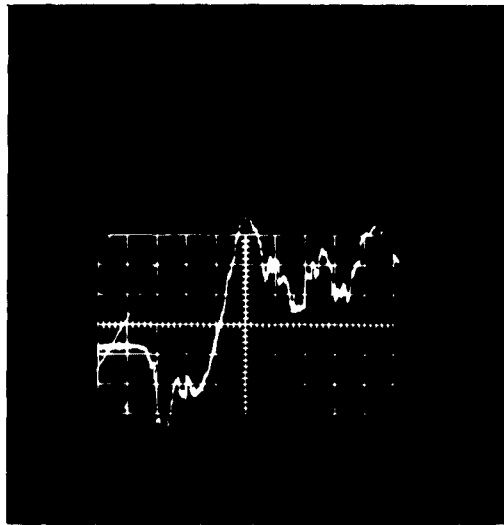


Figure 18. Impact Penetration of a Cylindrical Shell Model into Water

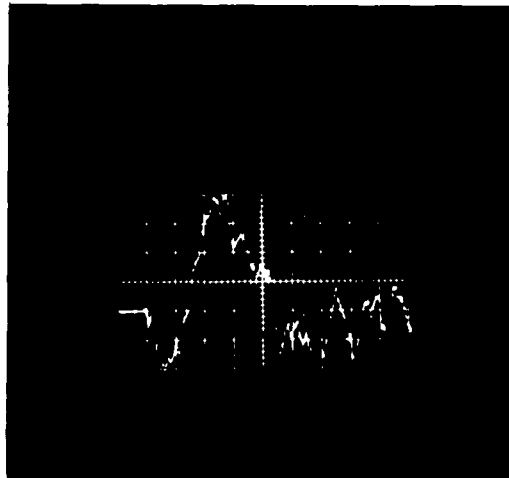
ϵ , Axial Strain (188 μ in/in/grid spacing)
 Compression \longrightarrow



Time (100 μ sec/grid spacing) \longrightarrow

Figure 19a. (Impact Begins at 130 μ sec from left)

ϵ , Axial Strain (188 μ in/in/grid spacing)
 Compression \longrightarrow



Time (100 μ sec/grid spacing) \longrightarrow

Figure 19b. (Impact Begins at 90 μ sec from left)

Figure 19. Axial Strain vs. Time at Two Circumferential Positions 120° Apart and 2 in. behind Impacted End. Pressurized Cylindrical Shell ($V_0 = 11.5$ ft/sec, $p_0 = 8.5$ psig, $\bar{p} = .165$, $h = .008$ ", Aluminum)

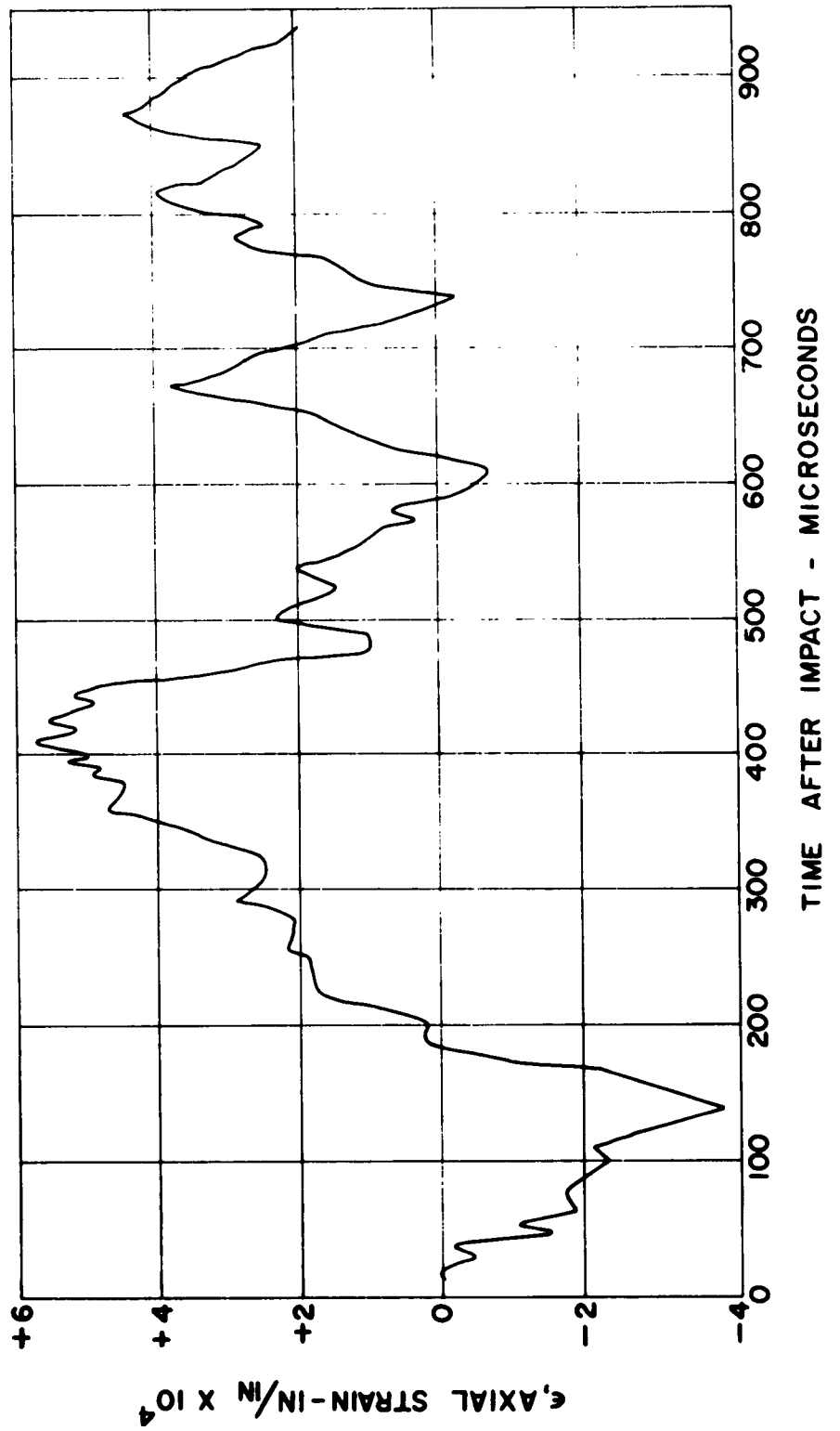
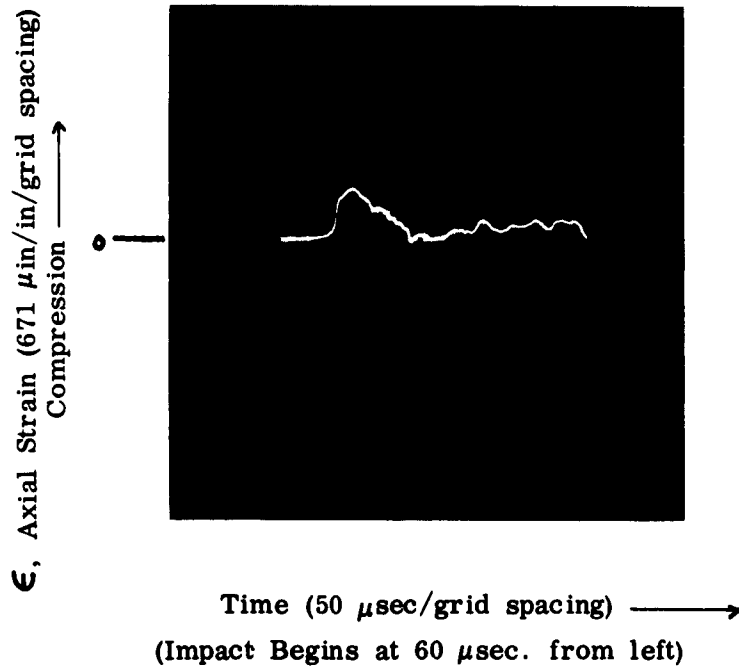
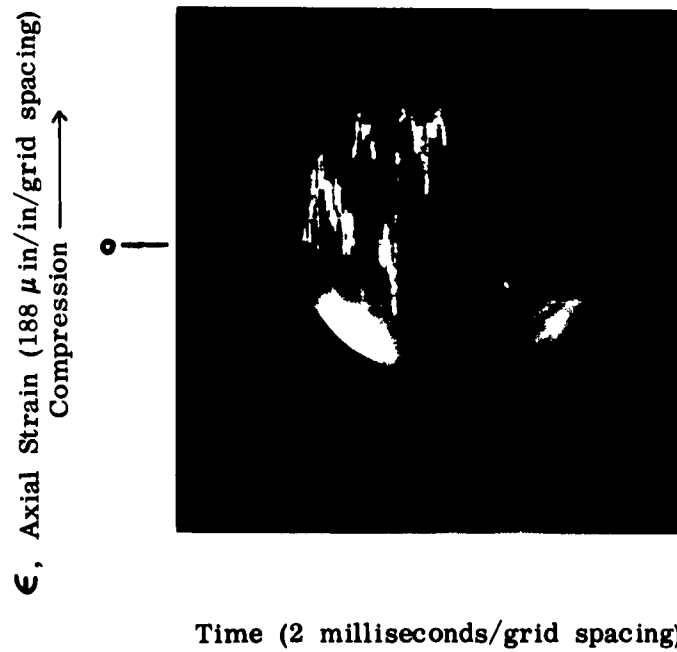


Figure 20. Axial Strain at 2 in. behind Impact End vs. Time ($V_0 = 11.5$ ft/sec, $P_0 = 8.5$ psig, $\bar{p} = .165$, $h = .008$ ", Aluminum) Internally Pressurized Cylindrical Shell

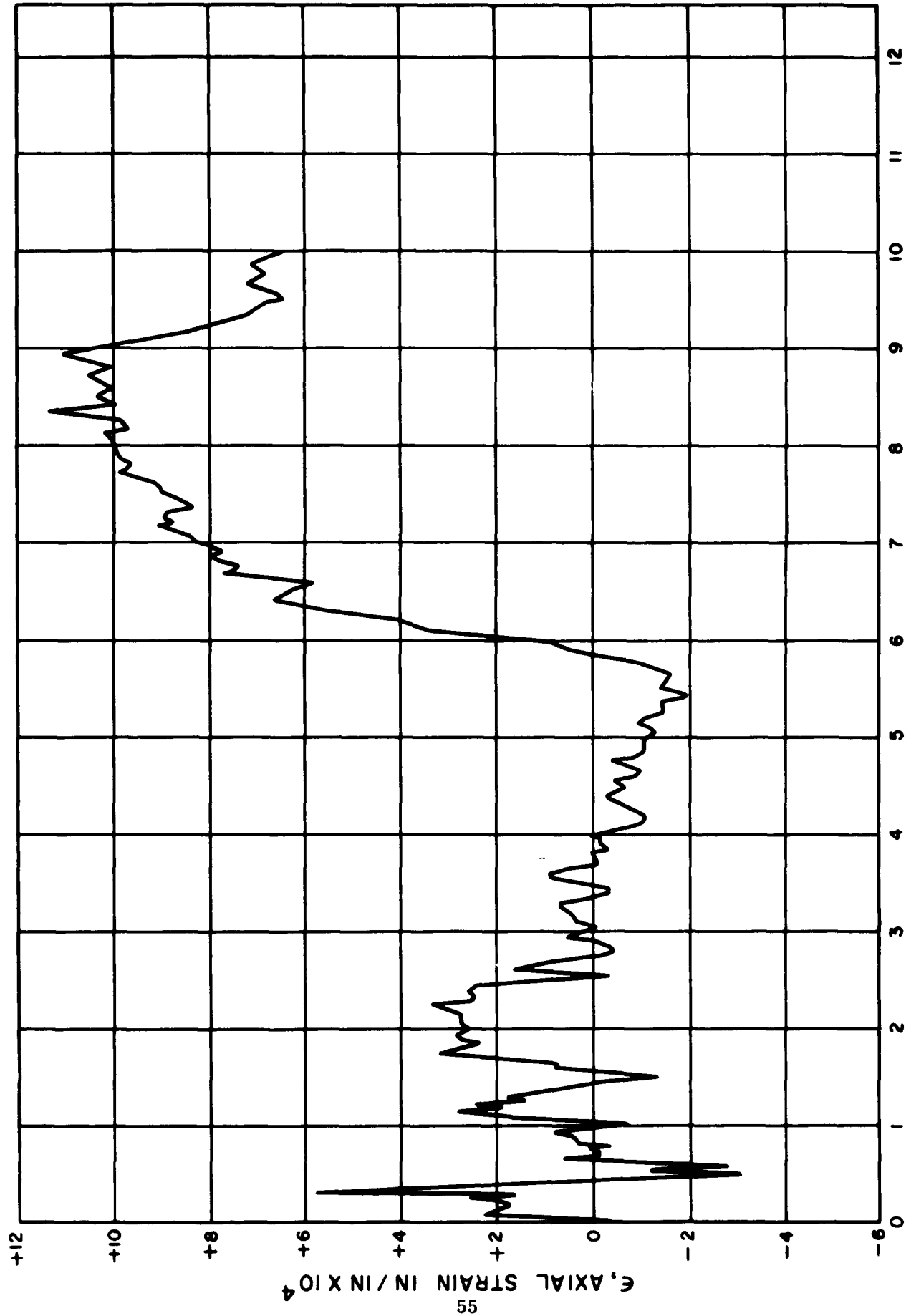


a. Short Time Trace



b. Long Time Trace

Figure 21. Axial Strain vs. Time for an Internally Pressurized Cylindrical Shell ($V_0 = 23 \text{ ft/sec}$, $p_0 = 8.5 \text{ psig}$, $\bar{p} = .165$, $h = .008''$, Aluminum)



TIME AFTER IMPACT (MILLISECONDS)

Figure 22. Axial Strain at 2 in. behind impact End vs. Time ($V_0 = 11.5$ ft/sec, $P_0 = 17.0$ psig, $\bar{p} = .330$, $h = .008$ ", Aluminum) Internally Pressurized Cylindrical Shell

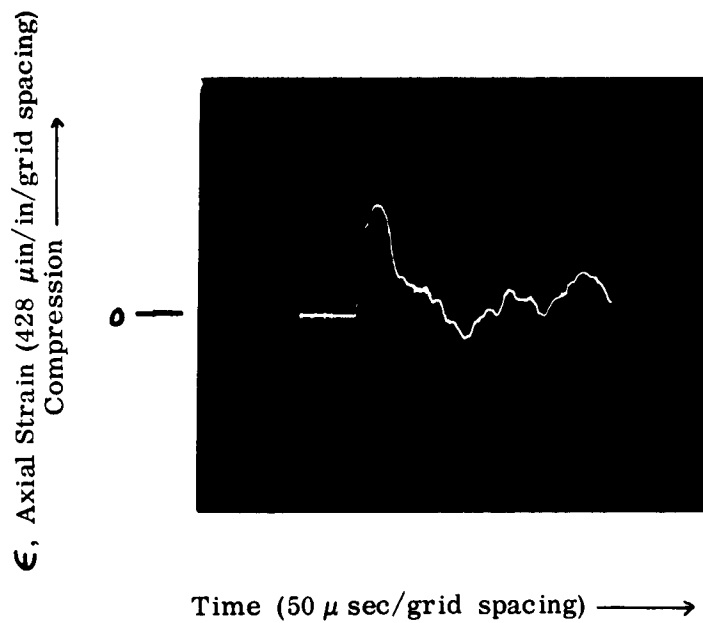


Figure 23a. (Impact Begins at 80 μ sec. from left)

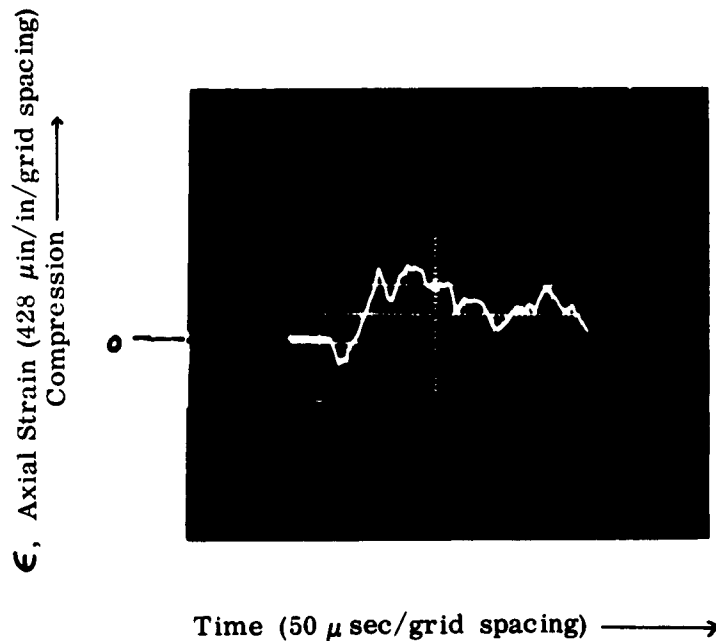


Figure 23b. (Impact Begins at 60 μ sec. from left)

Figure 23. Axial Strain vs. Time at Two Circumferential Positions 120° Apart and 2 in. behind Impacted End. Pressurized Cylindrical Shell ($V_0 = 23$ ft/sec, $p_0 = 17.0$ psig, $\bar{p} = .330$, $h = .008''$, Aluminum)

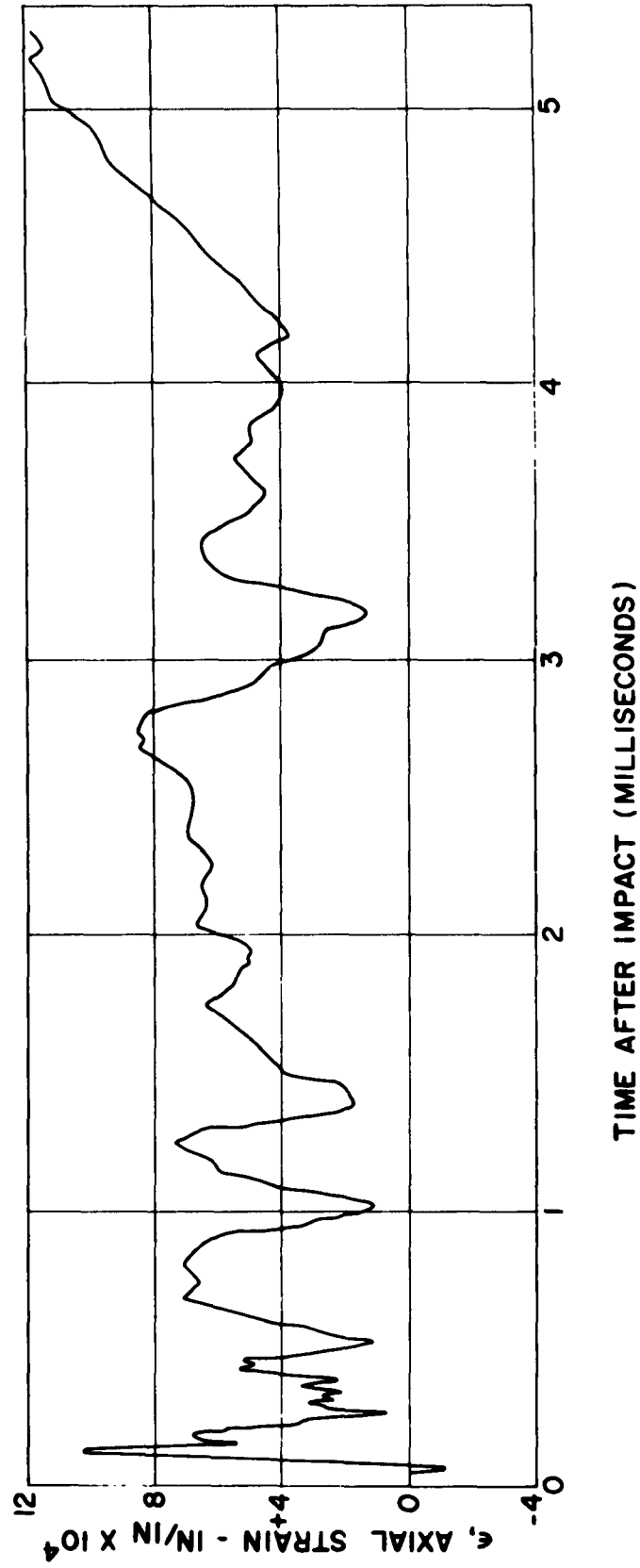


Figure 24. Axial Strain at 2 in. behind Impact End vs. Time ($V_0 = 23$ ft/sec, $P_0 = 17$ psig, $\bar{p} = .330$, $h = .008$ ", Aluminum) Internally Pressurized Cylindrical Shell

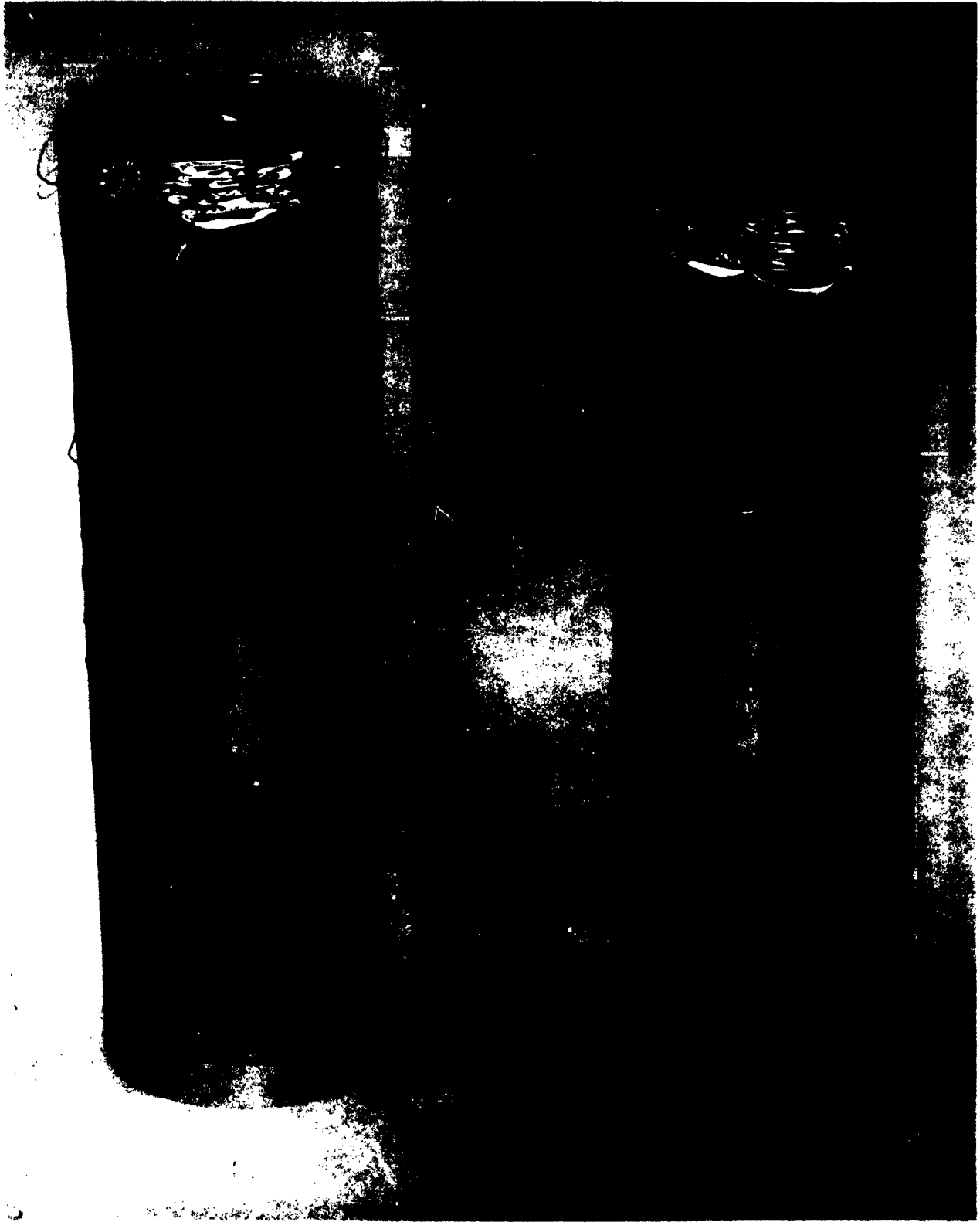


Figure 25. Cylindrical Shells after Impact ($V_0 = 23$ ft/sec, $p_0 = 17$ psig (left)
 $p_0 = 8.5$ psig (right), $h = .008$ ", Aluminum)



Figure 26. Partially Expanded Cylindrical Shell Showing Collapse Pattern
(Aluminum, .004" Thk, 5.700" Dia., 30" initial length)

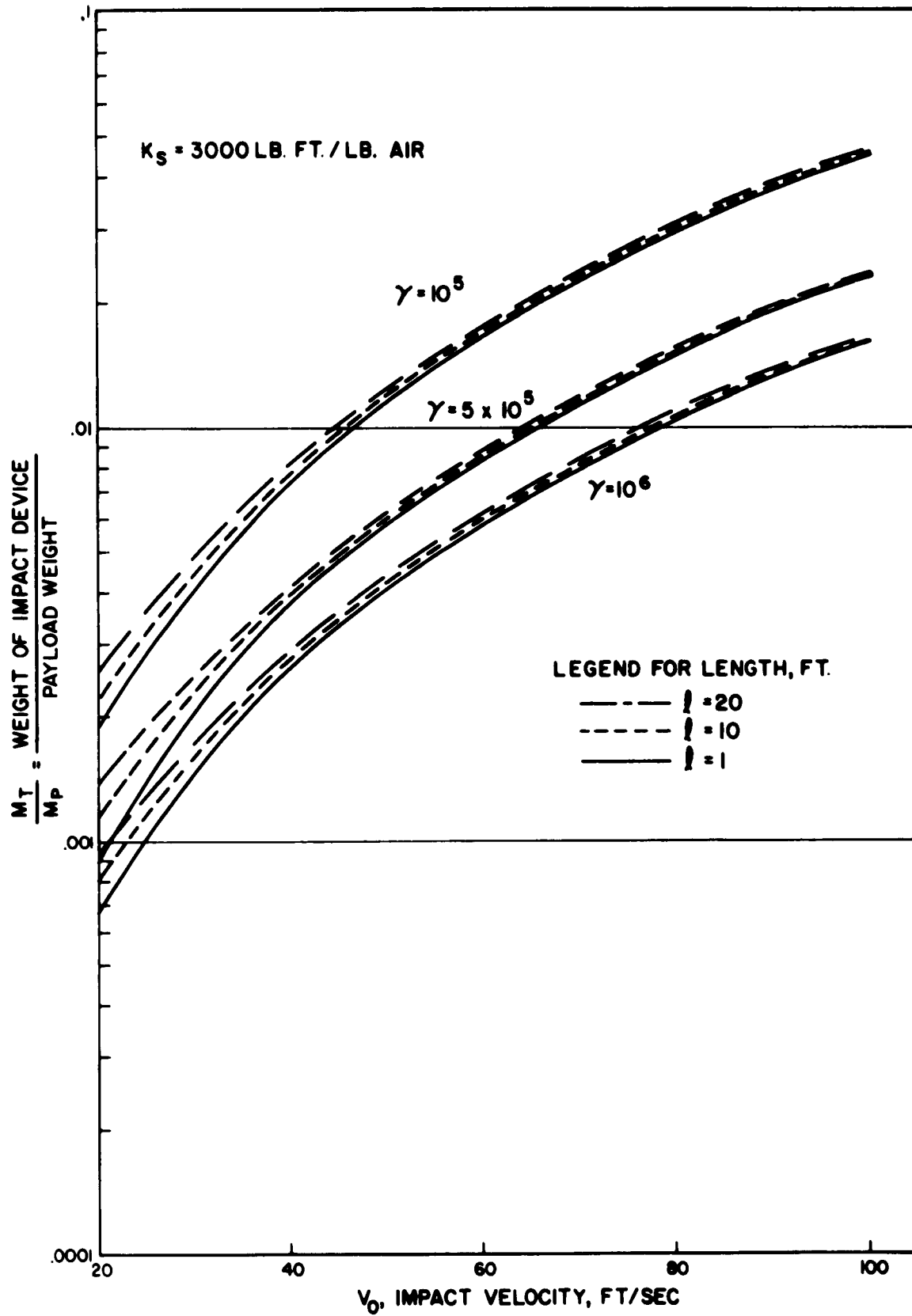


Figure 27. Weight Ratio Vs. Impact Velocity - Collapsible Shell (Vertical Cylinder), Air Pressurized

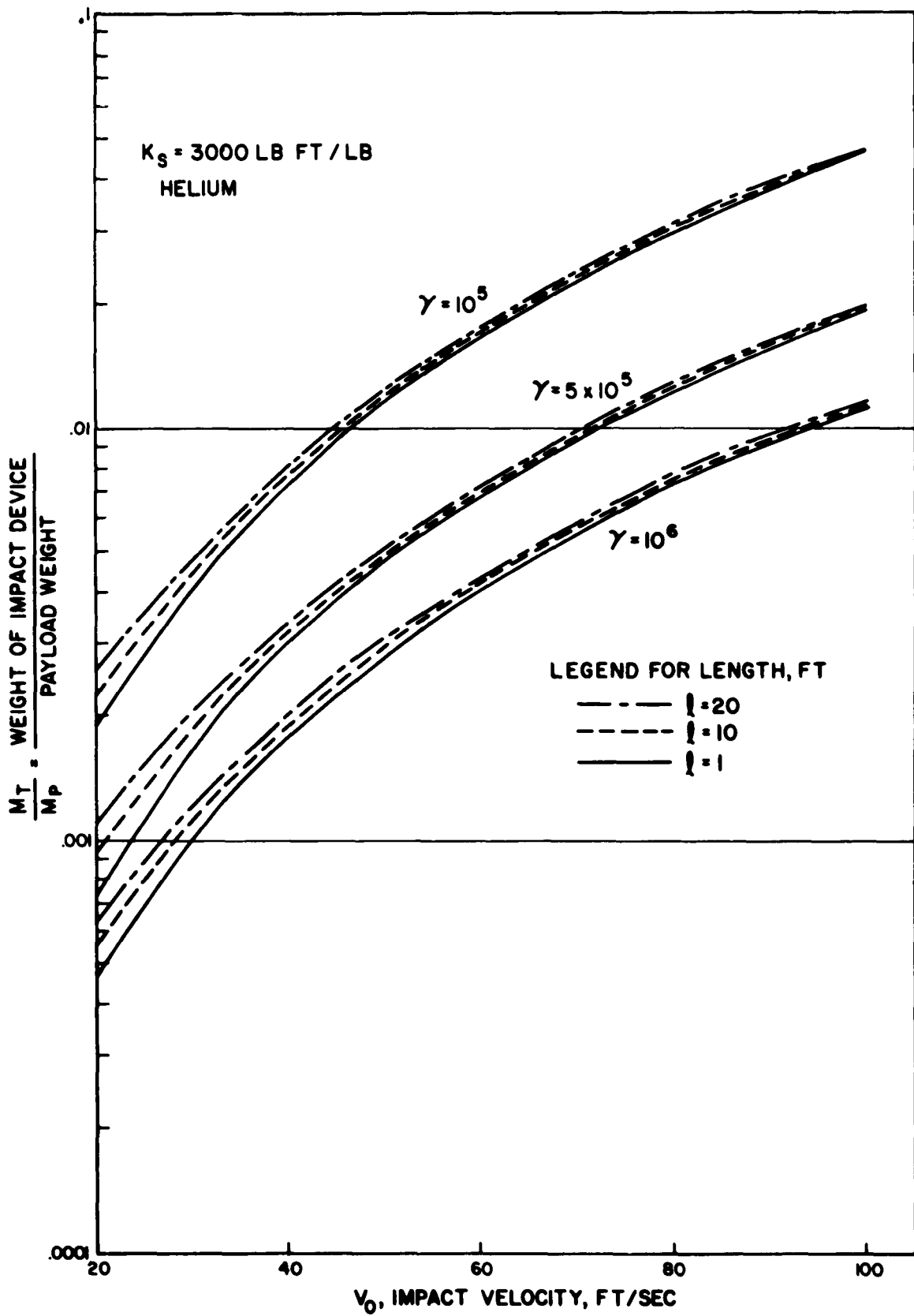


Figure 28. Weight Ratio Vs. Impact Velocity - Collapsible Shell (Vertical Cylinder), Helium Pressurized

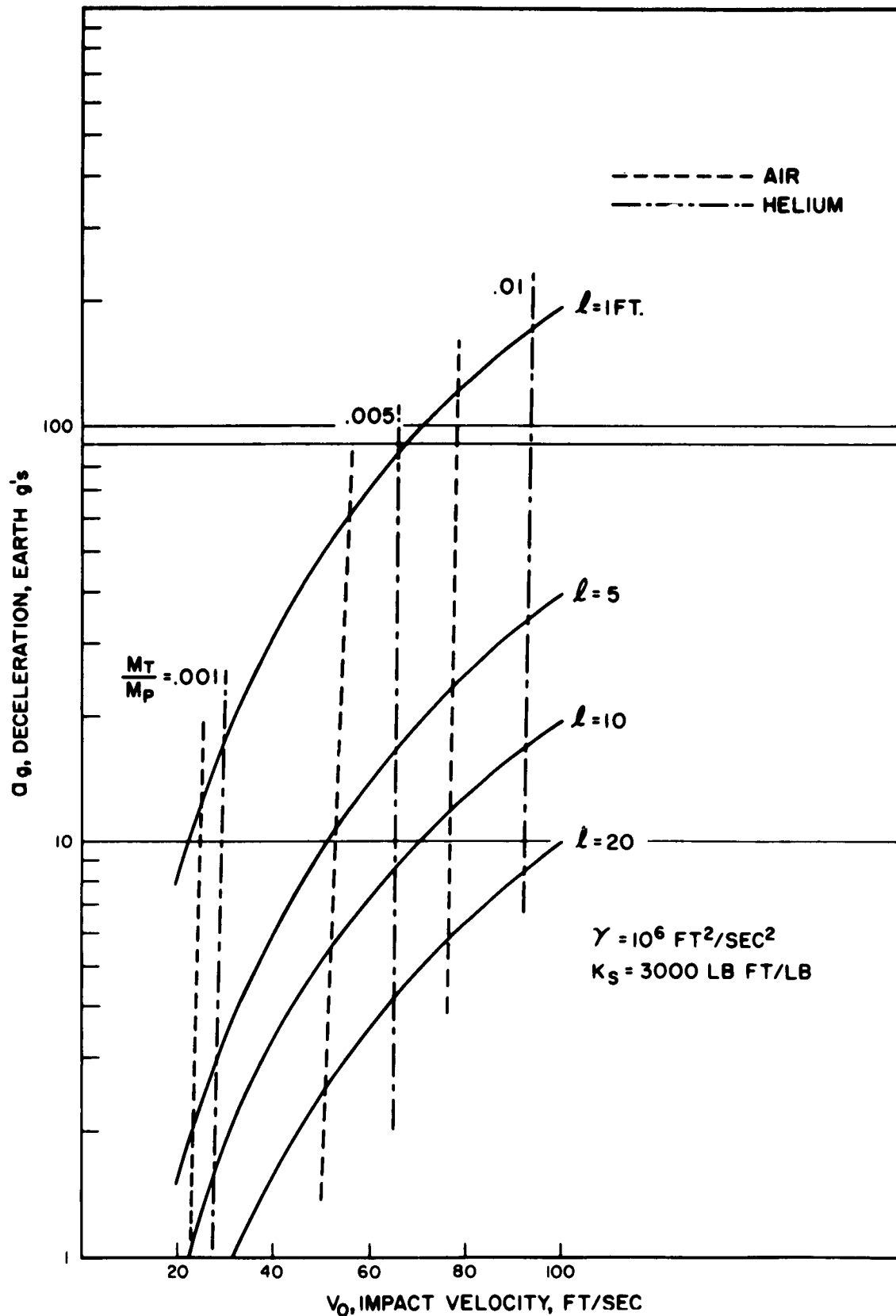


Figure 29. Deceleration of Collapsible Shell (Vertical Cylinder) with Constant Internal Pressure

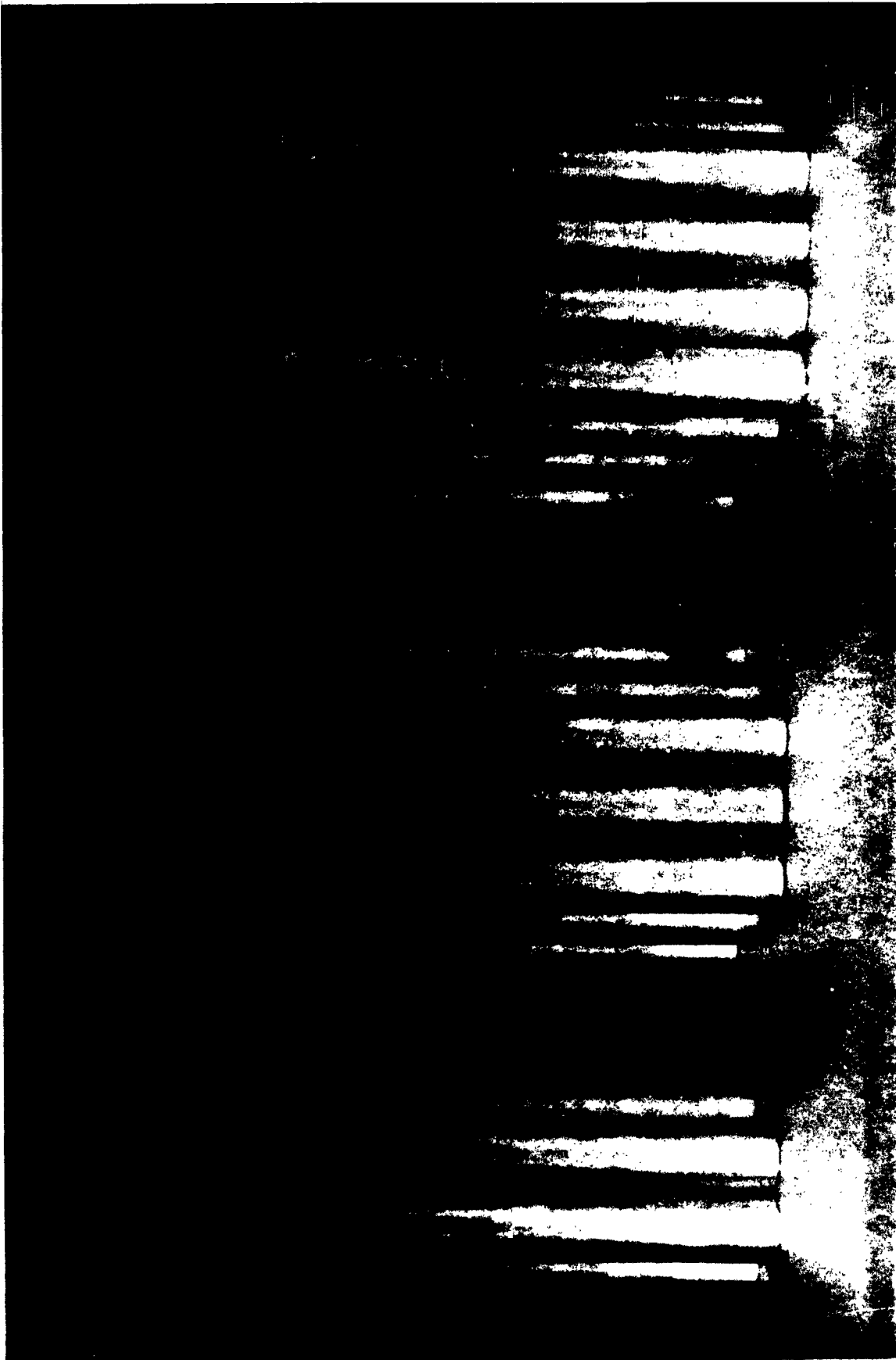


Figure 30. Arrays of Cylindrical Shells (Tube dimensions 1" Dia., .002" Thk., 8" Lgth, Aluminum)

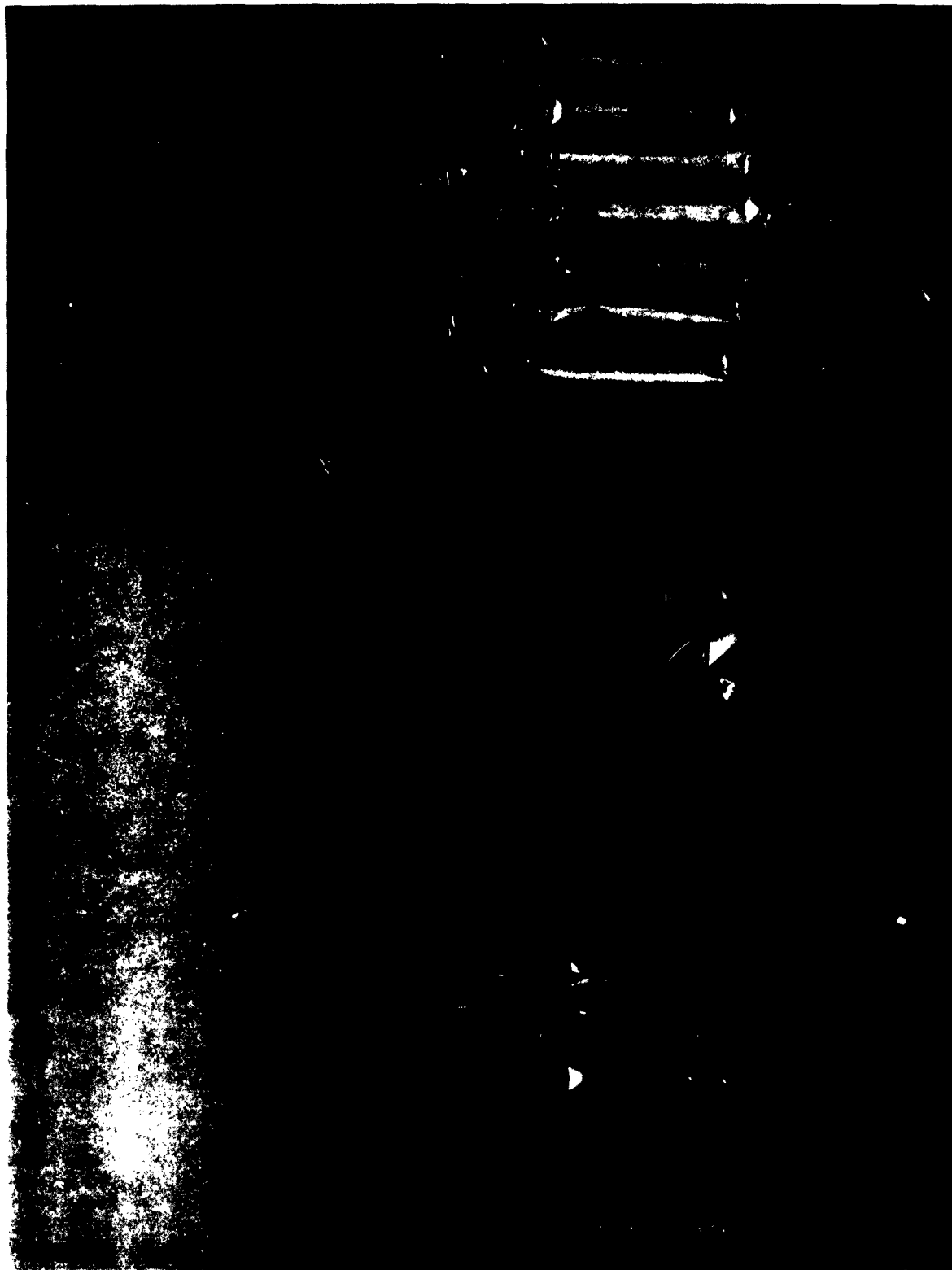


Figure 31. Collapsed Arrays of Cylindrical Shells

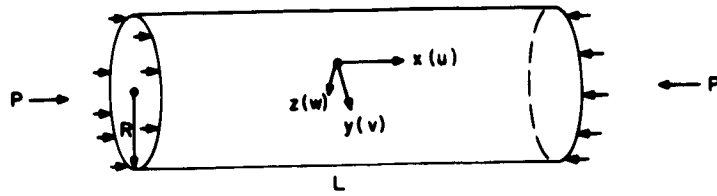


Figure 32. Shell Coordinates

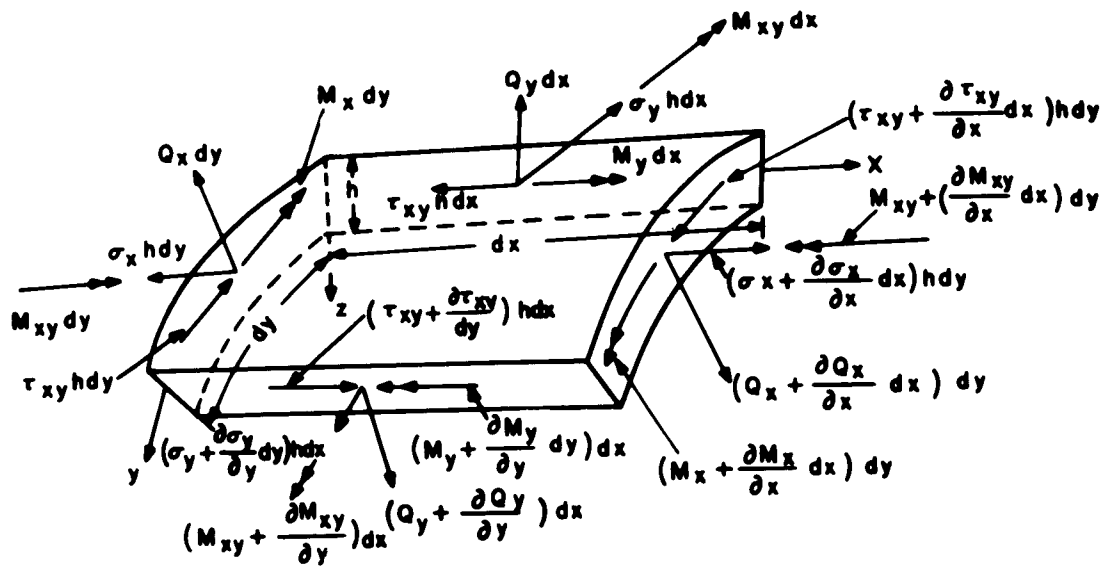


Figure 33. Shell Element Notations

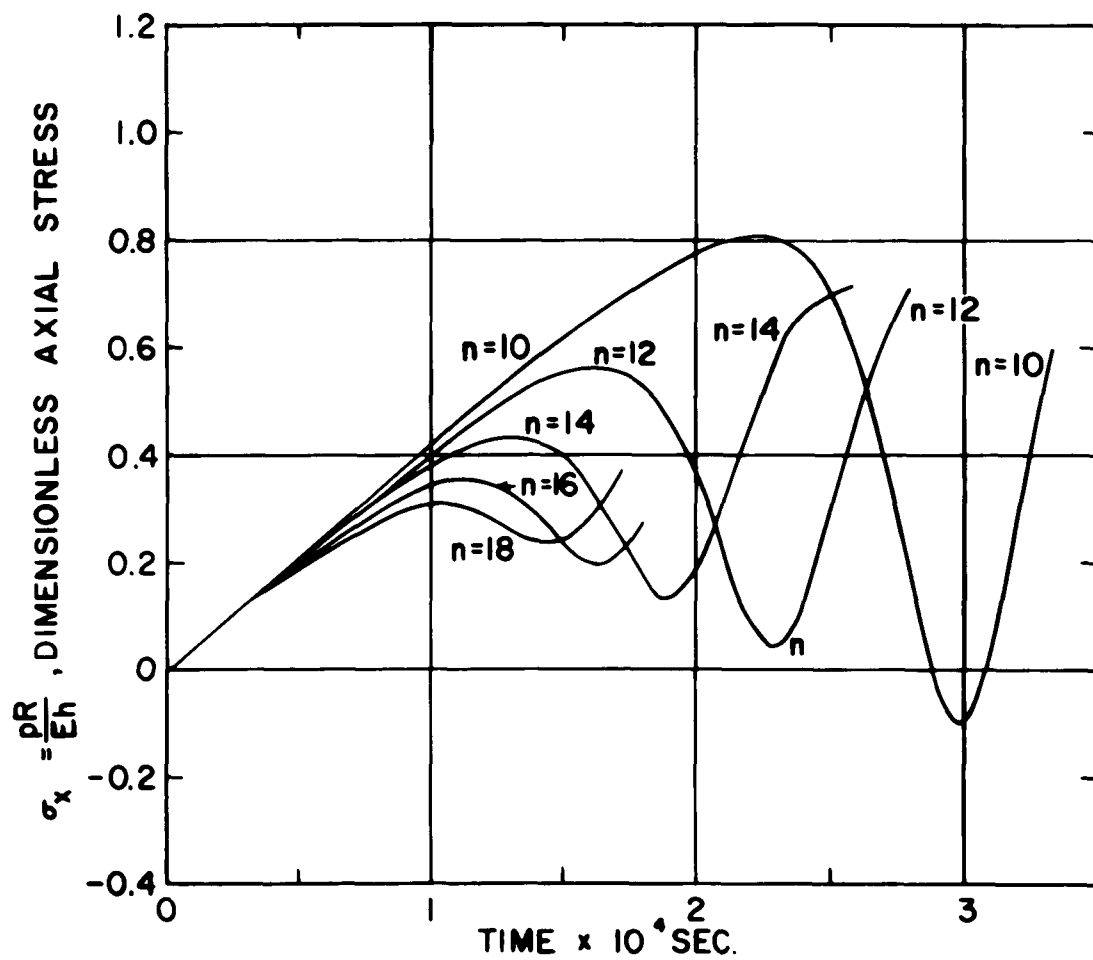


Figure 34. Axial Stress vs. Time ($V_0 = 11.5$ ft/sec, $h = .004''$, Aluminum)

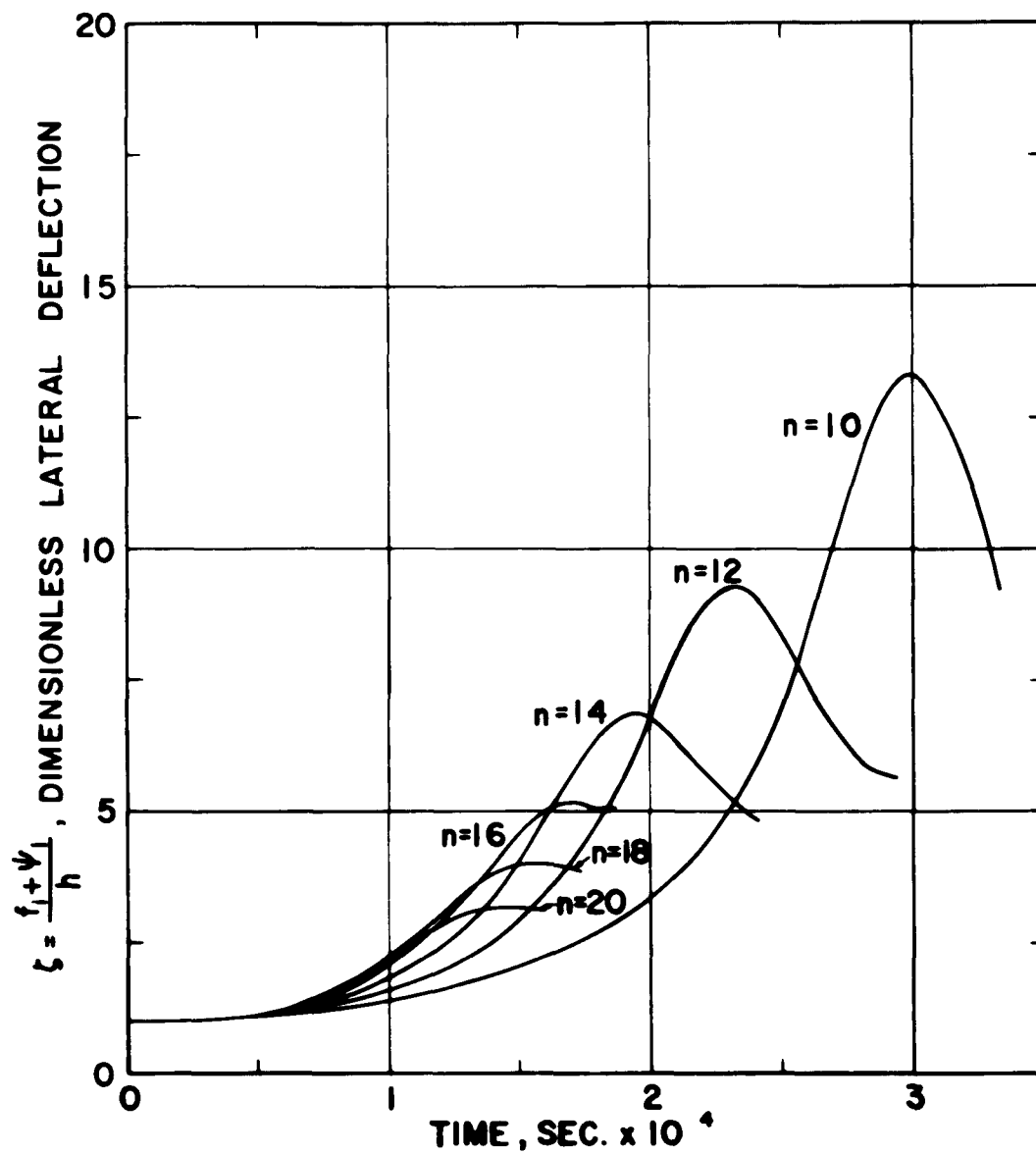


Figure 35. Lateral Deflection of Shell Wall vs. Time
 ($V_0 = 11.5$ ft/sec, $h = .004$ ", Aluminum)

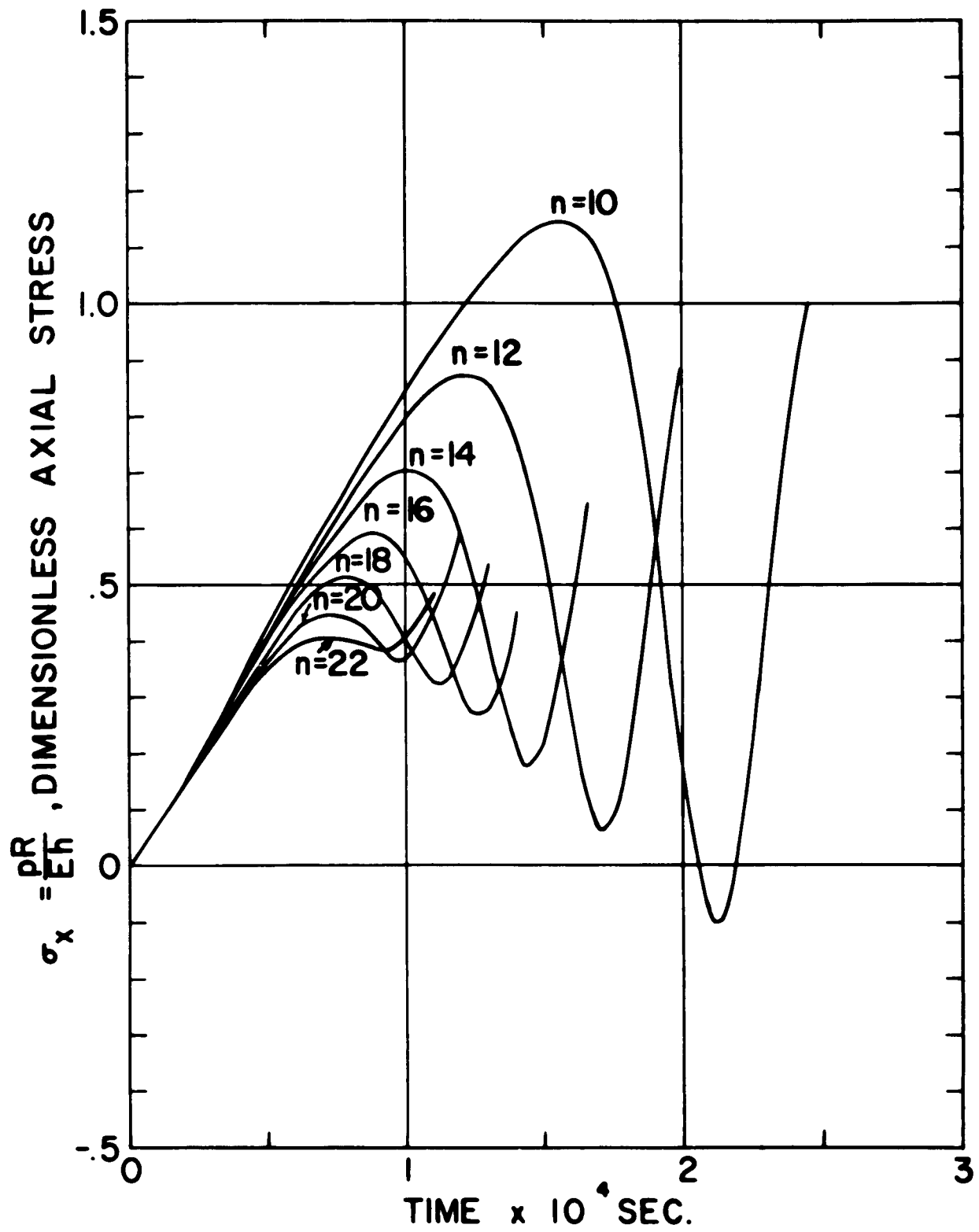


Figure 36. Axial Stress vs. Time ($V_0 = 23$ ft/sec, $h = .004$ ", Aluminum)

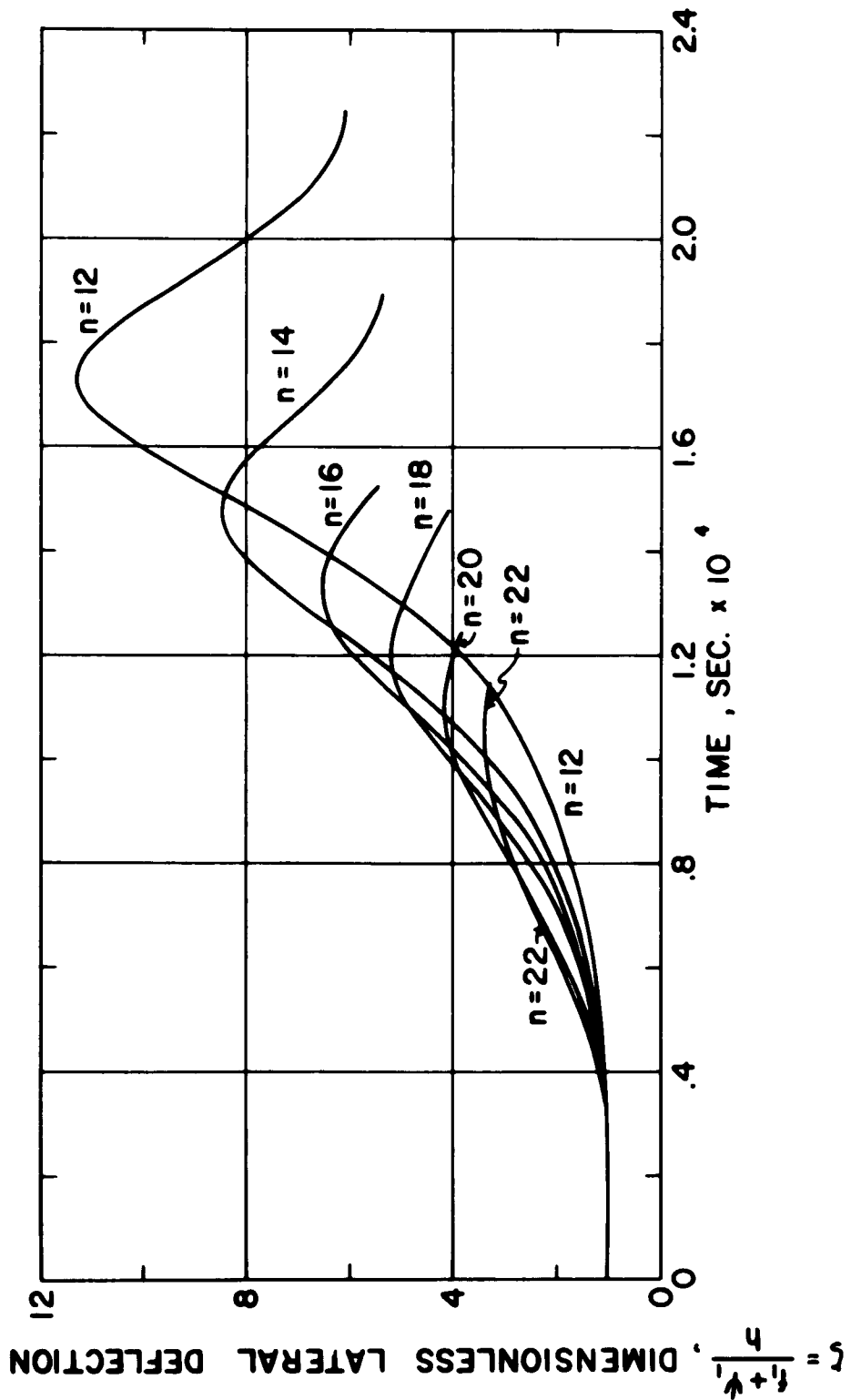


Figure 37. Lateral Deflection of Shell Wall vs. Time
 ($V_0 = 23$ ft/sec, $h = .004''$, Aluminum)

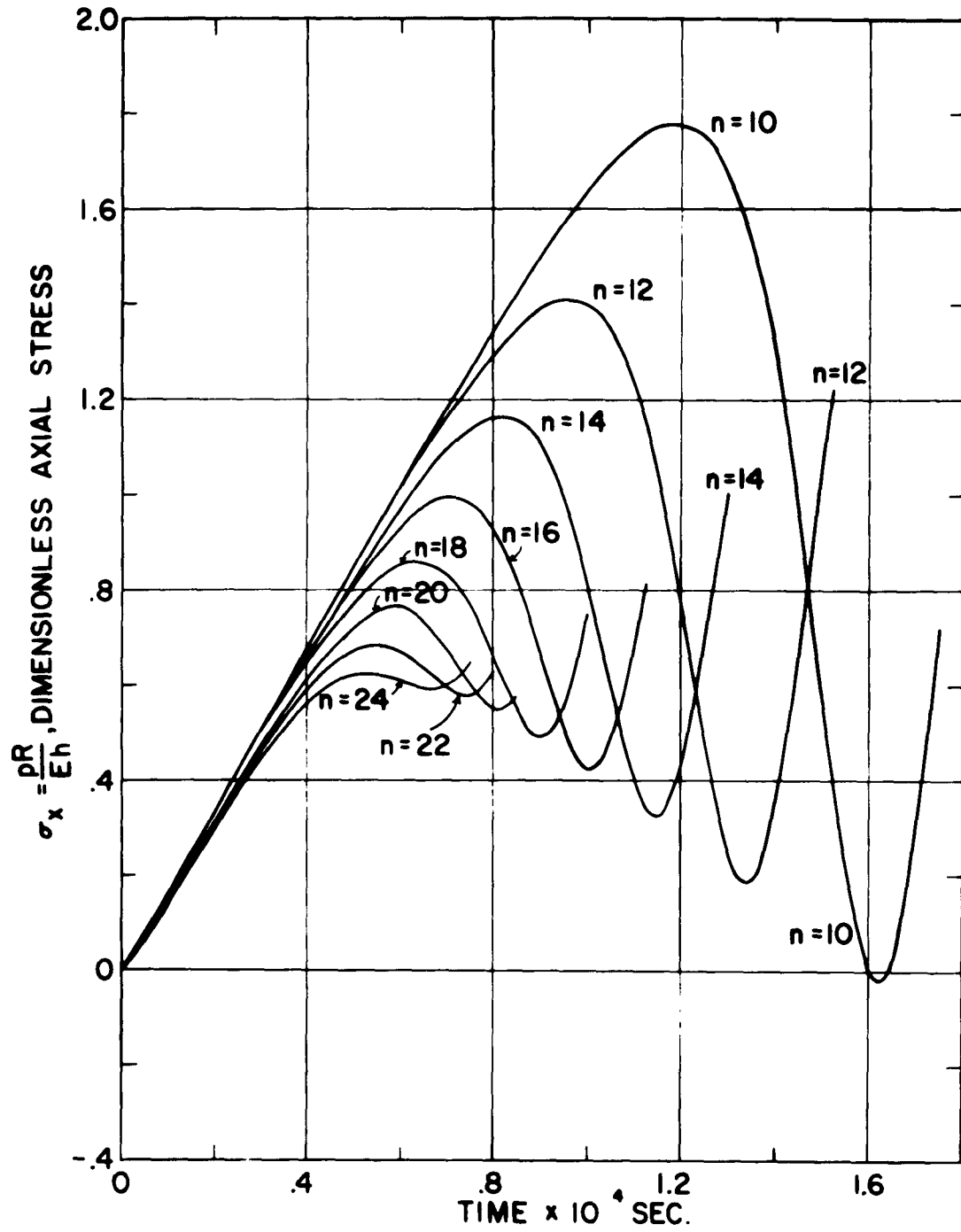


Figure 38. Axial Stress vs. Time ($V_0 = 46$ ft/sec, $h = .004$ ", Aluminum)

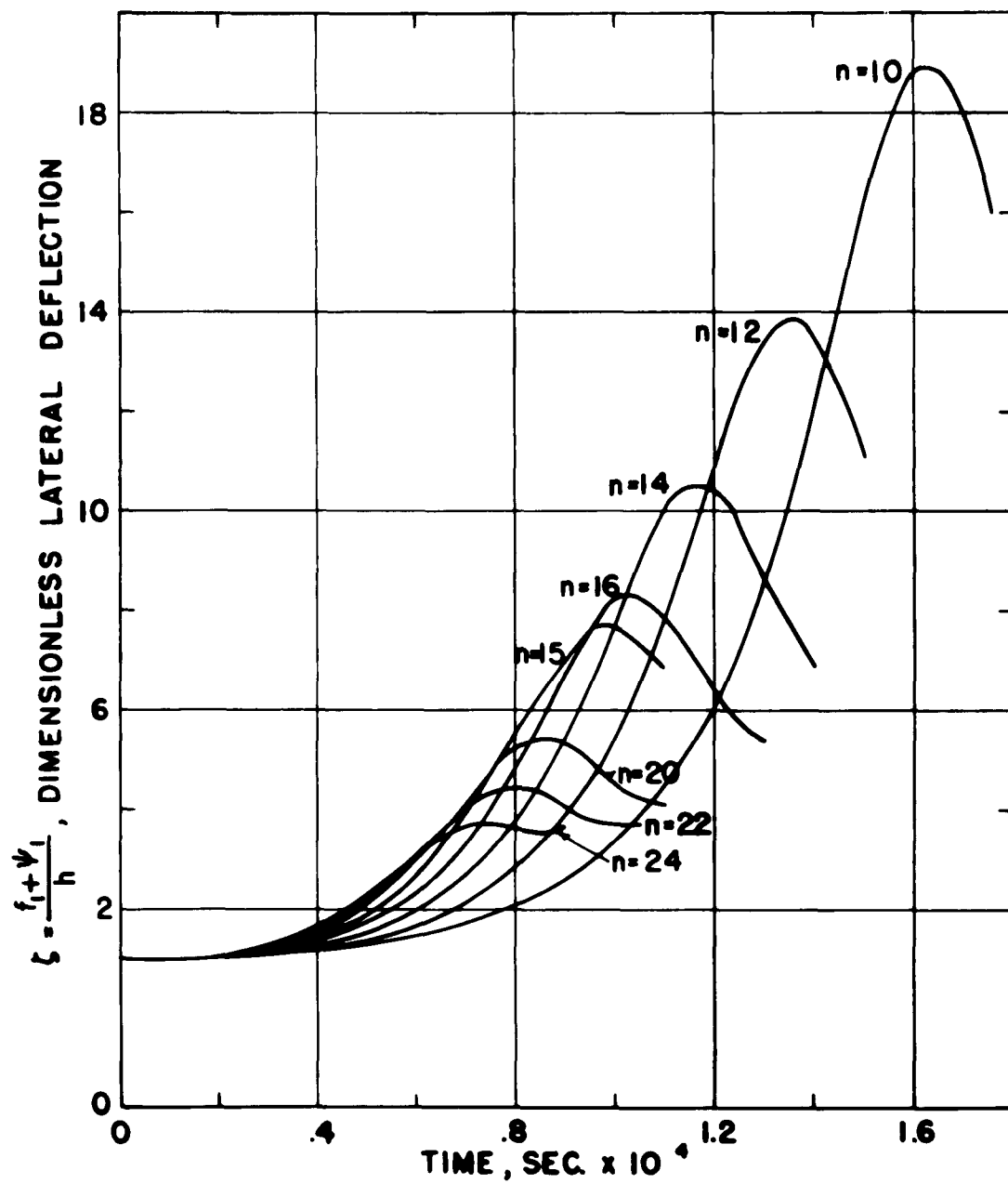


Figure 39. Lateral Deflection of the Shell Wall vs. Time
 ($V_0 = 46$ ft/sec, $h = .004$ ", Aluminum)

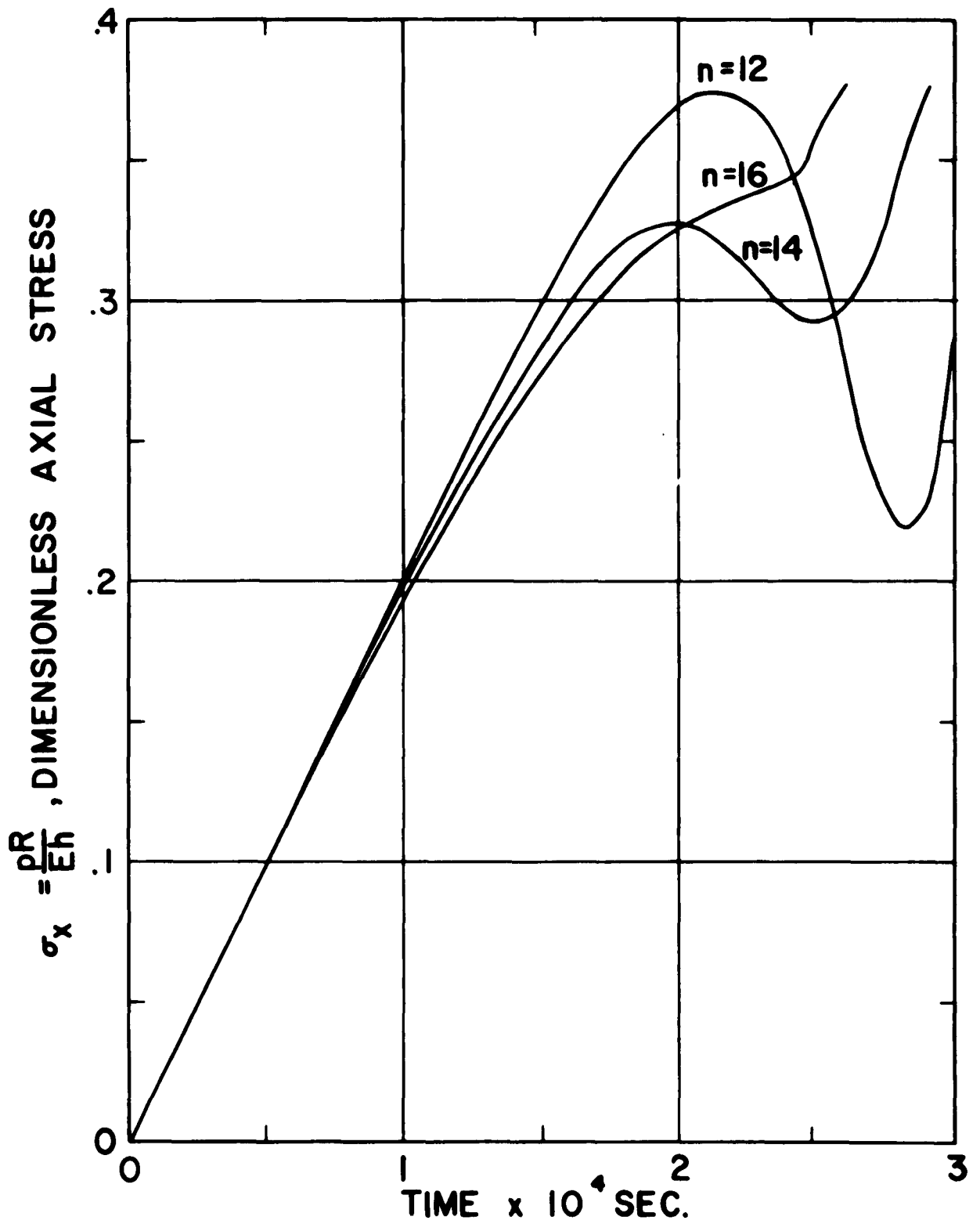


Figure 40. Axial Stress vs. Time ($V_0 = 11.5$ ft/sec, $h = .008''$, Aluminum)

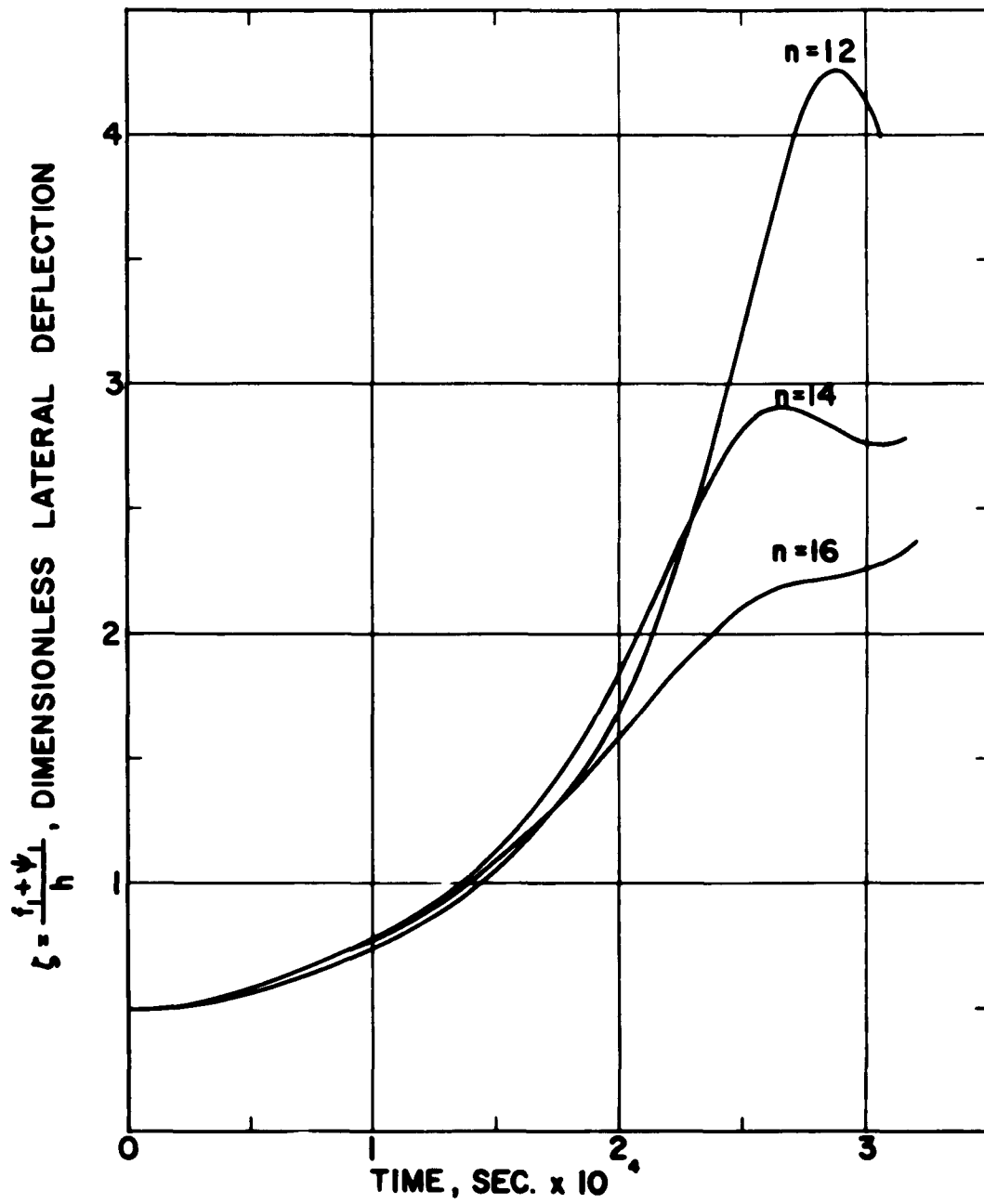


Figure 41. Lateral Deflection of the Shell Wall vs. Time
 ($V_0 = 11.5$ ft/sec, $h = .008$ ", Aluminum)

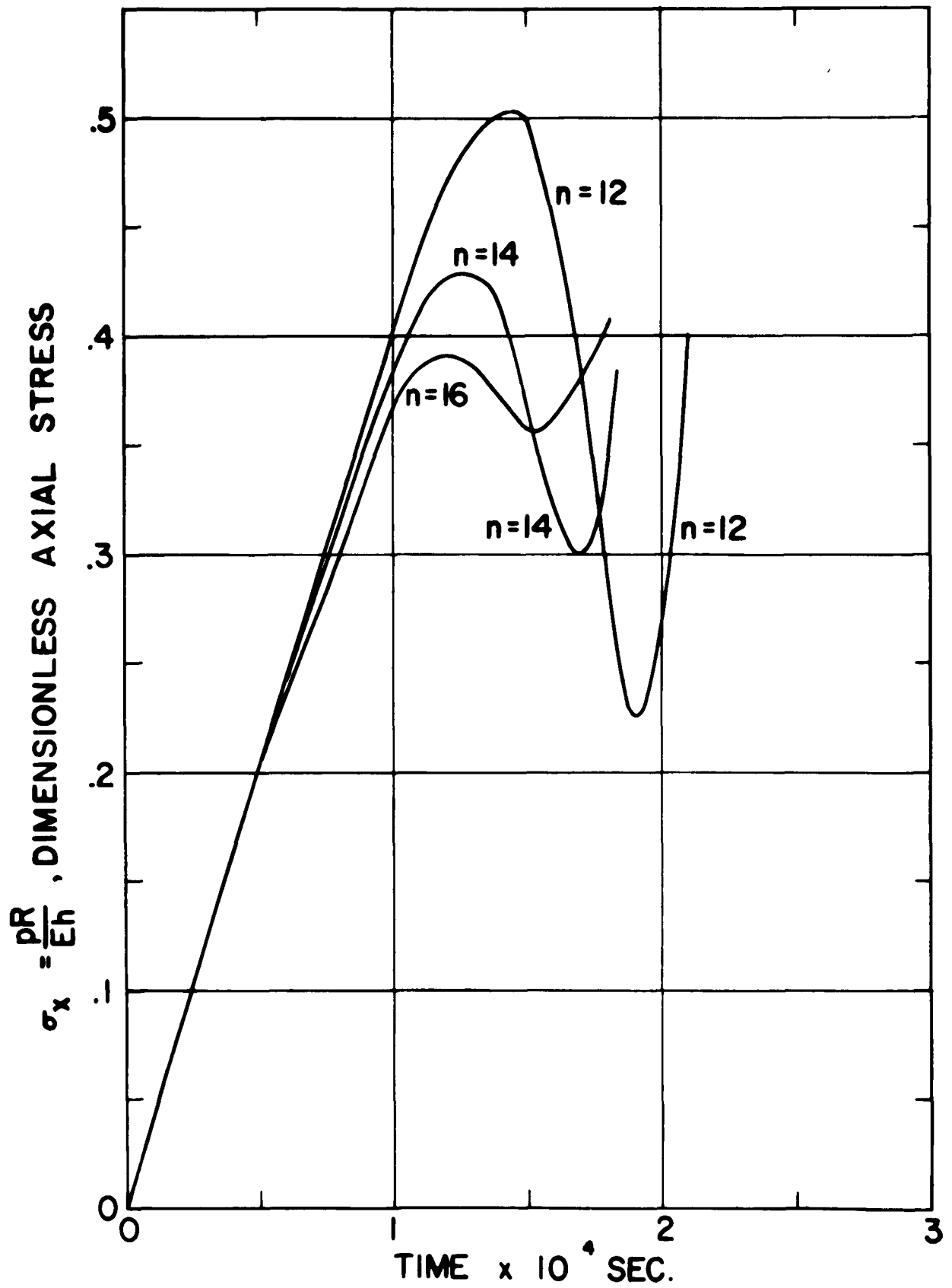


Figure 42. Axial Stress vs. Time ($V_0 = 23$ ft/sec, $h = .008''$, Aluminum)

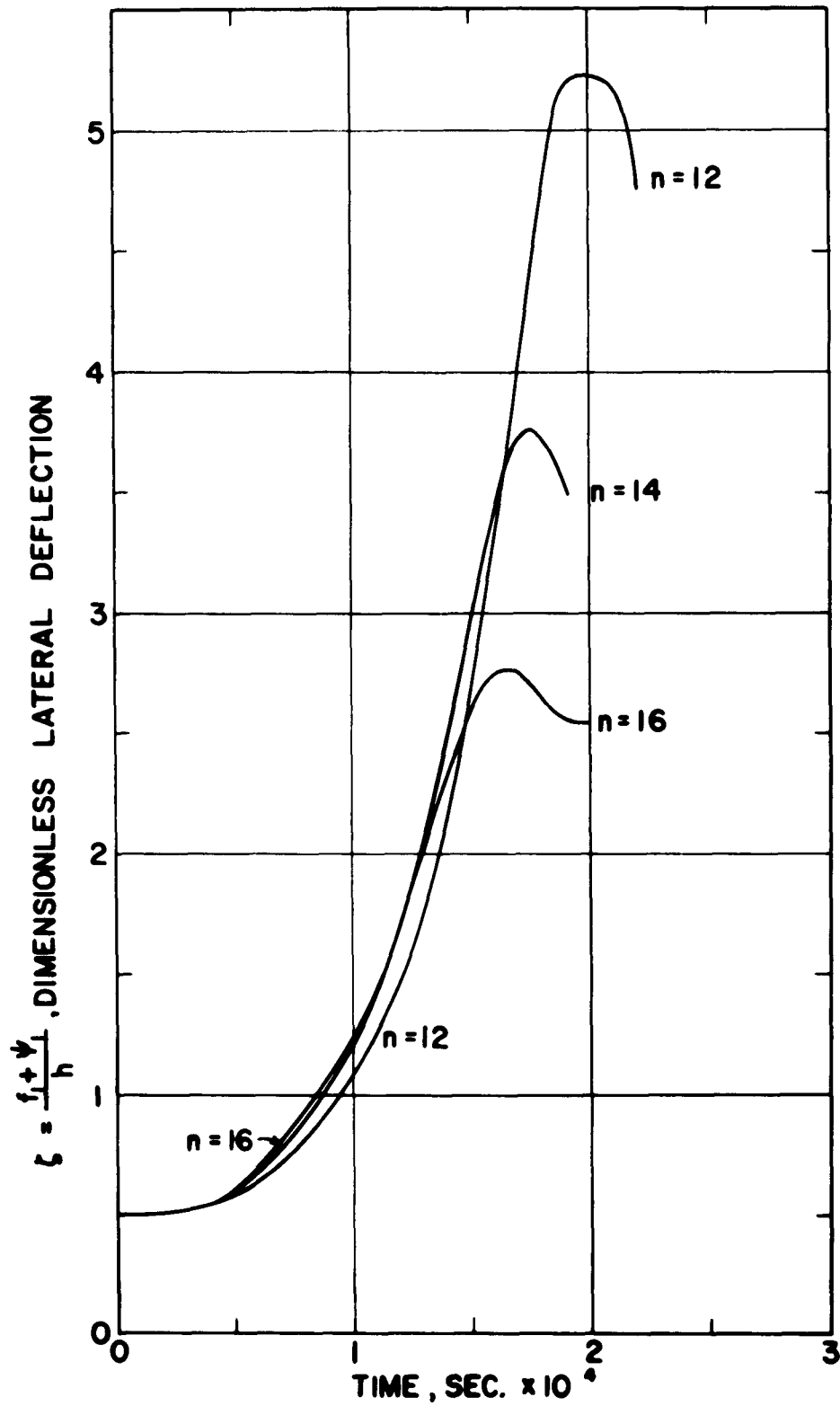


Figure 43. Lateral Deflection of the Shell Wall vs. Time ($V_0 = 23$ ft/sec, $h = .008$ ", Aluminum)

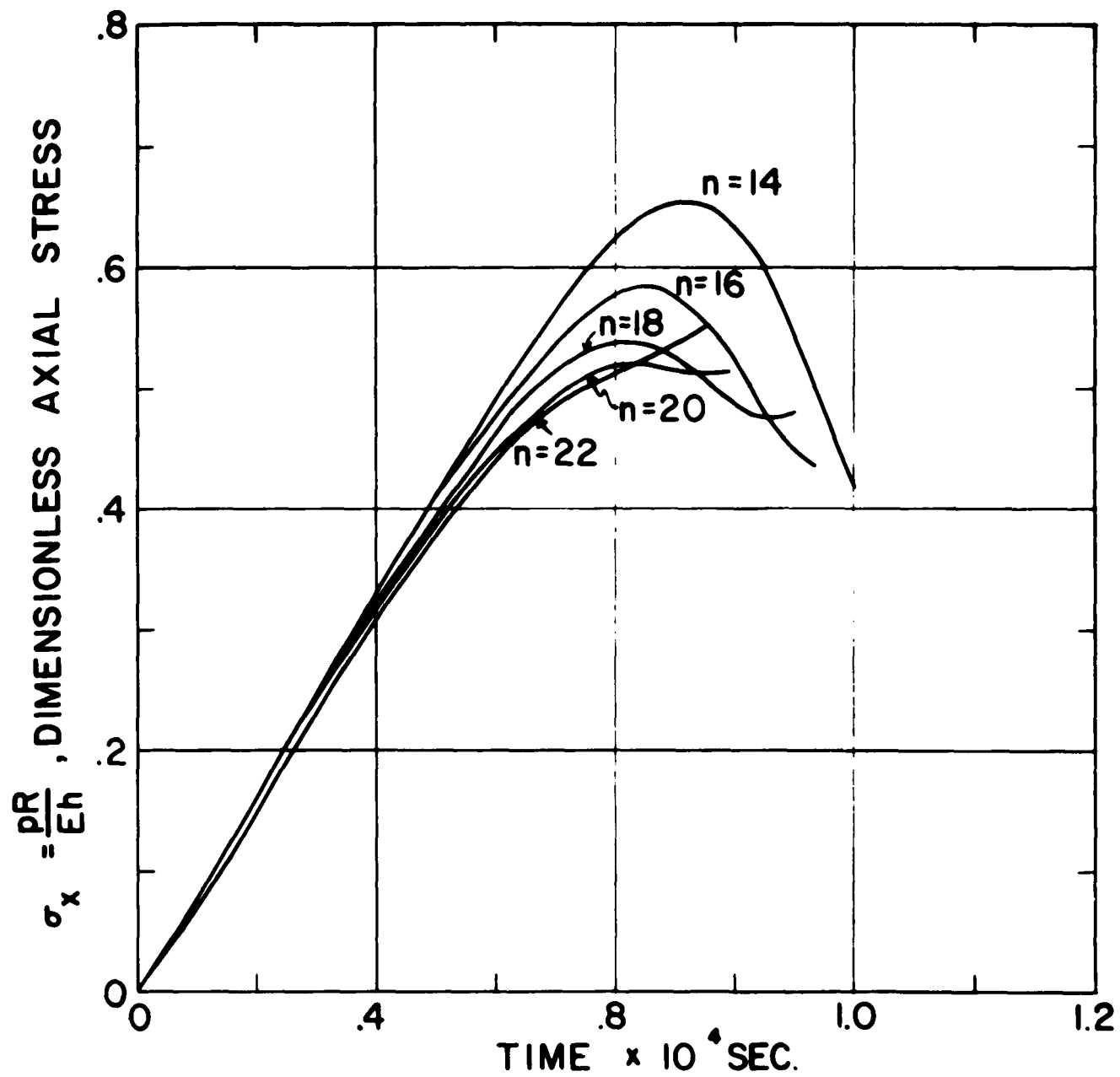


Figure 44. Axial Stress vs. Time ($V_0 = 46$ ft/sec, $h = .008''$, Aluminum)

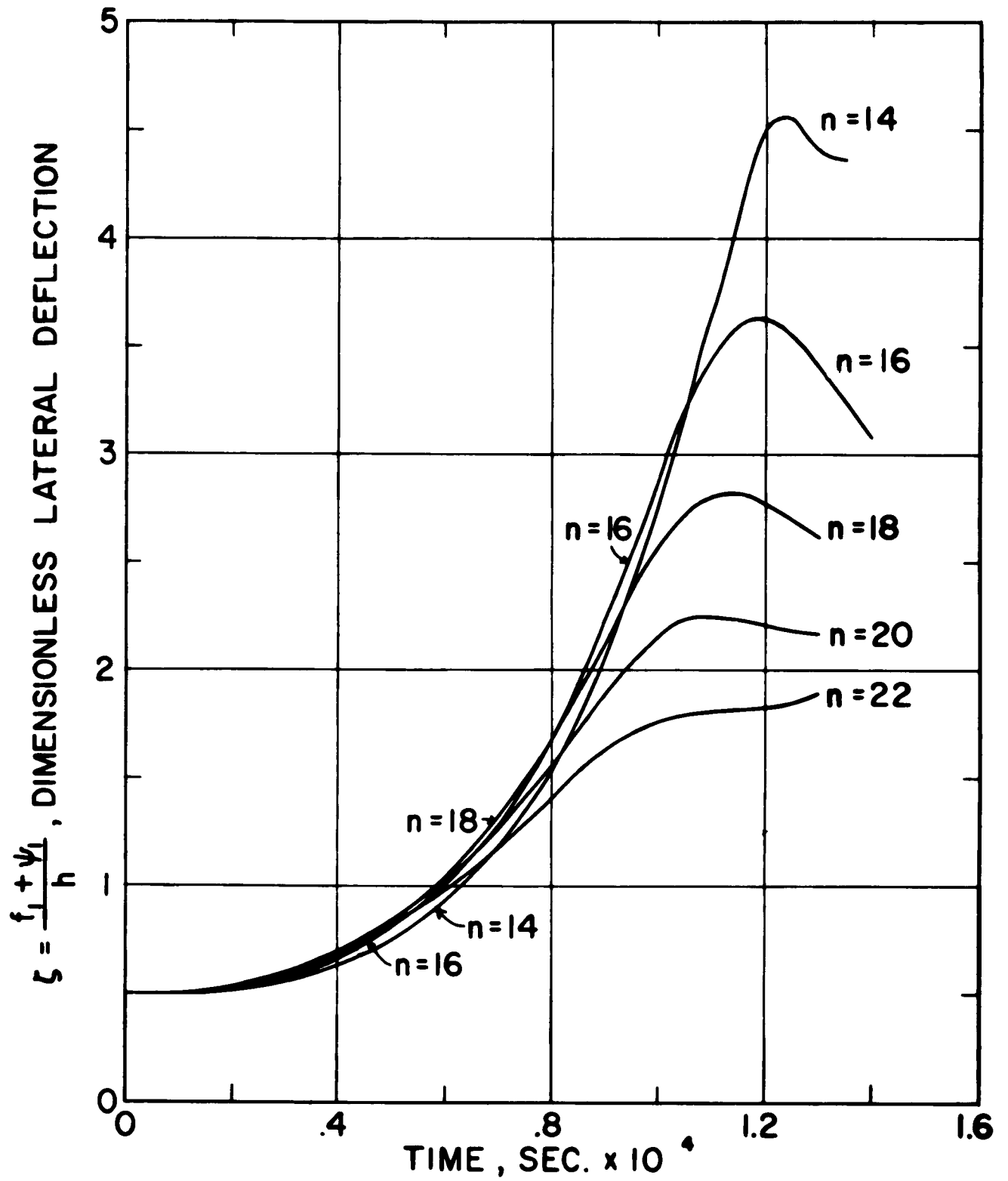


Figure 45. Lateral Deflection of the Shell Wall vs. Time
 ($V_0 = 46$ ft/sec, $h = .008''$, Aluminum)

Aeronautical Systems Division, Dir/Aeromechanics, Flight Dynamics Lab, Wright-Patterson AFB, Ohio. Rpt Nr ASD-TDR-62-774. DYNAMIC BUCKLING OF SHELL STRUCTURES SUBJECT TO LONGITUDINAL IMPACT. Final report, Dec 62, 77p. incl illus., 16 refs.

Unclassified Report

Investigations dealing with buckling of thin cylindrical and conical shells subject to axial impact are described. Studies consisted of experimental and theoretical efforts directed toward obtaining a qualitative and quantitative understanding of the dynamic buckling behavior of such shells under a variety of conditions. Conditions studied include different longitudinal conditions imposed on the impacted end of the shell and internal pressurization. In addition, methods of increasing the specific energy dissipation capacity of shells subject

1. Buckling
 2. Impact shock
 3. Shell buckling
 4. Mathematical analysis
 5. Dynamic buckling
- I. AFSC Project 1467
Task 146703
- II. Contract AF33(616)-
8248

- III. Missile & Space Div,
G. E. Space Tech Center,
King of Prussia, Pa.
- IV. A. P. Coppa, W. A. Mash
V. TIS R62 SD77
- VI. Aval fr OTS
- VII. In ASTIA collection

Aeronautical Systems Division, Dir/Aeromechanics, Flight Dynamics Lab, Wright-Patterson AFB, Ohio. Rpt Nr ASD-TDR-62-774. DYNAMIC BUCKLING OF SHELL STRUCTURES SUBJECT TO LONGITUDINAL IMPACT. Final report, Dec 62, 77p. incl illus., 16 refs.

Unclassified Report

Investigations dealing with buckling of thin cylindrical and conical shells subject to axial impact are described. Studies consisted of experimental and theoretical efforts directed toward obtaining a qualitative and quantitative understanding of the dynamic buckling behavior of such shells under a variety of conditions. Conditions studied include different longitudinal conditions imposed on the impacted end of the shell and internal pressurization. In addition, methods of increasing the specific energy dissipation capacity of shells subject

to axial impact were studied. A number of interesting results were obtained. It was demonstrated experimentally that buckling of a cylindrical shell is initiated during the first passage of the axial compression stress wave due to initial impact when the impact velocity is sufficiently high. Another significant experimental result obtained is that the asymmetrical (quasi-developable) form of shell buckling occurs as a result of a smooth transition from the asymmetrical (ring) form of buckling in some thin cylindrical shells subjected to an axially symmetric axial impact. Analytical results were obtained on the dynamical buckling behavior of cylindrical shells subject to a constant velocity end displacement. The method utilizes the finite deflection theory. It shows that both the upper critical stress and the number of circumferential waves increase and the time to initiate buckling decreases with increasing velocity of impact.

to axial impact were studied. A number of interesting results were obtained. It was demonstrated experimentally that buckling of a cylindrical shell is initiated during the first passage of the axial compression stress wave due to initial impact when the impact velocity is sufficiently high. Another significant experimental result obtained is that the asymmetrical (quasi-developable) form of shell buckling occurs as a result of a smooth transition from the asymmetrical (ring) form of buckling in some thin cylindrical shells subjected to an axially symmetric axial impact. Analytical results were obtained on the dynamical buckling behavior of cylindrical shells subject to a constant velocity end displacement. The method utilizes the finite deflection theory. It shows that both the upper critical stress and the number of circumferential waves increase and the time to initiate buckling decreases with increasing velocity of impact.

Aeronautical Systems Division, Dir/Aeromechanics, Flight Dynamics Lab, Wright-Patterson AFB, Ohio. Rpt Nr ASD-TDR-62-774. DYNAMIC BUCKLING OF SHELL STRUCTURES SUBJECT TO LONGITUDINAL IMPACT. Final report, Dec 62, 77p. incl illus., 16 refs.

Unclassified Report

Investigations dealing with buckling of thin cylindrical and conical shells subject to axial impact are described. Studies consisted of experimental and theoretical efforts directed toward obtaining a qualitative and quantitative understanding of the dynamic buckling behavior of such shells under a variety of conditions. Conditions studied include different longitudinal conditions imposed on the impacted end of the shell and internal pressurization. In addition, methods of increasing the specific energy dissipation capacity of shells subject

1. Buckling
 2. Impact shock
 3. Shell buckling
 4. Mathematical analysis
 5. Dynamic buckling
- I. AFSC Project 1467
Task 146703

II. Contract AF33(616)-8248

- III. Missile & Space Div, G.E. Space Tech Center, King of Prussia, Pa.
- IV. A. P. Coppa, W.A. Nash
- V. TIS R62 SD77
- VI. Aval fr OTS
- VII. In ASTIA collection

Aeronautical Systems Division, Dir/Aeromechanics, Flight Dynamics Lab, Wright-Patterson AFB, Ohio. Rpt Nr ASD-TDR-62-774. DYNAMIC BUCKLING OF SHELL STRUCTURES SUBJECT TO LONGITUDINAL IMPACT. Final report, Dec 62, 77p. incl illus., 16 refs.

Unclassified Report

Investigations dealing with buckling of thin cylindrical and conical shells subject to axial impact are described. Studies consisted of experimental and theoretical efforts directed toward obtaining a qualitative and quantitative understanding of the dynamic buckling behavior of such shells under a variety of conditions. Conditions studied include different longitudinal conditions imposed on the impacted end of the shell and internal pressurization. In addition, methods of increasing the specific energy dissipation capacity of shells subject

to axial impact were studied. A number of interesting results were obtained. It was demonstrated experimentally that buckling of a cylindrical shell initiated during the first passage of the axial compression stress wave due to initial impact when the impact velocity is sufficiently high. Another significant experimental result obtained is that the asymmetrical (quasi-developable) form of shell buckling occurs as a result of a smooth transition from the symmetrical (ring) form of buckling in some thin cylindrical shells subjected to an axially symmetric axial impact. Analytical results were obtained on the dynamical buckling behavior of cylindrical shells subject to a constant velocity and displacement. The method utilizes the finite deflection theory. It shows that both the upper critical stress and the number of circumferential waves increase and the time to initiate buckling decreases with increasing velocity of impact.

to axial impact were studied. A number of interesting results were obtained. It was demonstrated experimentally that buckling of a cylindrical shell initiated during the first passage of the axial compression stress wave due to initial impact when the impact velocity is sufficiently high. Another significant experimental result obtained is that the asymmetrical (quasi-developable) form of shell buckling occurs as a result of a smooth transition from the symmetrical (ring) form of buckling in some thin cylindrical shells subjected to an axially symmetric axial impact. Analytical results were obtained on the dynamical buckling behavior of cylindrical shells subject to a constant velocity and displacement. The method utilizes the finite deflection theory. It shows that both the upper critical stress and the number of circumferential waves increase and the time to initiate buckling decreases with increasing velocity of impact.

Aeronautical Systems Division, Dir/Aeromechanics,
Flight Dynamics Lab, Wright-Patterson AFB, Ohio.
Rep. Nr. ASD-TDR-62-774. DYNAMIC BUCKLING OF SHELL
STRUCTURES SUBJECT TO LONGITUDINAL IMPACT. Final
report, Dec 62, 77p. incl illus., 16 refs.

Unclassified Report

Investigations dealing with buckling of thin cylindrical and conical shells subject to axial impact are described. Studies consisted of experimental and theoretical efforts directed toward obtaining a qualitative and quantitative understanding of the dynamic buckling behavior of such shells under a variety of conditions. Conditions studied include different longitudinal conditions imposed on the impacted end of the shell and internal pressurization. In addition, methods of increasing the specific energy dissipation capacity of shells subject

to axial impact were studied. A number of interesting results were obtained. It was demonstrated experimentally that buckling of a cylindrical shell is initiated during the first passage of the axial compression stress wave due to initial impact when the impact velocity is sufficiently high. Another significant experimental result obtained is that the asymmetrical (quasi-developable) form of shell buckling occurs as a result of a smooth transition from the symmetrical (ring) form of buckling in some thin cylindrical shells subjected to an axially symmetric axial impact. Analytical results were obtained on the dynamical buckling behavior of cylindrical shells subject to a constant velocity end displacement. The method utilizes the finite deflection theory. It shows that both the upper critical stress and the number of circumferential waves increase and the time to initiate buckling decreases with increasing velocity of impact.

1. Buckling
2. Impact shock
3. Shell buckling
4. Mathematical analysis
5. Dynamic buckling
I. AFSC Project 1467
Task 146703

II. Contract AF33(616)-8248

III. Missile & Space Div,
G.E. Space Tech Center,
King of Prussia, Pa.

IV. A. P. Coppa, W.A. Mash
V. TIS R62 S077

VI. Avail fr OTS

VII. In ASTIA collection

Aeronautical Systems Division, Dir/Aeromechanics,
Flight Dynamics Lab, Wright-Patterson AFB, Ohio.
Rep. Nr. ASD-TDR-62-774. DYNAMIC BUCKLING OF SHELL
STRUCTURES SUBJECT TO LONGITUDINAL IMPACT. Final
report, Dec 62, 77p. incl illus., 16 refs.

Unclassified Report

Investigations dealing with buckling of thin cylindrical and conical shells subject to axial impact are described. Studies consisted of experimental and theoretical efforts directed toward obtaining a qualitative and quantitative understanding of the dynamic buckling behavior of such shells under a variety of conditions. Conditions studied include different longitudinal conditions imposed on the impacted end of the shell and internal pressurization. In addition, methods of increasing the specific energy dissipation capacity of shells subject

to axial impact were studied. A number of interesting results were obtained. It was demonstrated experimentally that buckling of a cylindrical shell is initiated during the first passage of the axial compression stress wave due to initial impact when the impact velocity is sufficiently high. Another significant experimental result obtained is that the asymmetrical (quasi-developable) form of shell buckling occurs as a result of a smooth transition from the symmetrical (ring) form of buckling in some thin cylindrical shells subjected to an axially symmetric axial impact. Analytical results were obtained on the dynamical buckling behavior of cylindrical shells subject to a constant velocity end displacement. The method utilizes the finite deflection theory. It shows that both the upper critical stress and the number of circumferential waves increase and the time to initiate buckling decreases with increasing velocity of impact.

Aeronautical Systems Division, Dir/Aeromechanics, Flight Dynamics Lab, Wright-Patterson AFB, Ohio. Rpt Nr ASD-TDR-62-774. DYNAMIC BUCKLING OF SHELL STRUCTURES SUBJECT TO LONGITUDINAL IMPACT. Final report, Dec 62, 77p. incl illus., 16 refs.

Unclassified Report

Investigations dealing with buckling of thin cylindrical and conical shells subject to axial impact are described. Studies consisted of experimental and theoretical efforts directed toward obtaining a qualitative and quantitative understanding of the dynamic buckling behavior of such shells under a variety of conditions. Conditions studied include different longitudinal conditions imposed on the impacted end of the shell and internal pressurization. In addition, methods of increasing the specific energy dissipation capacity of shells subject

1. Buckling
 2. Impact shock
 3. Shell buckling
 4. Mathematical analysis
 5. Dynamic buckling
- I. AFSC Project 1467

II. Contract AF33(616)-8248

III. Missile & Space Div, C.E. Space Tech Center, King of Prussia, Pa.

IV. A. P. Coppa, W.A. Mash

V. TIS R62 SD77

VI. Aval fr OTS

VII. In ASTIA collection

Aeronautical Systems Division, Dir/Aeromechanics, Flight Dynamics Lab, Wright-Patterson AFB, Ohio. Rpt Nr ASD-TDR-62-774. DYNAMIC BUCKLING OF SHELL STRUCTURES SUBJECT TO LONGITUDINAL IMPACT. Final report, Dec 62, 77p. incl illus., 16 refs.

Unclassified Report

Investigations dealing with buckling of thin cylindrical and conical shells subject to axial impact are described. Studies consisted of experimental and theoretical efforts directed toward obtaining a qualitative and quantitative understanding of the dynamic buckling behavior of such shells under a variety of conditions. Conditions studied include different longitudinal conditions imposed on the impacted end of the shell and internal pressurization. In addition, methods of increasing the specific energy dissipation capacity of shells subject

to axial impact were studied. A number of interesting results were obtained. It was demonstrated experimentally that buckling of a cylindrical shell is initiated during the first passage of the axial compression stress wave due to initial impact when the impact velocity is sufficiently high. Another significant experimental result obtained is that the asymmetrical (quasi-developable) form of shell buckling occurs as a result of a smooth transition from the symmetrical (ring) form of buckling in some thin cylindrical shells subjected to an axially symmetric axial impact. Analytical results were obtained on the dynamical buckling behavior of cylindrical shells subject to a constant velocity end displacement. The method utilizes the finite deflection theory. It shows that both the upper critical stress and the number of circumferential waves increase and the time to initiate buckling decreases with increasing velocity of impact.

to axial impact were studied. A number of interesting results were obtained. It was demonstrated experimentally that buckling of a cylindrical shell is initiated during the first passage of the axial compression stress wave due to initial impact when the impact velocity is sufficiently high. Another significant experimental result obtained is that the asymmetrical (quasi-developable) form of shell buckling occurs as a result of a smooth transition from the symmetrical (ring) form of buckling in some thin cylindrical shells subjected to an axially symmetric axial impact. Analytical results were obtained on the dynamical buckling behavior of cylindrical shells subject to a constant velocity end displacement. The method utilizes the finite deflection theory. It shows that both the upper critical stress and the number of circumferential waves increase and the time to initiate buckling decreases with increasing velocity of impact.